[illegible]/ME/65-7

THE USE OF A COANDA NOZZLE WITH PARALLEL SECONDARY INJECTION FOR THE THRUST VECTORING OF A TWO-DIMENSIONAL COMPRESSIBLE FLUID

THESIS

Presented to the Faculty of the School of Engineering

of the Air Force Institute of Technology

Air University

in Partial Fulfillment of the

Requirements for the Degree of

Master of Science

by

Philip P. Panzarella, B.S., A.E.
1/Lt USAF

Graduate Aerospace-Mechanical Engineering

March 1965

Preface

Up to the early 1960's, fluid jets were primarily controlled and vectored by mechanical systems. These systems were and still are complex, heavy, and difficult to adapt to either high temperature environments such as exist in rocket exhausts, or low temperature environments such as exist in space. Mechanical systems also become unreliable in extreme environments and require costly and heavy backup systems to insure consistent operation. These difficulties have caused interest in pure fluid control systems. Two types of pure fluid control devices being investigated today are the turbulence inducer and the wall attachment (coanda-effect) nozzle. The latter device has demonstrated its superiority over the turbulence inducer in vectoring (switching) a fluid and it is a modification of this device that is discussed in this paper. The Coanda-Effect nozzle is a device in which a two-dimensional fluid stream is thrust vectored (switched) by injecting a secondary fluid perpendicular to it.

The purpose of this experimental study was to determine the effect of parallel injection of a secondary fluid jet on the thrust vectoring of a two-dimensional fluid in a coanda nozzle. Nozzle geometries similar to those used by Kisby (Ref 9) and Opfell (Ref 20) were explored in order that a comparison could be made between the parallel and perpendicular secondary injection technique. Major consideration was given to supersonic (Choked flow) operation of the nozzle; however, some data on subsonic operation of the nozzle is presented. The notation used in this report and the non-dimensionalization procedure followed have, wherever possible, been made

consistent with Refs 9 and 20 so that easy comparison of results and trends could be accomplished.

I wish to thank Major W. C. Robison for the direction and support given me in his capacity as my thesis advisor. I would also like to thank Mr. Frank Jarvis and Mr. John Parks for the assistance rendered me in the laboratory.

Philip P. Pansarella

Contents

Contents (Contd)

List of Figures

List of Figures (Contd)

List of Figures (Contd)

List of Figures (Contd)

List of Tables

List of Symbols

A_t - Nozzle throat area, in^2.

b - Nozzle throat width, in.

C_p - Wall pressure coefficient.

d - Nozzle setback distance, in.

d/b - Setback ratio.

db - Decibels.

F_o - Axial nozzle thrust, lbf.

F_s - Lateral nozzle thrust, lbf.

F_s/F_o - Lateral thrust ratio.

$\frac{F_s/F_o}{\dot{M}_s/\dot{M}_o}$ - Lateral thrust efficiency ratio.

k - Ratio of specific heats.

L - Sidewall length, in.

$\dot{M}_o$ - Nozzle (primary) mass flow rate, lbm/sec.

$\dot{M}_s$ - Injection (secondary) mass flow rate, lbm/sec.

$\dot{M}_s/\dot{M}_o$ - Secondary mass flow ratio.

P_a - Ambient pressure, in. Hg.

P_b - Separation-bubble pressure, in. Hg.

P_o - Nozzle total pressure, in. Hg.

P_s - Wall static pressure, in. Hg.

P_o/P_a - Nozzle total pressure ratio.

$(P_o/P_a)_s$ - Secondary total pressure ratio.

Rey_b - Reynolds number based on b.

T_o - Primary flow total temperature, ^oF.

T_s - Injection (secondary) flow total temperature, ^oF.

V_t - Flow velocity at throat, ft/sec.

List of Symbols (Contd)

X	- Distance along the sidewall, in. (see Fig. 2).
X_r	- Flow attachment point distance, in. (see Fig. 2).
x/b	- Non-Dimensional wall distance.
θ	- Sidewall divergence angle, degrees.
ρ_t	- Density of throat, slugs/ft^3.
μ_t	- Absolute viscosity at throat, lbf-sec/ft^2.

Abbreviations

AFIT	- Air Force Institute of Technology
ASME	- American Society of Mechanical Engineers
Cps	- Cycles per second
DDC	- Defense Documentation Center

Abstract

An experimental investigation was performed to determine the effect of parallel injection of a secondary fluid on a two-dimensional coanda-effect nozzle used as a thrust vectoring (jet-switching) device. The effect of leakage in the vortex area of a conventional coanda-effect nozzle utilizing perpendicular secondary injection was also determined. The coanda-effect nozzle used in the investigation had a wall divergence half angle of 10° and a setback ratio that varied from 4 to 7. Pressure ratios investigated varied from 1.63 to 3.39. Successful thrust vectoring was accomplished within the above limits of setback and pressure ratios.

The injection of secondary fluid parallel to the centerline of the nozzle caused the primary jet to deflect toward the secondary jet and to attach to the nozzle sidewall nearest the secondary jet. A 1 to 10 decibel drop in the overall noise level resulted when the parallel secondary fluid was injected into the nozzle.

Attachment of the primary jet to the nozzle was stable and was sustained by "coanda-effect" flow in the separation region formed between the primary jet and the wall after secondary injection was discontinued. The wall attachment point was insensitive to increases in pressure ratio; however, the attachment point moved downstream along the nozzle wall as setback ratio increased from 4 to 7. The amount of secondary mass flow needed to switch the primary fluid jet increased with increasing setback ratio and with increasing pressure ratio. Lateral thrust increased with increasing setback ratio and decreased with increasing pressure ratio. The maximum lateral thrust

for the minimum secondary injection flow occurred between a setback ratio of 4 and 5. The time required for the primary fluid jet to switch from one nozzle wall to the other was found to be .001 seconds.

Interferometer and Schlieren photographs of the thrust vectoring phenomena that occurred throughout the investigated setback and pressure ratio range are included in the report.

GAM 65A/ME/65-7

THE USE OF A COANDA NOZZLE WITH PARALLEL SECONDARY INJECTION FOR THE THRUST VECTORING OF A TWO-DIMENSIONAL COMPRESSIBLE FLUID

I. Introduction

The Coanda-Effect - Background

In 1933, Henri Coanda, a Rumanian engineer working in France, observed that if a wall was placed near a fluid exiting from an orifice, the fluid would attach to the wall. This effect can be explained as follows. When a fluid jet with a turbulent boundary exits into an ambient fluid which has an equal or lower viscosity, the turbulent boundary entrains fluid from the ambient fluid field. Normally the entrained fluid is replaced from the surroundings and the only noticeable effect that can be observed is the spreading of the exiting fluid jet. Now if a wall is placed near the exiting jet, the fluid cannot be replaced from the surroundings because the wall "blocks off" the replacing fluid. Since fluid is still being entrained by the jet, the pressure in the region between the jet and the wall decreases and eventually the pressure differential across the fluid jet causes the jet to move towards the wall. If the wall is long enough, the jet will attach to it, forming a vortex, and assuming a stable position. The stability of the attached jet is explained by the fact that the portion of the fluid turned back at the attachment point is just enough to satisfy the entrainment requirements of the boundary of the jet that is facing the wall. This

wall attachment phenomena is termed the "Coanda-Effect" and is illustrated in Fig. 1a.

Coanda-Effect Nozzles - Previous Work

Since it is difficult and mechanically complex to construct variable geometry nozzles, that is, to provide for movement of the wall in the vicinity of the jet, a method was needed to deflect the main jet near the wall. The first person to efficiently accomplish this was Mr. B. H. Horton of the U.S. Army's Harry Diamond Laboratories in 1958. The primary jet was deflected by injecting a secondary fluid perpendicular to it, making use of momentum transfer effects. This was the first true purely fluid control device and was called a "Coanda-Effect Nozzle", Fig. 1b. Application of Coanda-Effect Nozzles includes fluid amplifiers, digital counters, missile steering, jet engine controls, analog integrators, flow diverters, turning rate sensors, and aircraft flight controls.

In 1960 Bourque and Newman (Ref 5) developed a mathematical model for a two-dimensional coanda-effect nozzle using an incompressible fluid jet. A method for determining the mean pressure in the separation-bubble and the jet attachment point was formulated. Also in 1960, Sawyer (Ref 22) completed an experimental study using an incompressible fluid exiting from a two-dimensional coanda-effect nozzle. Sawyer's work indicated that the jet spread coefficient was a function of the curvature of the jet and that the values for the jet attachment point and the mean separation-bubble pressure predicted by Bourque and Newman were correct. Both Bourque and Newman and Sawyer based their work on a method developed by Dodds (Ref 8).

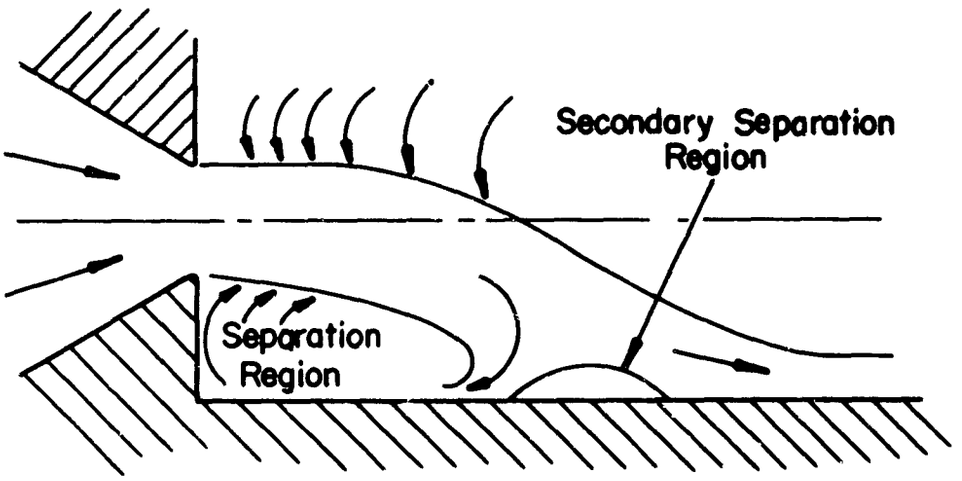

a. Schematic model of the coanda effect

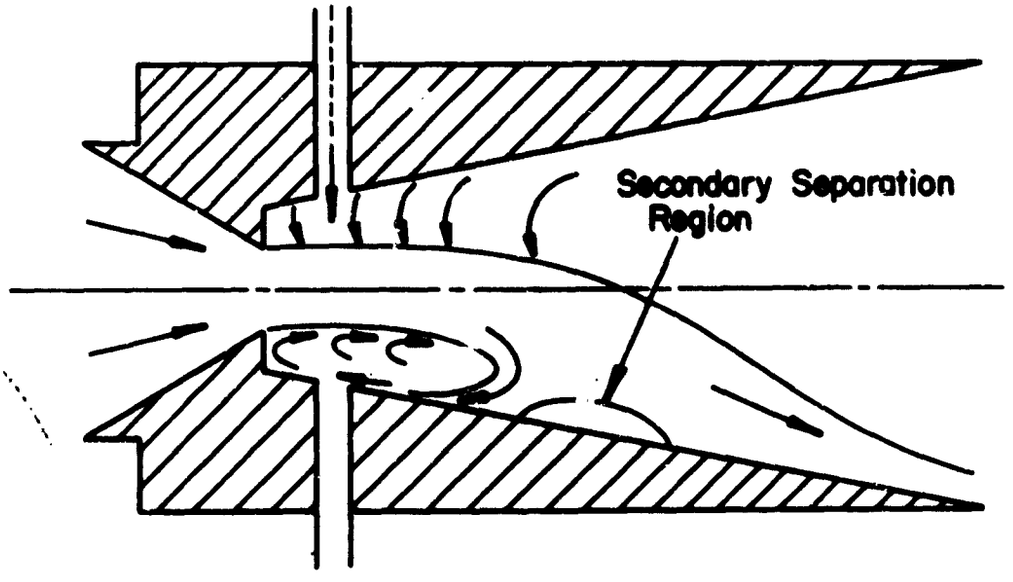

b. Schematic model of conventional coanda-effect nozzle

Fig. 1

Schematic Representation of the Coanda-Effect

Olson (Ref 19), in 1962, developed a theory for the prediction of the attachment point and the mean separation-bubble pressure of a two-dimensional compressible jet exiting adjacent to a flat plate. The model of the flow proposed by Olson took into account the curvature of the fluid jet. In a comment on this article, by A. E. Mitchell, it is pointed out that although the Dodds', et al, method of determining attachment point and separation-bubble pressure was based on an incompressible analysis, it agreed closely enough (especially at low mach numbers) with Olson's work so that it could be used. Also pointed out in this article is the fact that Dodds' method contains less empirical parameters than Olson's method, and therefore it affords a much more direct means of determining attachment point and mean separation-bubble pressure.

All the work done by the above investigators was done on relatively small scale coanda nozzles. In 1963 Elsby (Ref 9) of the Air Force Institute of Technology performed an experimental study on relatively large scale choked-flow, two-dimensional, coanda-effect nozzles with perpendicular, high velocity injection of the secondary fluid. It was found that thrust vectoring could be accomplished in this type of nozzle by injection of the secondary fluid into the separation-bubble. The injection destroyed the low pressure region in the separation-bubble causing the main jet to move away from the attached wall towards a centered position. Further injection deflected the main jet towards the opposite wall where it attached and remained after the secondary injector flow was discontinued. Opfell (Ref 20), also at the Air Force Institute of Technology, extended this work in

1964. This investigation was primarily concerned with subsonic flow in a two-dimensional coanda-effect nozzle and included the perpendicular injection of both high velocity and low velocity secondary fluid. It was concluded that there were two distinct modes of switching. The first mode was the one reported by Elsby, et al, that is, that injection into the separation-bubble caused the jet to switch to the opposite wall. The second mode of switching was caused by the perpendicular injection of secondary fluid from the wall opposite to the wall where the main jet was attached. In this case, entrainment was set up in the region between the secondary jet and the main jet, lowering the pressure and eventually causing a large enough pressure differential across the jet to allow it to break away from the attached wall, overcome the adverse momentum effects imposed on it by the secondary fluid stream, and attach to the wall from which the secondary fluid was issuing. This "attraction" switching suggested an alternate approach in the thrust vectoring of a fluid through use of a coanda nozzle, than the one initially proposed by B. W. Horton. Opfell also pointed out that the pure momentum model of jet switching was in error and that a new model, which was called the entrainment model, should be investigated to account for both the momentum and entrainment effects encountered during the thrust vectoring process.

The Problem

The model of the coanda-effect nozzle that Opfell used at the time "attraction" switching occurred was detrimental to the switch because the perpendicular "attraction" jet set up momentum transfer and pressure differential forces that acted in a direction opposite

to the motion of the switching primary jet. The nozzle used by Opfell also required large secondary mass flows to execute the "attraction" switch and was not able to consistently switch the jet when operating under "attraction" conditions. For these reasons, it was decided to redesign the nozzle so that the adverse momentum and pressure differential characteristics would be eliminated, and so that jet switching could be consistently demonstrated during subsonic and supersonic flow of the primary fluid. A comparison between the parallel injector coanda-effect nozzle and the coanda-effect nozzles used by both Elsby and Opfell was desirable and, therefore, the variable geometry aspect of these nozzles was retained. The redesigned nozzle was then tested to obtain basic information on the ability of the nozzle to thrust vector a supersonic two-dimensional compressible fluid.

In both Elsby's and Opfell's work leakage of the nozzle in the vicinity of the junction of the converging and diverging sections of the nozzle was listed as a source of experimental error. It was decided as a secondary problem to devise a way of sealing these coanda nozzles and thus, to qualitatively determine the effect leakage had on the results. The sealing technique discovered in this part of the investigation was incorporated into the redesigned nozzle used in the latter part of the study.

Assumptions

The primary and secondary jets were assumed to be two-dimensional for this study. As can be seen in Fig. 4, page 14, the main jet exiting from the redesigned coanda-effect nozzle is indeed two-dimensional; however, the secondary fluid streams exiting from the injectors drilled

in the diverging base blocks of the nozzle are not two-dimensional. The secondary jets were assumed to be two-dimensional because of the nearness of the walls of the testing chamber to the issuing jets as compared to the distance between the sidewall of the nozzle and the centerline of the primary jet stream. The boundary layer buildup on the glass walls of the testing chamber was assumed to be negligible. Gravitational effects were neglected since the coanda-effect nozzle was mounted vertically on the test stand.

Objectives and Criteria

The primary objective of this experimental study was to determine the effect of parallel injection of a secondary fluid on a coanda nozzle used as a device for thrust vectoring a two-dimensional compressible fluid. A secondary objective was to compare the parallel injection coanda nozzle with a conventional (perpendicular injection) coanda nozzle. The definition of optimum conditions under which thrust vectoring occurred in the parallel injection nozzle was also desired. Successful thrust vectoring in the test nozzle was considered to occur when the attached main jet could be made to switch and attach to the opposite wall as a result of injection of the secondary fluid. Optimum conditions for thrust vectoring were considered to exist when a maximum lateral thrust force was obtained with a minimum secondary fluid flow rate.

Scope

Due to the comparison desired between the parallel injector coanda nozzle and the conventional nozzle used by Elsby, it was

decided to restrict the investigation to the optimum switching conditions suggested by Elsby's data. After a study of Elsby's work was made and after reviewing the divergence angles commonly used in the diverging sections of fluid flow devices, it was decided that the design conditions were to be: Divergence angle (θ) equal to 10°; setback ratio (d/b) equal to 4 through 7; and a nozzle pressure ratio, that is the ratio of the total pressure in the nozzle stagnation chamber to the ambient pressure (P_o/P_a), that yielded primary flow Mach numbers in the low supersonic range. The basic geometric parameters of the nozzle are defined in Fig. 2.

Thrust vectoring phenomena and the geometry of the flow were observed with photographic and pressure sensing techniques. Schlieren and Interferometer optical systems were used for the photographic analysis while static pressures taken at specified points along the nozzle sidewall were used for the determination of attachment point and lateral thrust measurement.

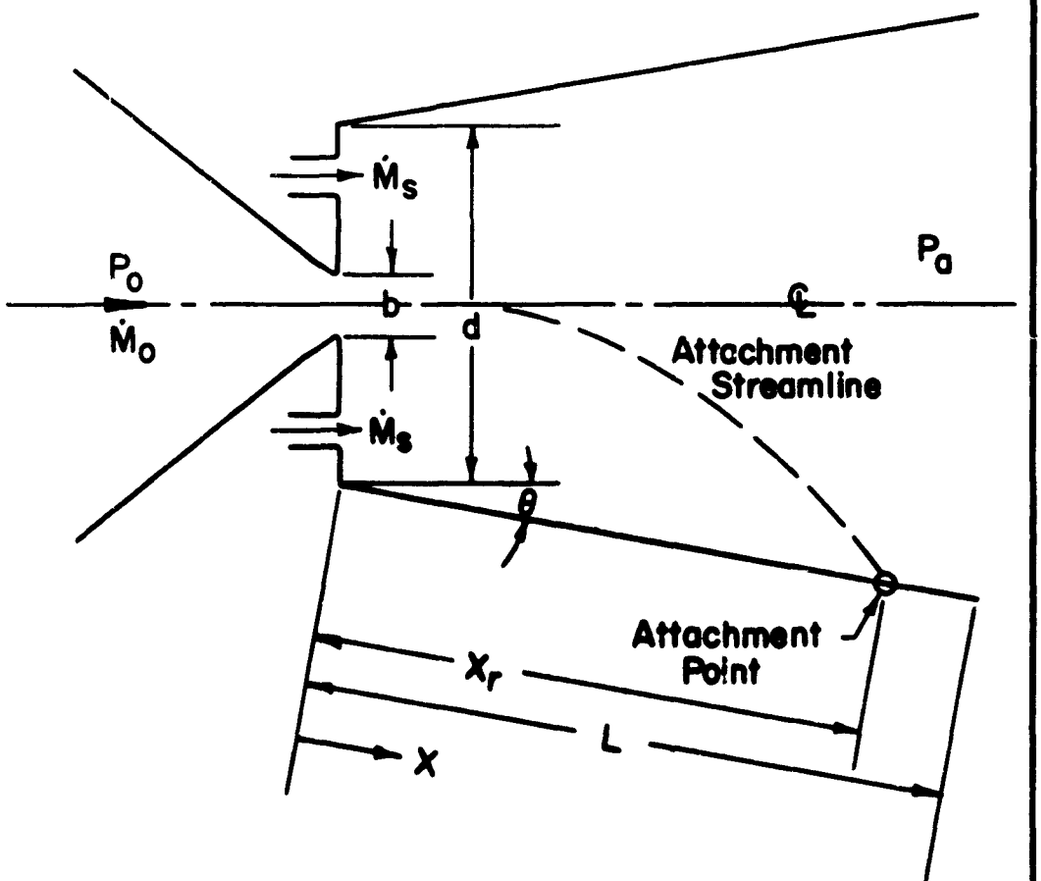

Fig. 2

Basic Coanda Nozzle Parameters

II. Apparatus

Design Considerations

The Coanda-Effect Nozzle used in this study was a modification of the nozzle used by Kisby (Ref 9). The main modification to the nozzle consisted of the design of a pair of parallel injectors in accordance with criteria recommended by Barrère' (Ref 4:383), and installation of these injectors into the diverging section of the nozzle. One wall of the diverging section of the nozzle was also modified to accommodate 14 instead of the 9 static pressure taps previously installed in it. During the modification, redesign, and manufacture, extreme care was taken to conserve the original dimensions of the nozzle. This was done so that a basis of comparison would exist between the results obtained with the parallel injector coanda-effect nozzle and those obtained with the nozzle used by Kisby. The applicable physical parameters of Kisby's nozzle are listed below for the convenience of the reader:

θ = 10^0

d/b = variable from 4 to 7

A_t = 0.125 sq. in.

L = 4.60 in.

Assembly and Sealing of Nozzle

The components of the coanda-effect nozzle, that is, the converging blocks and the sidewall blocks, were machined from ½ inch brass stock.

The circular base plate of the test section was machined from ½ inch aluminum stock and had a slot cut in its center. Two frames

were mounted on the base plate adjacent to the slot and parallel to the long side of the slot. These frames were held in position by Allenhead bolts inserted from beneath the base plate and into holes tapped in the bottom of the frames. Formica cement was placed between the base plate and the bottom of the frame to insure an air-tight seal. The converging blocks of the nozzle were then inserted between the walls formed by the frames and into the slot cut in the base plate. These blocks were held in position by four bolts which fitted through holes drilled in both the blocks and the frame. The horizontal surface of the convergent block had a keyway cut into it to accept a key-tab in the base of the diverging section of the nozzle, a threaded hole was also tapped in each block below the keyway so that the traversing assembly bolt could be accommodated.

In assembling the apparatus, a thin layer of formica cement was brushed into the keyway of the converging section and the diverging blocks were mated to it and positioned at a specific setback ratio (d/b). Now the sides of the converging and diverging blocks that would contact the glass walls of the test section were coated with a thin layer of formica cement. The glass walls with their aluminum supporting rings were then bolted to the two supporting frames and the cement was allowed to dry. When the formica cement was fully cured, a thin flexible film existed between the glass wall of the test section and the brass blocks, thus forming a leakproof gasket. The entire assembly was then attached to the settling chamber by bolts inserted through the holes drilled in the base plate and into the

tapped holes in the settling chamber cap. Figures 3 and 4 show the nozzle components in various stages of assembly.

Each wall of the converging section of the coanda nozzle had a 30° convergence angle and had an injector inserted in its horizontal surface at throat exit plane. These injectors were constructed so that the flow exiting from them would be parallel to the primary jet flow. The diverging walls had a divergence angle of 10°. There were 9 static pressure taps in one wall of the diverging section and 14 static pressure taps in the other wall of the diverging section. Stainless steel tubes were inserted in each of the 23 static pressure taps. These tubes were sealed and cemented in place with Epoxy resin. The detail drawing of the modified coanda-effect nozzle can be found in Appendix C.

Fluid Supply System

Dry, oil-free air was supplied by two electrically driven compressors. The larger compressor which provided air at a maximum line gauge pressure of 93 psi was used as a source of air for the primary flow. The secondary injection air was provided by a smaller compressor which supplied air at a maximum line pressure of 80 psi. Full flow regulation of both of the air supplies was obtained by diverting excess air to an exterior exhaust. This procedure provided a nearly steady mass flow rate for each experimental condition. The total pressure in the nozzle settling chamber was regulated by a set of hand operated valves connected in parallel upstream of the settling chamber. Secondary injection air was regulated with one quick-acting

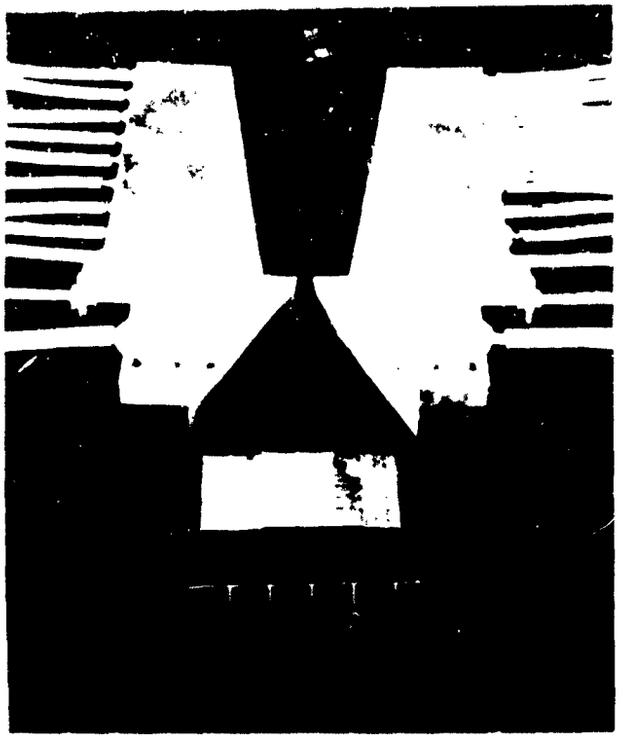

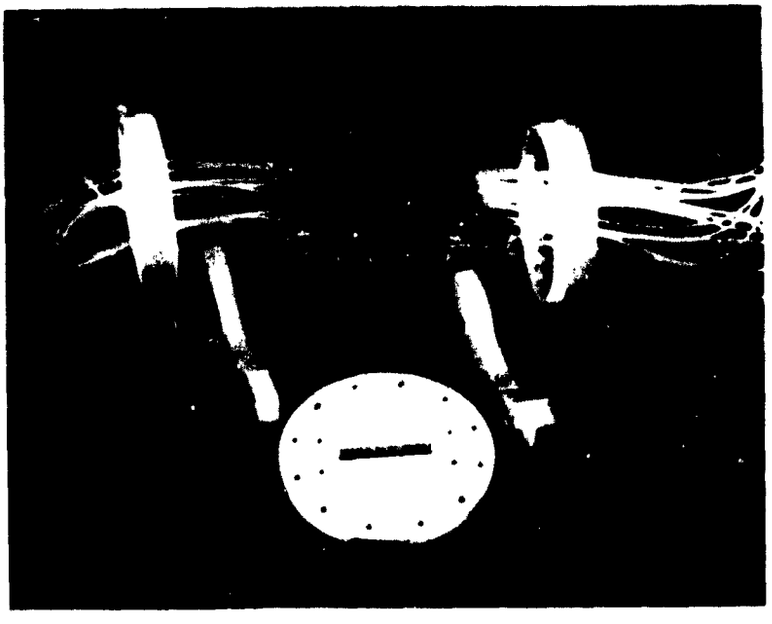

Fig. 3

Parallel Injector Ccanda Nozzle

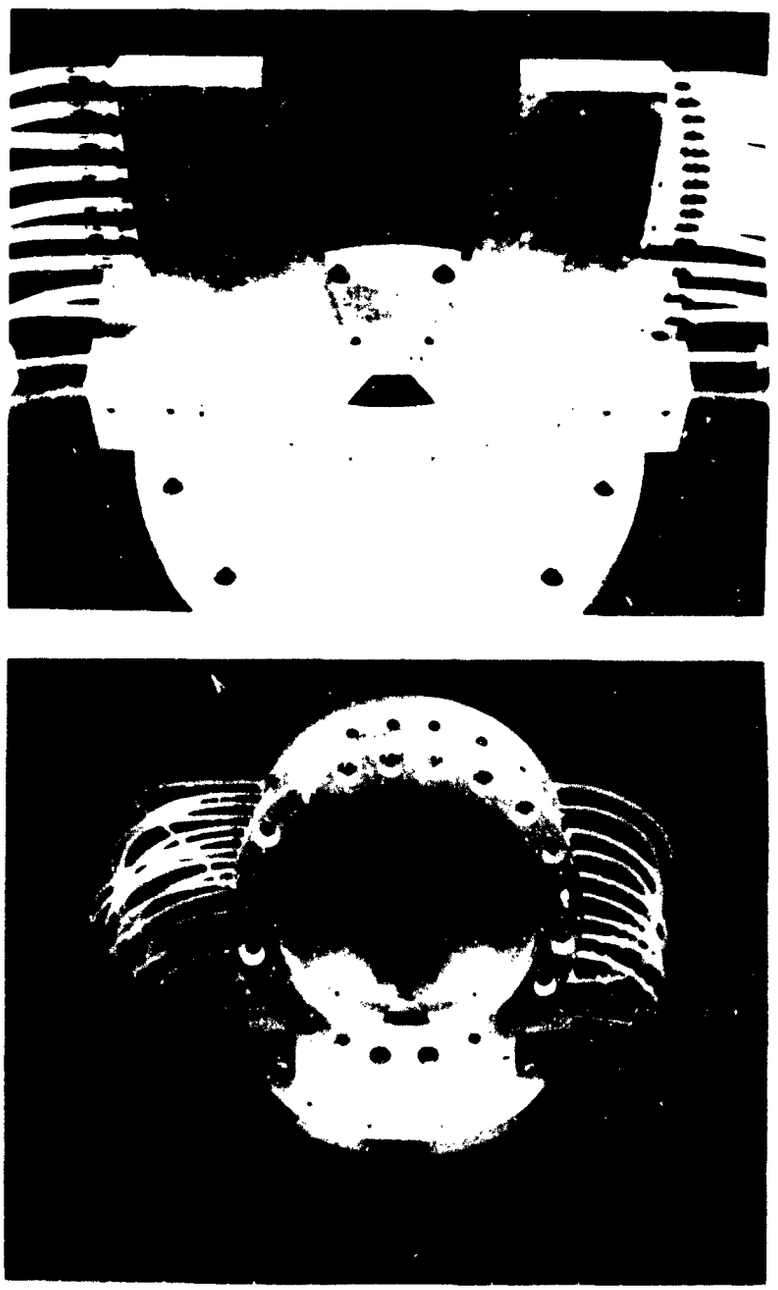

Fig. 4

Parallel Injector Coanda Nozzle

valve located upstream of two simple on-off flow valves. A schematic representation of the fluid supply system is shown in Fig. 5.

Instrumentation

The stagnation flow temperatures were measured using a potentiometer connected to copper-constantan thermocouples located in the flowmeter pipes upstream of the measuring device. The thermocouples were installed in accordance with ASME standards. The mass flow rates of both the primary and secondary air streams were determined by a method reported in the 1961 ASME Flowmeter Computation Handbook (Ref 1). A 1.05 inch diameter sharp-edged orifice with flange taps installed in a 2 inch diameter schedule-40 pipe was used to measure the flow rate of the primary air, while a .500 inch diameter sharp-edged orifice with flange taps installed in a 2 inch diameter schedule-40 pipe was used to measure secondary air flow rate. Both the flowmeters used in the test were installed in accordance with the standards listed in Ref 2.

The primary fluid pressure upstream of the orifice was measured with a 0 to 200 inch mercury dial manometer graduated in 1 inch increments. The secondary fluid pressure upstream of the orifice was measured with a 0-100 psi gauge graduated in one psi increments. The pressure drop across both the primary flow orifice and the secondary flow orifice was measured with a 30 inch water filled U-tube manometer connected to flange taps. The nozzle stagnation pressure was measured with a 0-200 inch mercury dial manometer graduated in 1 inch increments. This manometer was connected to a static pressure port located in the wall of the settling chamber. The difference between

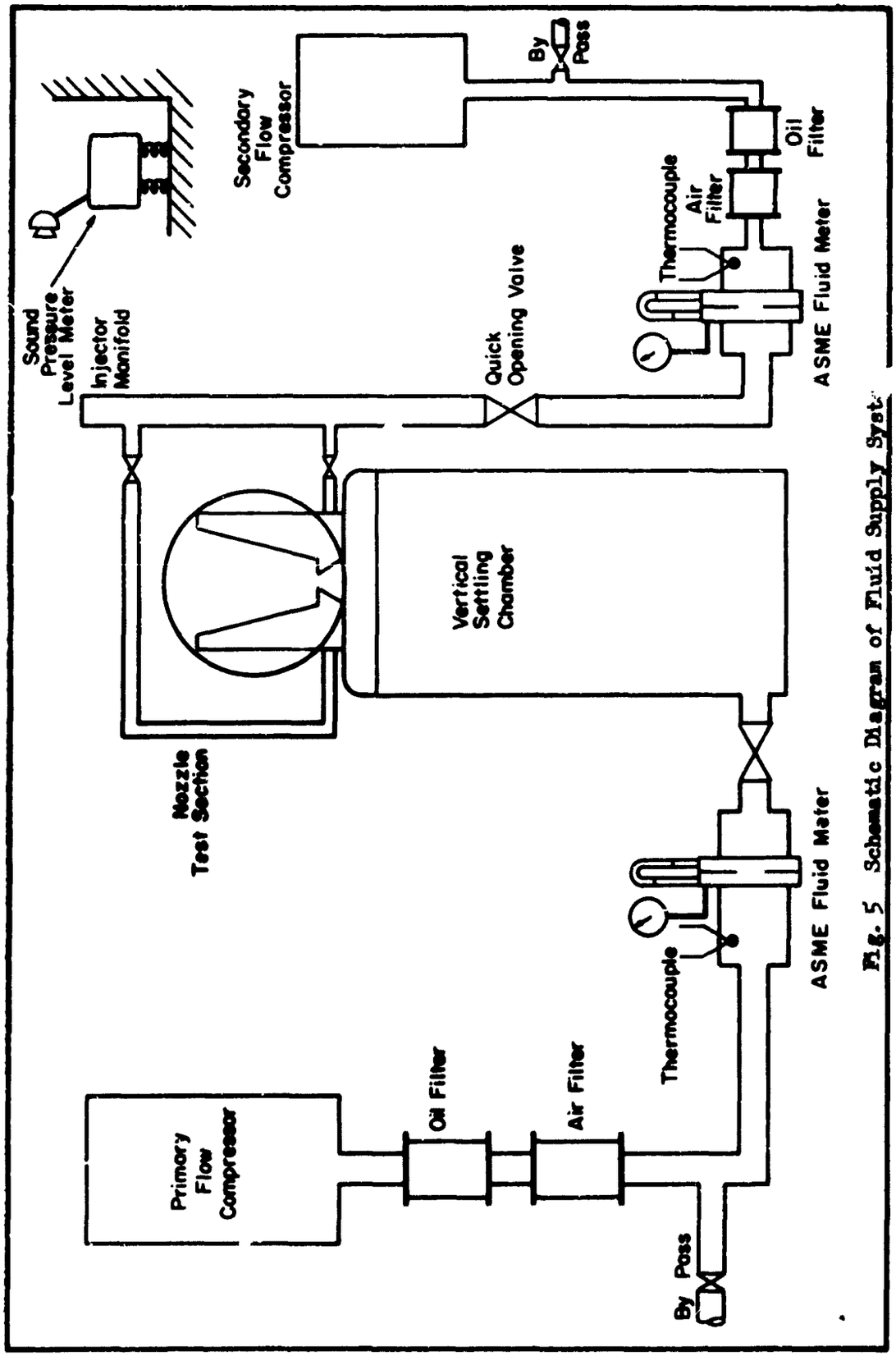

Fig. 5 Schematic Diagram of Fluid Supply Syst

the total and static pressure measured in the settling chamber was neglected because the area ratio of the settling chamber to the nozzle throat was more than 400 to 1. The static pressure on the diverging walls of the nozzle was measured using twenty-three, 30 inch, U-tube, mercury manometers. The static pressure taps were connected to the manometers through 3/32 inch stainless steel and ¼ inch plastic tubing.

Optical Equipment

A Mach-Zender type interferometer (Fig. 6) was used as the primary optical system for viewing thrust vectoring phenomena which occurred in the parallel injector coanda nozzle. A continuous source zirconium arc lamp with a wave length of approximately 5460 angstrom units was used as the light source for the interferometer. The reader is referred to Ref 15 for a complete description of this type of interferometer. The interferometer was converted to a schlieren optical system by inserting a piece of pasteboard in front of the combining splitter, so that the light not passing through the test section was completely blocked off, and inserting a knife edge at the focal point of the light beam ahead of the viewing point. Omission of the knife edge in the above procedure converted the interferometer into a shadowgraph device. The zirconium arc lamp was used as the light source for the schlieren and shadowgraph systems. Photographs were taken using a camera fitted with a Polaroid film holder. When using the interferometer as a schlieren or shadowgraph system half of the light was blocked off, and the shutter speed had to be changed.

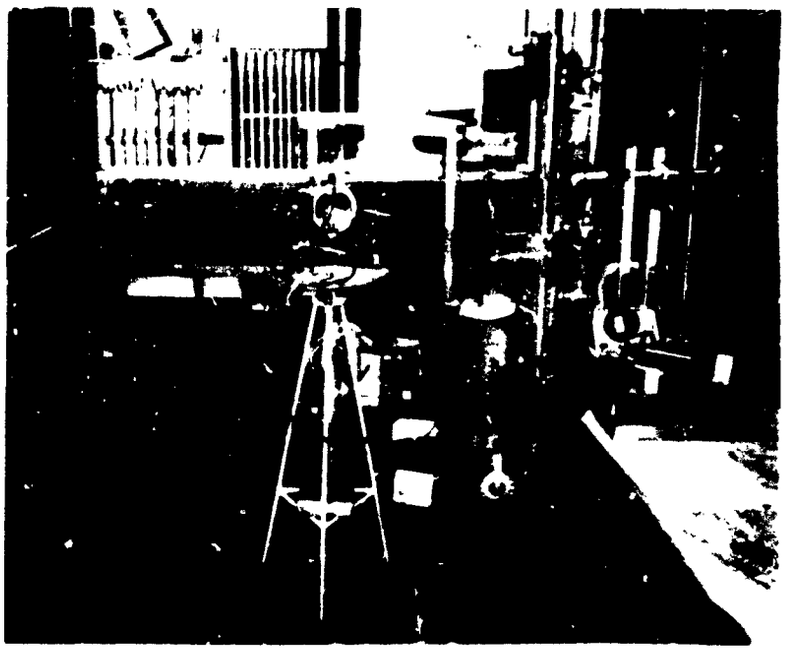

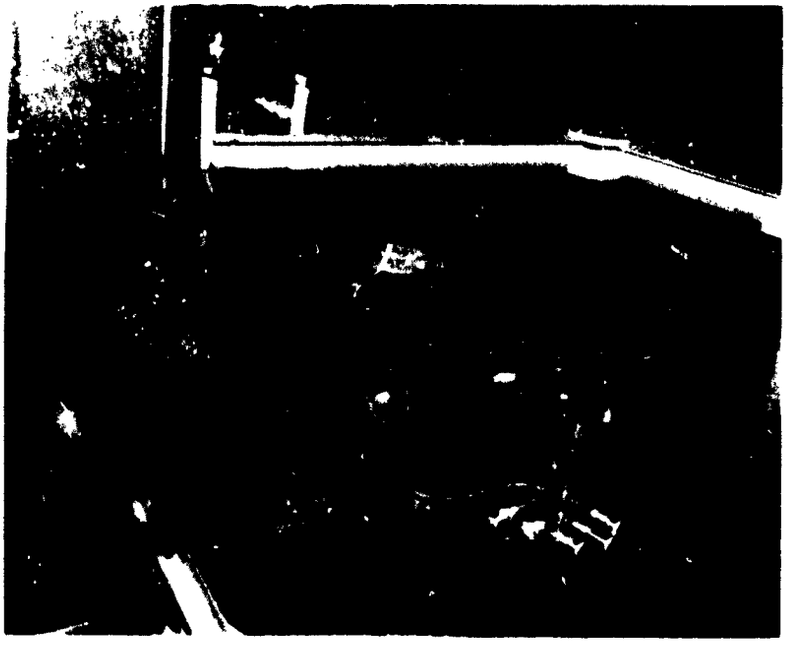

Fig. 6

Mach-Zender Interferometer

Polaroid type 47 film was used for both interferometer and schlieren photographs.

A fastax camera was used at 7,000, 4,000, and 1,000 frames per second to make high speed, interferometer, schlieren, and shadowgraph films of the thrust vectoring phenomena. A timing signal was placed on the film so that jet switching time of the main fluid stream could be measured. The film used in the fastax camera was Dupont 16 mm, 931A rapid reversal for black and white photography and Eastman-Kodak ERB 430 for the color photography.

Sound Recording Equipment

A General Radio type 1550-A Octave Band Noise Analyzer with a frequency range of 20 to 10,000 cps was used to record the change in noise level at the position indicated in Fig. 6. The noise analyzer is calibrated in decibels and yields noise data in eight distinct band widths which are 20 to 75 cps, 75 to 150 cps, 150 to 300 cps, 300 to 600 cps, 600 to 1200 cps, 1200 to 2400 cps, 2400 to 4800 cps, and 4800 to 10,000 cps. The analyzer can also be used to give an overall noise level in the band width 20 to 10,000 cps. A complete description of this equipment can be found in Ref 10. This equipment was incorporated into the test apparatus so that any noise reduction that occurred by using parallel injection of the secondary fluid could be sensed.

III. Experimental Procedure

General

Data runs were made on the parallel injector nozzle at setback ratios (d/b) of 4, 5, 6, and 7. The nozzle was operated at pressure ratios of 1.86, 2.20, 2.89 and 3.39 for a setback ratio of 4, at pressure ratios of 1.86, 2.20, 2.60 and 2.89 for a setback ratio of 5, at pressure ratios of 1.80, 1.86, 2.20 and 2.35 for a setback ratio of 6, and at pressure ratios of 1.63, 1.70, 1.87 and 1.91 for a setback ratio of 7. The criterion that established the maximum pressure ratio to be used at a specific setback ratio was the limit at which the secondary jet could cause switching of the primary fluid jet.

Typical Test Run

A typical test run was conducted in the following manner:

(1) Set up and seal nozzle at the desired setback ratio.

(2) Attach primary fluid jet to the desired nozzle sidewall.

(3) Establish nozzle pressure ratio (P_o/P_a).

(4) Record necessary data to measure $\dot{M}_o$ and T_o.

(5) Switch primary jet through use of parallel injection of the secondary fluid and record data to measure $\dot{M}_s$ and T_s.

(6) Cut off injection of secondary fluid and conduct the static pressure survey.

Test Procedure

The nozzle was set up and sealed in the desired geometrical configuration following the method given on Page 10 of this report.

Attachment of the jet to the desired sidewall was accomplished by injecting fluid from the secondary injector near the sidewall on which attachment was to occur and then opening valves to start the primary fluid flowing through the nozzle. This procedure caused the primary fluid to attach to the designated nozzle wall in all cases. The primary fluid jet was switched by injecting the secondary fluid on the side of the primary jet opposite to where the initial separation-bubble was formed. The mechanism that explains these phenomena is discussed in detail in the Results Section of this study.

Noise level and schlieren and interferometer photographs were obtained on subsequent data runs which immediately followed the static pressure survey run. The purpose of these runs was to record the change in noise level associated with the parallel injection of the secondary fluid and to record photographically the switching of the jet from one nozzle wall to the other. These additional runs also served as a check on the mass flow rate data and the temperature data obtained on the original test run.

After all the necessary data for a specific setback ratio was obtained, the nozzle assembly was dismantled from the settling chamber and soaked 18 to 24 hours in commercial grade acetone. This soaking was necessary to break the formica cement seal formed between the brass nozzle blocks and the glass test section walls. The nozzle was then taken apart, cleaned, reassembled, and sealed in the next setback ratio configuration.

The minimum secondary mass rate of flow required to switch the main jet from one nozzle sidewall to the other was obtained by opening the supply line to the secondary injector near the wall where

the primary jet was attached and then starting the secondary fluid compressor, thus allowing the pressure in the injector stagnation chamber to gradually build up. When the primary jet switched, the necessary data was recorded to determine the mass rate of flow of the secondary fluid. The gradual buildup technique gave consistent and repeatable data at the individual test conditions.

Since the jet switching encountered in this test occurred almost instantaneously, a high speed (7,000 frames per second), 16 millimeter film was made to record this phenomena. This film further documented the switching characteristics in the parallel injector coanda-effect nozzle and shows the switching phenomena using interferometer, schlieren, and shadowgraph optical techniques.

IV. Data Reduction Methods

Determination of Primary and Secondary Mass Flow Rates

The method used in this study for the calculation of both the primary and secondary fluid mass flow rates is given in the ASME Flowmeter Computation Handbook (Ref 1) published in 1961. This method is particularly useful in that the iterative procedure required by the older method (Ref 2) has been carried out for most commonly used flow pipe-orifice combinations and the iterative results are listed in the form of tables. The newer mass flow computation method simply requires knowledge of the flow-pipe diameter, the flow-pipe schedule number, the type of orifice being used and its diameter, the type of fluid being used, and the temperature of the fluid. Fluid mass flow rates are easily found since all of these quantities are usually known. The newer method also eliminates the use of costly computer time and special programs for quick computation of mass flow rates.

Determination of Jet Attachment Location

Crossley (Ref 7:120) and Sawyer (Ref 22:552) defined the jet attachment location as the point on the nozzle sidewall where the maximum static pressure occurred, but Olson (Ref 19:27) determined that the attachment point was upstream of this location. A. E. Mitchell (Ref 16:31), in a comment on Olson's article, concluded that the method for jet attachment location proposed by Sawyer et al, was in close agreement with Olson's work at the lower Mach numbers. The jet attachment point was taken as the point of maximum wall static pressure because only low Mach number flow was used in this study.

The attachment point, for the various setback ratios, was taken from pressure coefficient versus non-dimensional wall distance plots (Figs. 53, 54, 55, and 56).

Determination of Nozzle Thrust

A nozzle thrust comparison was made using theoretical axial thrusts and computing lateral forces from the pressures measured along the nozzle wall. The theoretical axial forces were the forces that the choked flow exiting from the throat and the secondary injector exerted on the nozzle. These forces were found from the isentropic thrust equation for a fluid exiting from a choked convergent nozzle (Ref 23:103). The equation used was:

$$F_0 = P_0 A_t \left[2\left(\frac{2}{k+1}\right)^{\frac{1}{k-1}} - \frac{P_a}{P_0}\right]$$

where the appropriate throat area and stagnation pressure were used to yield the forces exerted by the primary and secondary flow, respectively, on the nozzle. The lateral forces acting on the nozzle were determined by a mechanical integration of the static pressure versus distance curve obtained from measurements made on the diverging walls of the nozzle. The curve was extrapolated to the nozzle throat so that a pressure could be determined between the throat of the nozzle and the first static pressure tap. This integration yielded a resultant force acting perpendicular to the nozzle sidewalls. The addition of the axial component of the resultant force to the two analytically determined forces was defined to be the thrust of the nozzle. The component of the resultant force that was normal to the nozzle centerline was defined to be the lateral thrust of the nozzle.

The effects of friction, lateral momentum, and the pressure acting on the area between the nozzle throat and the setback nozzle walls were ignored in the thrust analysis.

Determination of Reynolds Number

The method used to determine the Reynolds number based on the width of the nozzle throat was the same as that used by Elsby (Ref 9:115). The derivation is presented for the convenience of the reader.

The Reynolds number, based on the nozzle throat width (b), is given by

$$Rey_b = \frac{\rho_t \ V_t \ b}{\mu_t}$$

but

$$V_t = \frac{\dot{M}_o}{\rho_t \ A_t}$$

and

$$\dot{M}_o = \frac{0.532 \ P_o \ b}{\sqrt{T_o}} \qquad \text{(Ref 23:85)}$$

therefore,

$$Rey_b = \frac{0.532 \ P_o \ b}{\mu_t \sqrt{T_o}}$$

Determination of Separation-Bubble Pressure

Separation-bubble pressure, that is the average pressure within the vortex, was experimentally determined from the interferometer

photographs taken during this study using a modification of the method described in Ref 15. The method used consists of first finding the density in the separated region by using the formula

$$\rho = \rho_1 - \left(\frac{\rho_0 \gamma_0}{n_0 - 1}\right) \frac{1}{L} E$$

and then using the perfect gas law ($P = \rho RT$) to yield the pressure in the separation-bubble. The temperature used was assumed to be the stagnation temperature of the main fluid stream.

V. Discussion and Results

Effects of Sealing on Switching Requirements

Six test runs were performed in the initial phase of the study to obtain data so that a comparison between the switching requirements of the sealed conventional (perpendicular secondary injector) coanda nozzle and Elsby's (partially sealed) conventional coanda nozzle could be made. The first two test runs were performed to indicate what effect nozzle leakage had on the total nozzle pressure ratio required to obtain the "full flow" limiting condition described by Elsby in Ref 9 as a flow condition where the main fluid stream spontaneously attaches to both nozzle walls. The runs were performed at a setback ratio of 4 and at total nozzle pressure ratios of 4.80 and 4.72 respectively. The results of these runs indicated that a 7½% reduction in pressure ratio was obtained using the sealed nozzle. The remaining four runs were designed to indicate what change in the secondary mass flow rate required for jet switching occurred by using the sealed nozzle. Two of these runs were conducted at a setback ratio (d/b) of 4 and a pressure ratio of approximately 2.70, the other two were conducted at a setback ratio (d/b) of 6 and a pressure ratio (P_o/P_a) of 3.06. The results of these runs showed that the use of the sealed nozzle reduced the secondary mass flow rate required for jet switching by 33% at a setback ratio of 4, and by 35% at a setback ratio of 6. A summary of these results is shown in Table I.

Switching Mechanism-Parallel Injector Coanda Nozzle

The switching mechanism for the parallel injector coanda nozzle is radically different from the conventional switching mechanism

TABLE I

Change in Flow Parameters Due to Nozzle Sealing: $\theta = 10°$

Run No.	1		2		3		4		5		6	
Type Nozzle	Sealed Nozzle	Elsby Nozzle	Sealed Nozzle	Elsby Nozzle	Sealed Nozzle	Elsby Nozzle	Sealed Nozzle	Elsby Nozzle	Sealed Nozzle	Elsby Nozzle	Sealed Nozzle	Elsby Nozzle
P_o/P_a	4.80	5.15	4.72	5.15	2.69	2.70	2.70	2.70	3.07	3.07	3.06	3.06
$\dot{M}_s/\dot{M}_o$					.112	.167	.113	.167	.0834	.125	.0834	.125
d/b	4	4	4	4	4	4	4	4	6	6	6	6
% Change in Mass Flow					33.4		32.6		33.6		33.6	
% Change in Pressure Ratio	6.8		8.4									
Phenomenon	Full Flow		Full Flow		Jet Switching		Jet Switching		Jet Switching		Jet Switching	

described by Bourque and Newman (Ref 5), Sawyer (Ref 22), Dodds (Ref 8), and others. A brief review of the conventional switching mechanism is repeated here for the convenience of the reader.

When a fluid jet with a turbulent boundary exits into an ambient fluid field which has an equal or lower viscosity, the turbulent boundary entrains fluid from the ambient field. If a wall is placed near the issuing jet, this entrainment is disrupted and eventually a low pressure region is formed between the jet and the wall. The low pressure region causes the jet to deflect and attach to the wall. At this time a vortex is formed between the jet and the wall and the fluid stays attached to the wall. This phenomena is called the coanda effect. Now the conventional method for switching this fluid jet from the attached wall is to introduce a secondary fluid jet into the vortex (separation region) at right angles to the jet. This has two effects, it destroys the low pressure region and vortex, and it produces a momentum deflection of the primary jet. Both of these effects cause the jet to move away from the attaching wall. Once the jet is detached from the wall it is moved, say in the vicinity of another wall, by a force which results from the momentum transfer between the main fluid jet and the secondary fluid jet. Since the main jet is now in the vicinity of another wall, the coanda effect described above takes over and the jet attaches to the other wall. The above sequence is illustrated in Figs. 9 and 10, pages 52 and 53.

In the case of the parallel injector coanda nozzle, the jet switching sequence (Fig. 7) starts when a secondary fluid flow that is parallel to the main stream is initiated on the side of the main

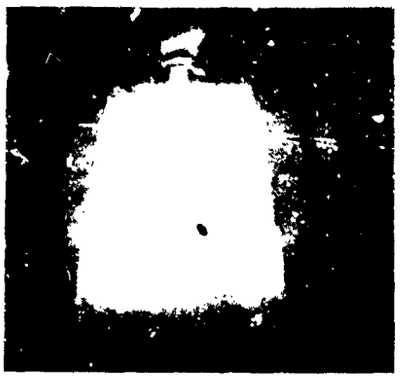

1

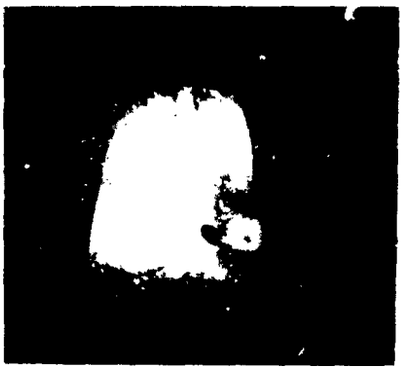

2

3

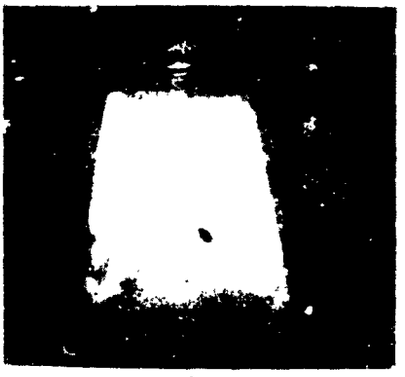

4

5

Sequence - Right to Left, 1 through 5

Fig. 7

Thrust Vectoring Sequence: Interferometer, d/b = 6, P_o/P_a = 1.87

fluid jet opposite to the side facing the attached wall. The secondary jet does not attach to the nozzle wall nearest it because although the pressure in the area between the secondary jet and the wall is decreased by the entrainment of fluid from the region by the jet, this decrease is small because the area from which the entrained fluid is taken is large with respect to the jet, and because the secondary jet is three-dimensional. Consequently, only a slight difference in pressure exists across the boundaries of the high energy secondary jet, $(P_o/P_a)_s = 5$ to 7. The small pressure difference is not enough to cause the jet to move closer to the wall and therefore the jet remains parallel to the centerline of the nozzle. The secondary jet also entrains fluid from the quasi-ambient region between it and the primary fluid jet. The entrainment by both the primary and secondary jet rapidly reduces the pressure in the region between the two jets to a level that is lower than the pressure existing between the main jet and the attaching wall. A pressure differential now exists across the boundaries of the main fluid jet and the main jet moves towards the secondary jet. This movement causes the attachment point of the main jet to move downstream along the nozzle wall until it detaches from the wall, destroying the vortex that formerly existed between it and the wall. As the main jet passes through the centerline of the nozzle, it comes under the influence of a strong vortex system which has been formed between the secondary jet and the nozzle wall nearest it. This vortex is caused by the entrainment of the fluid in the region between the wall and the turbulent boundary of the secondary jet, and by the circulation induced by the secondary jet itself in this region. The vortex "attracts" the main jet and causes it to

attach to the wall. Upon attachment, a portion of the fluid flows back into the vortex and a stable "coanda-effect" situation is established (see Fig. 12). The secondary jet can now be discontinued, setting up pure coanda-effect flow, and the primary jet remains attached to the nozzle sidewall.

The above mentioned pressure differential that exists across the boundary of the main fluid jet implies that the pressure on the side of the fluid jet away from the attachment wall is lower than the pressure on the side of the jet facing the attachment wall. In order to explain this, a discussion of the relationship of velocity of a fluid stream on the entrainment of fluid from a region adjacent to the stream is in order. Kivnick (Ref 11) demonstrated that the amount of fluid entrained from the surroundings by a turbulent jet increases as the velocity of the jet increased. The secondary jet operated during the test at a pressure ratio that was approximately three times greater than the pressure ratio of the primary fluid jet, and therefore had a higher velocity than the primary fluid jet. The surface area, based on ½ the circumference, of the secondary jet was larger than the surface area of the primary jet and since the velocity of the secondary jet was greater than the velocity of the primary jet, the entrainment of the secondary jet was greater than the entrainment of the primary jet. Now when parallel injection of the secondary flow is established in the nozzle, both the secondary jet and the primary jet are entraining fluid from the small region between the two jets at a rate that is greater than twice the rate that fluid is being entrained from the region between the primary jet and the wall. This causes the pressure on the surface of the primary jet facing away from the attachment

wall to decrease faster than the pressure on the surface facing the attachment wall and therefore, a pressure differential is created across the primary jet. The pressure differential causes the jet to detach from the attachment wall and switch to the opposite nozzle wall.

It was determined, from timing marks coded on a high speed (7000 frames/sec) film, that the jet switching time in a parallel injector nozzle was .001 seconds. This value agrees well with the jet switching times given in current literature. Schlieren and interferometer photographs showing the vectoring sequence for various setback ratio configurations of the parallel injection coanda nozzle are shown in Figs. 11 through 34.

Effect of Continued Injection into Separation-Bubble

During the test, when using the parallel injector coanda nozzle, it was noted that continued injection of secondary fluid into the separation region formed between the wall of the nozzle and the primary jet caused a stronger vortex to form within the separation region (Fig. 30). The stronger vortex lowered the mean pressure within the separation-bubble and induced a greater pressure differential across the boundaries of the attaching jet. The effect of the increased pressure differential was to increase the curvature of the primary fluid jet, and move the jet attachment point upstream along the nozzle sidewall towards the nozzle throat. This is opposite to the behavior that Elsby reported in the study on perpendicular injection coanda-effect nozzles where it is stated that the continued injection of fluid into the separation-bubble, caused the jet curvature

to decrease and the jet attachment point to move downstream along the nozzle until jet detachment and switching occurred. Opfell also reported that the effect of secondary injection into the separation-bubble was to move the jet attachment point downstream along the nozzle wall to the exit. The movement of the attachment point upstream when secondary fluid is injected into the separation region is a distinguishing feature of the flow in a parallel injection coanda-effect nozzle.

Sidewall Attaching Phenomena

The separation-bubble approached a circular shape as the nozzle pressure ratio (P_o/P_a) was decreased in the parallel injector coanda-effect nozzle. The shape of the separation-bubble roughly resembled an ellipse at the higher nozzle pressure ratios. This can be seen by referring to Figs. 11 through 34. A similar effect was noted by Elsby in Ref 9. Another interesting feature of the attaching flow was a roughly triangular shaped separation region that was observed above the attachment point. This region, called the secondary separation region, was first noticed while viewing the high speed film taken at a nozzle setback ratio of 4 and can be seen in Fig. 7, sequence photograph 4. The high speed film also showed a weak vortex occupying this region which would suggest that a pressure lower than ambient existed in the region.

The static pressure survey that was performed did not indicate the presence of the low pressure region (see Fig. 54). This can be explained by noting that a true static pressure is not measured at any distance along the wall after the separation point, instead a pressure

that is composed of static and dynamic components is measured. The dynamic pressure component is brought about by the fluid that is flowing at an angle to the nozzle wall towards the nozzle exit. It is this component that covers up the presence of the second separated region and the weak vortex inside it. Analysis of the variation of the surface pressure coefficient (C_p) with non-dimensional wall distance (x/b), Figs. 53 through 56, does give an indication of the presence of the second separation region by the steep negative slope just downstream of the attachment point. The steep negative slope indicated a rapidly decreasing pressure, and it can be seen from Figs. 53 through 56 that the steepness of the slope, and therefore the pressure in the second separated flow region, decreased with increasing setback ratio (d/b). The presence of a second separated region was not reported by Elsby or Opfell; however Reeves and Lees (Ref 21) demonstrated its presence in supersonic separated and reattaching laminar flows.

The boundary layer buildup on the surface of the jet opposite the attaching wall is shown in Fig. 11. The rapidity of the buildup indicates that the boundary of the jet is indeed turbulent and that fluid is being entrained from the surroundings.

Sidewall Static Pressure Measurements

The results of the sidewall pressure analysis are shown in Figs. 53 through 56 and are presented as a variation of pressure coefficient (C_p) versus the non-dimensional wall distance x/b. It can be seen from these plots that at a specific setback ratio (d/b), the point of maximum static pressure varied by less than one nozzle width (b)

during the increase of pressure ratio (P_o/P_a). This contradicts the statements made by Elsby (Ref 9:23) et al, which indicate that the maximum static pressure point is moved downstream along the sidewall as the pressure ratio (P_o/P_a) is increased.

Figures 53 through 57 show that the effect of increasing the setback ratio was to move the maximum static pressure point downstream along the nozzle wall. This result agrees with statements made by Elsby, Opfell, and others. The pressure coefficient plots show that the separation-bubble pressure remained fairly constant at one setback ratio during the increases of the pressure ratio; this observation also agrees with Elsby's results (Ref 9:27).

During the test, a static pressure analysis of the wall opposite to the jet attachment wall was performed (Figs. 62 through 65). The results of this study showed that a pressure which was less than ambient and which increased with increasing pressure ratio, and decreased with decreasing setback ratio, acted along the wall. The distribution of this lower than ambient pressure was such that it started at zero at the nozzle throat, increased to its maximum value at a point 3 nozzle widths downstream of the throat, and then decreased until it equalled atmospheric pressure at the nozzle exit. The lower pressure resulted from the inability of the area surrounding the exiting primary jet to replace fluid entrained by the jet from that area. The roughly triangular distribution of the lower pressure can be explained as follows. As the primary jet exits the nozzle plane, the turbulent boundary layer starts to build up (Ref 3) and fluid begins to be entrained from its surroundings; this explains the initial increasing pressure distribution. Now as the jet proceeds downstream,

the jet spreads and velocity decreases, thus decreasing the primary jet entrainment from the surroundings. The decreased entrainment from the area surrounding the jet causes the pressure in the area to decrease and this continues until the jet exits the nozzle. The deflection of the primary jet towards the attachment wall also contributes to the decreasing pressure profile for as the fluid jet moves towards the attachment wall, the boundary of the jet opposite to the attachment wall can entrain fluid from a larger area, and thus contribute less and less to the pressure distribution.

Jet Attachment Location

Both Elsby and Opfell reported in their work that the jet attachment point moved downstream along the nozzle wall as pressure ratio or setback ratio was increased. Figure 57 shows that increasing setback ratio did indeed move the attachment point downstream from a non-dimensional distance (x/b) of 7 to 10; however, increasing the pressure ratio had relatively little effect on the movement of this point. In fact, the jet attachment point remained in a nearly fixed position for the variation in pressure ratios considered in this study.

Again a contradiction exists between geometrically similar conventional and parallel injector coanda-effect nozzles, this time in the area of the effect increasing nozzle pressure ratio has on the jet attachment location. The contradiction can be explained by noting that at a given setback and pressure ratio, the effect of leakage would be to increase the separation-bubble pressure to a value that is greater than the separation-bubble pressure without nozzle leakage. This increased pressure would cause the jet attachment point to be

located downstream of the attachment point obtained with a sealed nozzle.

The constant attachment point location with increasing nozzle pressure ratio as obtained with the parallel injector coanda-effect nozzle would be a desirable feature if the coanda nozzle was going to be used in a device where large changes in pressure ratio occurred.

Separation-Bubble Pressure

Mueller, in Ref 17, showed that an analytical method which was developed by Nash (Ref 18) for determination of the separation-bubble pressure in uniform supersonic flow over a two-dimensional backstep could be extended to the coanda nozzle case. He states that if the assumption made by Korst and Chapman (Ref 5) that the recompression of the attaching streamline up to the attachment point is isentropic can be accepted, then the separation-bubble pressure could be obtained by a trial and error solution of the expression,

$$\frac{P_r}{P_b} = N\left[\frac{P_a}{P_b} - 1\right] + 1$$

In this expression, P_r is the pressure measured on the nozzle wall at the attachment point, P_b is the separation-bubble static pressure, P_a is the static (ambient) pressure on the free boundary of the jet, and N is the recompression coefficient and is a function of the Reynolds number and Mach number before separation for a particular nozzle configuration. The initial Mach number in this study was calculated from the total nozzle pressure ratio and assuming isentropic flow.

Korst and Chapman stated that N = 1.0, while Nash (Ref 18), after showing that the criterion originally put forth by Korst and Chapman was not consistent with experimental data, suggested that N = .35.

Mueller suggests in his article that N = 2.0. An analysis of the separation-bubble pressure was made using the interferometer photographs obtained during this study to determine what value of N was suggested by the data. The result of this analysis is presented on a graph taken from Ref 17 in Fig. 8. As can be seen from this figure, the value obtained for N in this study was approximately .65 and lies between the values suggested by Korst and Chapman and Nash. It is considerably below the value put forth by Mueller.

Secondary Mass Flow Requirements for Thrust-Vectoring

Earlier in this report (see page 27), the extreme effects that leakage in the area of the separation-bubble had on the amount of secondary mass flow required to switch the jet were pointed out. For this reason and for others which are enumerated in the following paragraph, it is felt that the difference in the secondary mass flow requirements between the partially sealed nozzles of Elsby and Opfell and the sealed parallel injector coanda nozzle can not be entirely attributable to the change in secondary injection techniques.

At this point it is instructive to review the effect that increasing nozzle pressure ratio has on separation-bubble pressure. As the nozzle pressure ratio is increased, the velocity of the jet is increased, and the entrainment requirement on the attached boundary of the jet is increased. The increased entrainment required causes a decrease in the separation-bubble pressure, thus tending to "hold" the jet more firmly to the wall. It would seem then that an increased secondary mass flow requirement would be needed to switch the jet whichever method (i.e., parallel or perpendicular secondary injection)

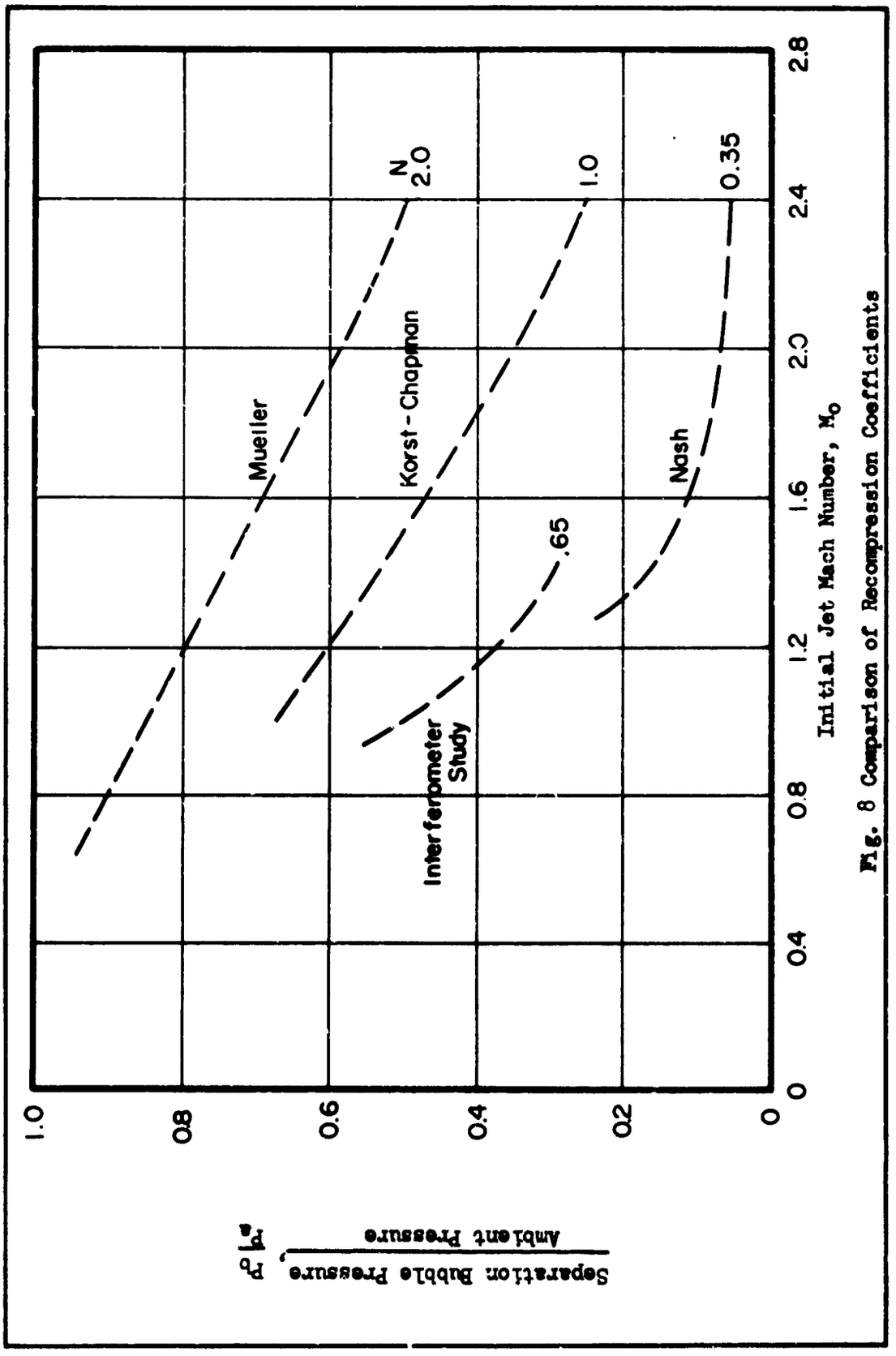

Fig. 8 Comparison of Recompression Coefficients

was used. The case of perpendicular secondary injection would especially indicate that an increased secondary mass flow would be required because more secondary fluid would be needed to destroy the lower bubble pressure, and because the momentum deflection of the primary jet would be less effective due to the increased momentum of the high velocity main stream. Investigation of Elsby's and Opfell's results in this area reveals that the secondary injection mass flow required decreased with increasing pressure ratio, contradicting the physical picture presented above and the results obtained in this study. It is felt that the nozzle leakage, listed as a source of experimental error by both Elsby and Opfell, caused this contradiction. The results obtained with the parallel injector nozzle, Fig. 58, indicate that jet switching during the operation of this nozzle required an increased secondary mass flow rate as the nozzle pressure ratio was increased. The secondary mass flow ratio ($\dot{M}_s/\dot{M}_o$) required to thrust vector the primary fluid in the nozzle varied from .8 to .18 as the setback ratio was changed from 4 to 7. Further examination of the results reveals that an optimum condition, that is one which required a minimum amount of secondary injection for jet switching at a given pressure ratio, occurred between a setback ratio of 4 and 5 for the nozzle used in this study.

Opfell (Ref 20:74) reported that the secondary mass flow ratio ($\dot{M}_s/\dot{M}_o$) required to thrust vector the primary fluid by "attraction" switching was 11.2 when switching was accomplished with his injection port number 2, and was 14.9 when injection port number 3 was utilized. The mass flow ratios given above were taken at a setback ratio of 4, and a total nozzle pressure ratio of 2. A comparison of the data

obtained in this study at a pressure ratio of 4 and a nozzle pressure ratio of 2 was made with the results reported by Opfell at these same conditions. The comparison showed that a 93% reduction in the mass flow ratio ($\dot{M}_s/\dot{M}_o$) was obtained when using the parallel injection nozzle to vector the primary fluid.

An additional comparison between the secondary mass flow required to thrust vector a fluid in a coanda nozzle was carried out between a sealed version of the perpendicular secondary injection coanda-effect nozzle used by Elsby, and the parallel secondary injection coanda-effect nozzle used in this study. The results of the comparison between the two geometrically similar nozzles are shown in Fig. 61. The figure shows that the mass flow requirements for thrust vectoring increased for both coanda nozzles as the pressure ratio increased, and indicates that for the comparison range, the parallel injector coanda nozzle mass flow requirements for thrust vectoring were approximately 11.7% lower than the sealed perpendicular injector coanda nozzle requirements. This comparison shows the advantage that parallel injection of the secondary fluid has over the perpendicular injection of the secondary fluid when using relatively large scale coanda-effect nozzles as thrust vectoring devices.

Lateral Thrust

The results of a lateral thrust analysis were not reported for $\theta = 10^{\circ}$ by Elsby (Ref 9); however, for this case, Opfell (Ref 20:37) reported lateral thrust ratios (F_s/F_o) that varied sinusoidally between 32 and 39%, for setback ratios of 4 through 7. The parallel flow coanda nozzle yielded values of lateral thrust ratio that

increased from 9.6 to 18.2%, and lateral thrusts that varied from .415 lbf to .755 lbf, as the setback ratio increased from 4 to 7. The results obtained with the parallel injector nozzle seem reasonable because the primary jet moves through a greater deflection angle as setback ratio is increased (Figs. 11 through 34). Opfell's sinusoidal variation cannot be explained.

The effect of increasing the pressure ratio, at a given setback ratio, was to decrease the lateral thrust ratio (Fig. 59). The explanation of this is found by recalling that as the nozzle pressure ratio is increased, the separation-bubble pressure is decreased, causing a decrease in the pressure acting over the length of the attached wall and thus decreasing the lateral thrust. The variation of lateral thrust efficiency ratio $\left(\frac{F_s/F_o}{M_s/M_o}\right)$ with pressure ratio (P_o/P_a) is plotted in Fig. 60 and shows that for supersonic flow of the primary fluid, as the pressure ratio increases, the lateral thrust efficiency ratio decreases. A comparison between the data obtained with the nozzle used in this study ($\theta = 10^o$) and the results given in Refs 9 and 20 could not be accomplished because Elsby (Ref 9) only presented the thrust efficiency plot for $\theta = 20^o$ and 30^o respectively, and Opfell (Ref 20) did not present a plot of this nature.

Expanded Flow

At high pressure ratios (above 3.70) and setback ratios of 4 and 5, the spontaneous jet expansion noted by Elsby (Ref 9:20) occurred. The jet expansion was characterized by the attachment of the issuing jet to both nozzle walls (Figs. 35 and 36). Reduced pressure in the regions between the attached jet boundaries and the base of the nozzle

is shown in Fig. 36 and is indicated by the rapid expansion of the secondary jets issuing into this region, illustrated in Fig. 35. The effect of injection into this region was to move the boundaries of the jet closer together, decreasing the nozzle divergence angle θ. This is illustrated by Fig. 35.

Another effect that parallel secondary injection had on the expanded flow pattern was to move the primary flow thrust vector through an angle of 7 degrees, toward the side of the nozzle from which the secondary injection was issuing. The above two effects, that is, the moving of the boundaries downstream due to the satisfying of the primary jet entrainment requirements by the secondary flow and the movement of the thrust vector by injection of the secondary flow, would suggest the use of the parallel injection coanda nozzle as a steerable propulsive device in the high supersonic range where propulsive systems are commonly used. The secondary injection of fluid parallel to the supersonic main stream would also increase the thrust of the coanda-nozzle. The explanation of thrust increases in parallel flowing streams is given by Luts in Ref 14.

Noise Reduction Due to Secondary Injection

Lighthill (Ref 13) states that noise is radiated sound which represents energy extracted from the jet and propogated away through the atmosphere. The noise can be induced by fluctuating vortex movements or by the motion found in the turbulent boundary layers which are formed during high Reynolds number flow of fluid jets. It was pointed out by Lighthill that the main source of noise is the turbulent jet boundary layer and that the intensity of the noise is a

function of the root-mean-square (rms) velocity of this layer. Lighthill concluded that the only successful methods for reduction of jet noise would be those that decreased the rms turbulent velocity. This reduction, he suggested, could be done by either reducing the jet velocity (undesirable for propulsion applications), or diminishing the relative velocity of the jet and the air adjacent to it. The parallel injector nozzle used in this study falls into the latter category, and during the test a reduction in the noise level at a point (shown in Fig. 6) was noticed. The overall noise reduction in peak sound at this point is shown in Figs. 37 through 51 and varied from 1 to 11 decibels (db). This reduction is significant because a 10 db reduction in overall peak sound is the maximum reduction obtainable with present day flightweight, noise reduction devices, and this reduction is obtained during normal operation of the nozzle, inducing no performance loss and requiring no additional hardware. Additional significance in the noise reduction induced by the parallel injection of secondary fluid in a coanda-effect nozzle can be obtained by a further examination of Figs. 37 through 51 where it can be seen that the noise reduction takes place in the higher frequency ranges, that is above 1000 cps. The reduction of noise in these ranges greatly lessens the acoustic fatigue problems common to high mass rate of flow compressible fluid systems.

Limits of Jet Switching

During the test definite limits were reached beyond which the main jet could not be vectored. These limits were reflected in the maximum pressure ratio (P_o/P_a) used at a given setback ratio and were

P_o/P_a = 3.39 for d/b = 4, P_o/P_a = 2.89 for d/b = 5, P_o/P_a = 2.35 for d/b = 6, and P_o/P_a = 1.90 for d/b = 7. Fig. 58 shows that the limiting factor was the secondary mass flow rate. As can be seen from this graph, the secondary mass flow rate increases with increasing pressure ratio when the primary fluid flow is supersonic. Therefore, the maximum secondary mass rate of flow available limits the pressure ratio at which the primary jet will switch from one nozzle sidewall to the other. The reason for this behavior can be explained by noting that as the setback ratio (d/b) increases, the area from which the secondary jet entrains fluid increases and therefore the pressure drop in the area between the secondary jet and the nozzle sidewall decreases. Because the pressure drop in this region is decreased, less of a differential in pressure exists across the primary jet, and the main fluid jet has less of a tendency to move away from its attachment wall. It can be seen from this that increased entrainment, which requires increased pressure ratio and the associated increased secondary mass flow, is required to cause jet switching as the setback ratio is increased in the parallel injector coanda-effect nozzle.

Flow Bias Factors

Throughout the conduct of this study, it was assumed that the fluid in both the primary and secondary jet streams was dry, oil-free air. Examination of the Schlieren photographs presented in this report shows that droplets of water formed on the glass test section wall during the data runs. It was also noticed (using the interferometer system) that after each test run, a residue remained on the test section glass. The residue, believed to be formed by oil in the

air supply, was deposited so that after the attaching jet had been discontinued, its outline could be seen on the glass test section walls. This, of course, would bias the orientation of a new fluid jet exiting from the nozzle throat. The extent of the error induced by the two above factors could not be determined during this study.

VI. Conclusions

The following conclusions are based upon the results of this study:

1. The complete sealing of Elsby's coanda-effect nozzle decreased the secondary mass flow required for jet switching by 33% at a setback ratio (d/b) of 4, and by 34% at a setback ratio of 6.

2. The complete sealing of Elsby's coanda-effect nozzle decreased the pressure ratio required for jet switching by 7½% at a setback ratio (d/b) of 4, and a nozzle pressure ratio (P_o/P_a) of 4.76.

3. Thrust vectoring in a parallel secondary injection coanda nozzle is characterized by the deflection of the main jet towards the secondary jet. This is opposed to the thrust vectoring sequence encountered in perpendicular secondary injection coanda nozzles where the main jet is moved away from the secondary jet.

4. Continued injection into the attached flow separation-bubble does not cause jet detachment from the nozzle sidewall.

5. Secondary injection into the separation-bubble does not move the jet attachment point downstream along the nozzle sidewall.

6. Increasing nozzle setback ratio (d/b) moves the attachment point downstream along the nozzle sidewall.

7. The secondary injection flow required to cause thrust vectoring in a parallel injector coanda-effect nozzle increases with increasing nozzle setback ratio (d/b).

8. The secondary injection flow required to cause thrust vectoring in a parallel injection coanda-effect nozzle, increases with increasing nozzle pressure ratio when the primary nozzle flow is

supersonic.

9. The secondary injection flow required to cause thrust vectoring in a parallel injection coanda-effect nozzle was 11.7% less than the amount required by a geometrically similar sealed perpendicular injection coanda-effect nozzle.

10. The secondary injection flow required to cause thrust vectoring in a parallel injection coanda-effect nozzle was 93% less than the value reported by Opfell in Ref 9.

11. The lateral thrust ratio (F_s/F_o) increases with increasing setback ratio (d/b), and decreases with increasing pressure ratio (P_o/P_a).

12. The results of this study indicate that, for the conditions tested, the maximum lateral thrust for the minimum injection mass flow required to thrust vector a fluid through use of a parallel secondary injector coanda-effect nozzle, occurred between a setback ratio (d/b) of 4 and 5.

13. Noise level drops of from 1 to 11 decibels can be obtained by the secondary injection of fluid in a parallel secondary injector coanda-effect nozzle.

14. The jet switching time in a parallel injector coanda-effect nozzle is approximately .001 seconds.

15. The mean pressure in the separation-bubble in parallel injector coanda-effect nozzles can be found by using the formula $\frac{P_r}{P_b} = N\left[\frac{P_a}{P_b} - 1\right] + 1$, where N = 0.65.

VII. Recommendations

1. Construct a two-dimensional parallel secondary injector coanda-effect nozzle with variable mass flow rate secondary injectors so that an extension of the results presented in this study into high Mach number regions could be made, and so a matching of the entrainment requirements on the boundary of the main jet could be made.

2. Perform an investigation to analytically determine the value of the recompression coefficient N, and to further examine the flow in the secondary separation region reported in this study.

3. Utilize strain gauge instrumentation to measure lateral thrust of coanda nozzles.

Bibliography

1. A.S.M.E. Research Committee on Fluid Meters. Flowmeter Computation Handbook. New York: American Society of Mechanical Engineers, 1961.

2. A.S.M.E. Special Research Committee on Fluid Meters. Fluid Meters Their Theory and Application, Part I. New York: American Society of Mechanical Engineers, 1937.

3. Birkhoff, G. and E. H. Zaratonello. Jets, Wakes, and Cavities. New York: Academic Press, 1957.

4. Barrère, M. and others. Rocket Propulsion. New York: Elsevier Publishing Company, 1960.

5. Bourque, C. and B. G. Newman. "Reattachment of a Two-Dimensional Jet to an Adjacent Flat Plate". The Aeronautical Quarterly 11: 201-232 (August 1960).

6. Chapman, D. R. An Analysis of Base Pressure of Supersonic Velocities and Comparison with Experiments. TR No. 1051, Washington, D.C.: National Advisory Committee on Aeronautics, 1951.

7. Crossley, R. W. An Experimental Investigation of Pneumatic Jet-Type Amplifiers and Relays, Sc. D. Thesis, Massachusetts Institute of Technology: Cambridge, Massachusetts, September 1961.

8. Dodds, J. I. The Use of Suction or Blowing to Prevent Separation of a Turbulent Boundary Layer, Ph. D. Thesis, University of Cambridge; Cambridge, England, 1961.

9. Elsby, C. N. Jet Switching Phenomena in a Choked Flow Coanda-Effect Nozzle. Thesis, Air Force Institute of Technology: Wright-Patterson AFB, Ohio, August 1963.

10. General Radio Company. The Type 1550-A Octave Band Noise Analyzer. Cambridge, Massachusetts: General Radio Company, February 1955.

11. Kivnick, A. Mixing of Fluid Streams. M6-ORI-071(11), University of Illinois Experimental Station, September, 1953.

12. Korst, H., Chow, W., and G. W. Zumwalt. Research on Transonic and Supersonic Flow of a Real Fluid at Abrupt Increases in Cross Section. ME-TN-392-5, OSR-TR-60-72: University of Illinois, 1959.

13. Lighthill, M. J. "Jet Noise". American Institute of Aeronautics and Astronautics Journal, 1: 1507-1517 (July 1963).

14. Lutz, O. Gas Dynamic Mixing Processes. Thrust Increase by Jet Mixing. Translation, MOA-TIL-T5349, Ministry of Aviation, London, England, January 1964.

15. Massachusetts Institute of Technology. Aerodynamic Measurements, Chapter XII, Part I. Cambridge: Massachusetts Institute of Technology, 1952.

16. Mitchell, A. E. Reattachment of a Two-Dimensional Compressible Jet to An Adjacent Plate, Comment. New York: ASME, Symposium on Fluid Jet Control Devices, 1962.

17. Mueller, T. J. An Experimental Investigation of the Reattachment of Compressible Two-Dimensional Jets, A.S.M.E. paper 64-FE-18, New York: American Society of Mechanical Engineers, May 1964.

18. Nash, J. F. An Analysis of Two-Dimensional Turbulent Base Flow Including the Effect of the Approaching Boundary Layer, NPL Aeronautical Report 1036, 1963.

19. Olson, R. E. Reattachment of a Two-Dimensional Compressible Jet to an Adjacent Plate. New York: ASME, Symposium on Fluid Jet Control Devices, 1962.

20. Opfell, R. F. Jet Attachment Location and Switching Requirement in a Subsonic, Sonic Coanda Nozzle. Thesis, Air Force Institute of Technology: Wright-Patterson AFB, Ohio, August 1964.

21. Reeves, B. L. and Lees, L. "Supersonic Separated and Reattaching Laminar Flows: 1. General Theory and Application to Adiabatic Boundary Layer/Shock-Wave Interactions". American Institute of Aeronautics and Astronautics Journal, 2: 1907-1920 (November 1964).

22. Sawyer, R. A. "The Flow Due to a Two-Dimensional Jet Issuing Parallel to a Flat Plate". Journal of Fluid Mechanics, 9: 543-560 (December 1960).

23. Shapiro, A. H. The Dynamics and Thermodynamics of Compressible Fluid Flow, Volume I. New York: The Ronald Press Company, 1953.

Appendix A

Flow Photographs

The schlieren and interferometer photographs collected in this appendix were taken during the conduct of this study.

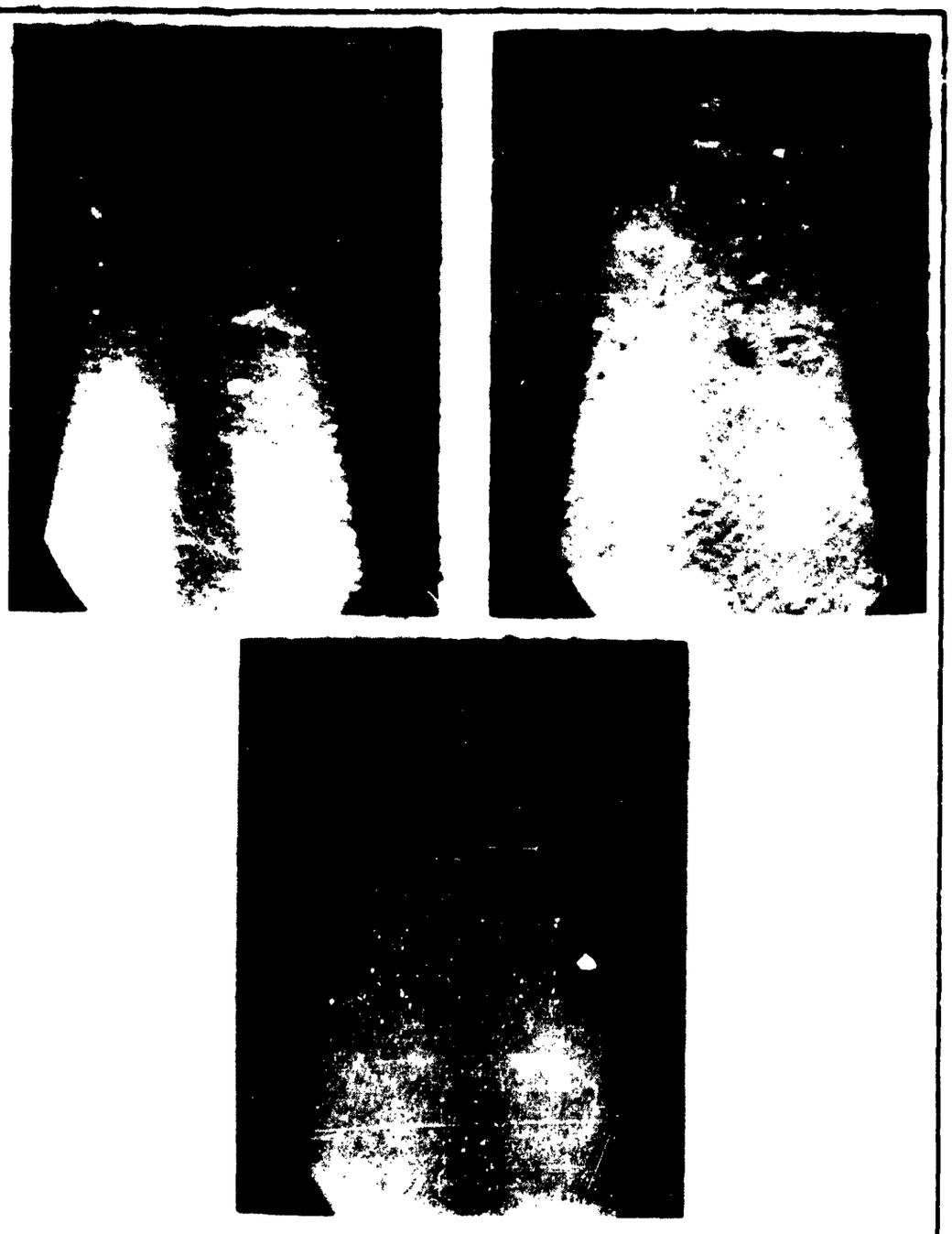

Perpendicular Injection Sequence - Right to Left

Fig. 9

Thrust Vectoring Sequence: Schlieren, d/b = 4, P_o/P_a = 3.20

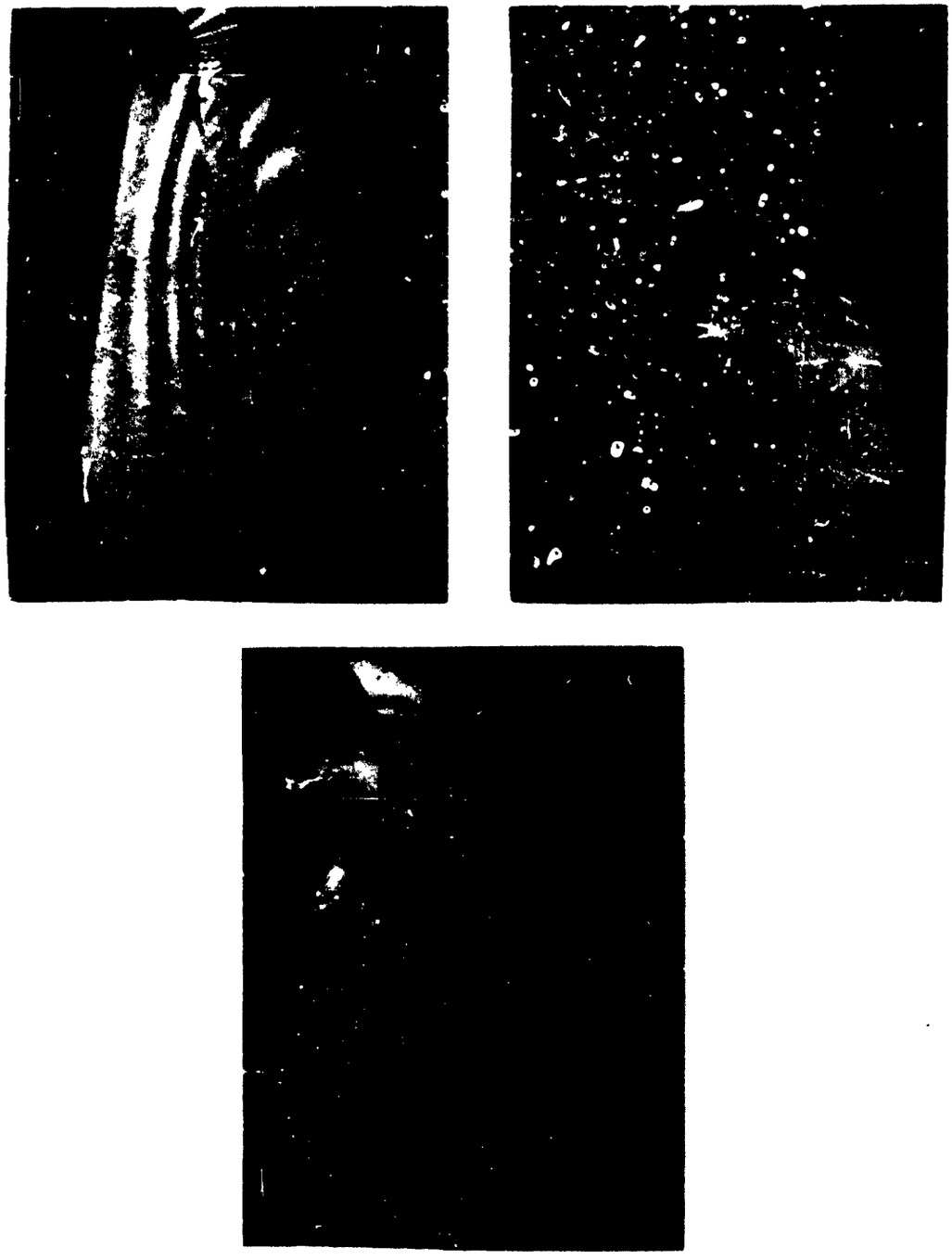

Perpendicular Injection Sequence - Right to Left

Fig. 10

Thrust Vectoring Sequence: Interferometer, d/b = 4, P_o/P_a = 3.20

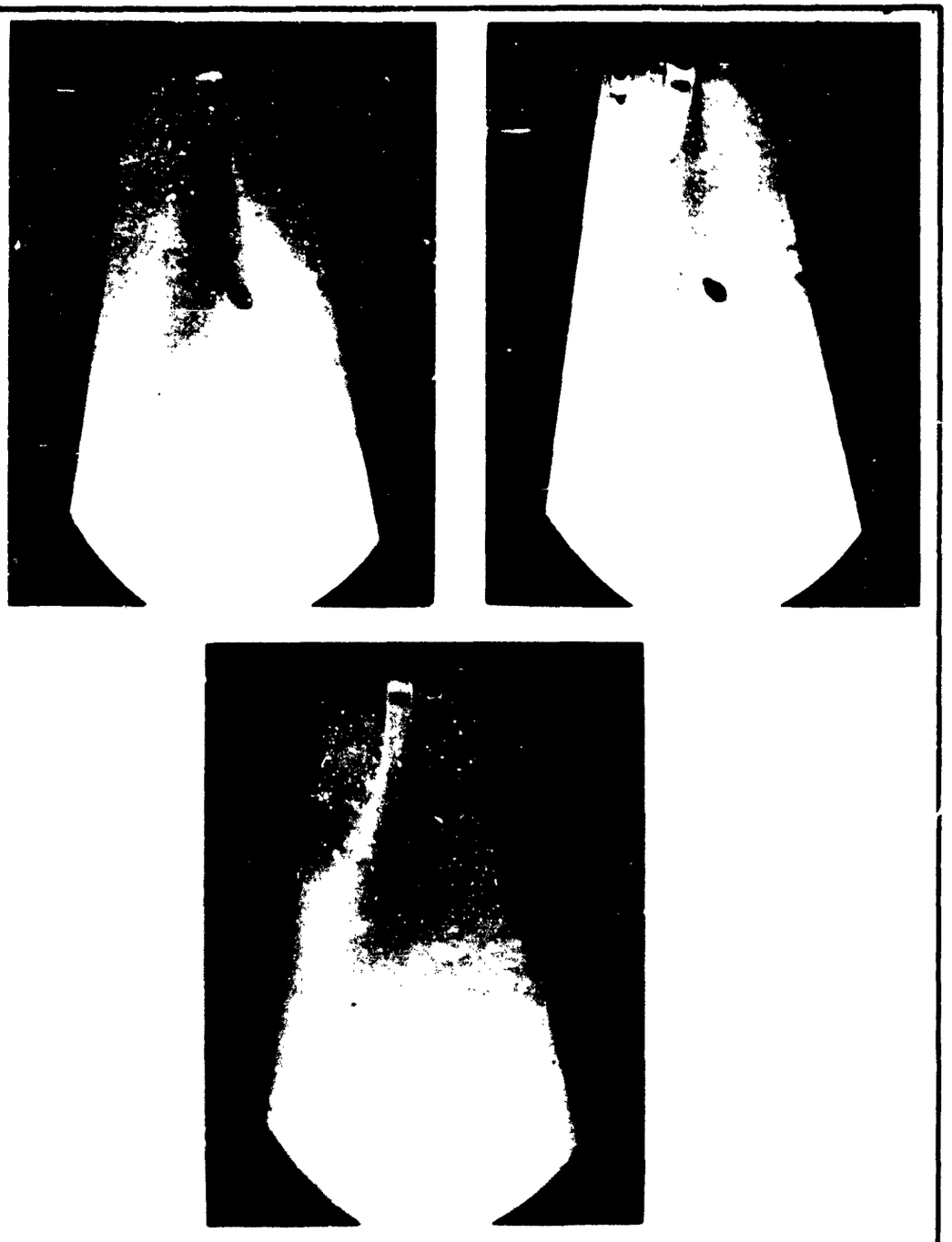

Parallel Injection Sequence - Right to Left

Fig. 11

Thrust Vectoring Sequence: Schlieren, d/b = 4; P_o/P_a = 1.86

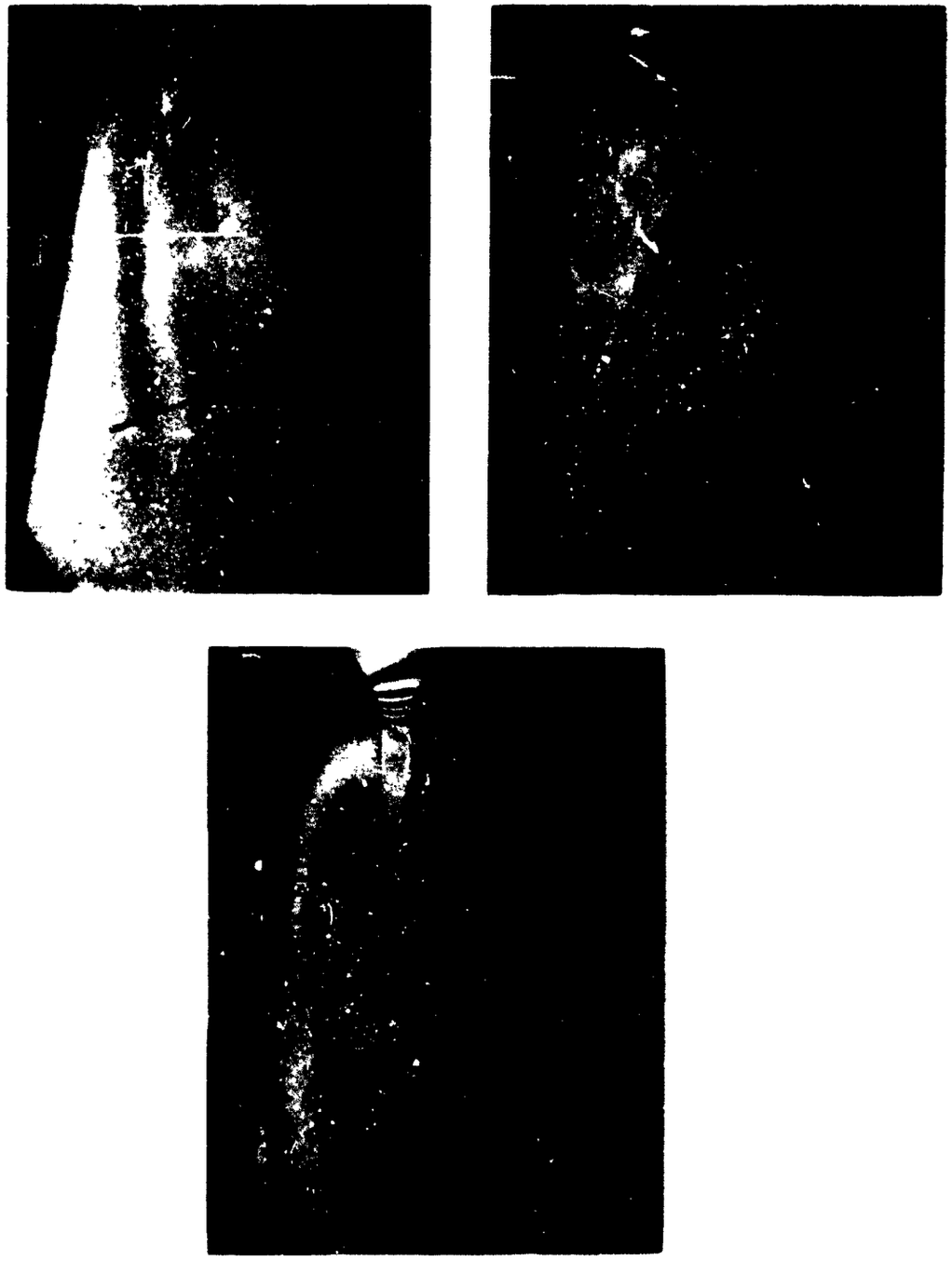

Parallel Injection Sequence - Right to Left

Fig. 12

Thrust Vectoring Sequence: Interferometer, d/b = 4; P_o/P_a =1.86

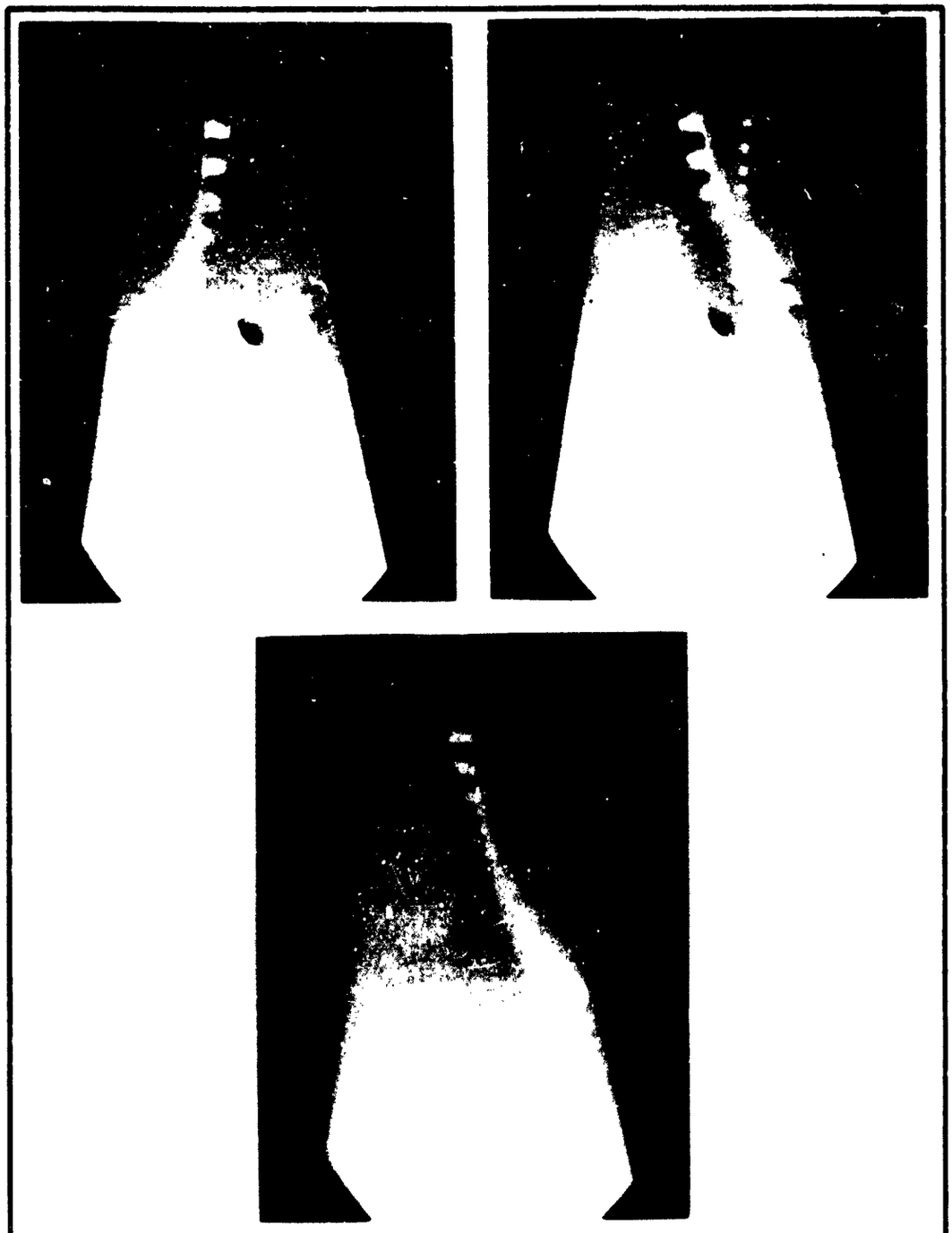

Parallel Injection Sequence - Left to Right

Fig. 13

Thrust Vectoring Sequence: Schlieren, d/b = 4; P_o/P_a = 2.89

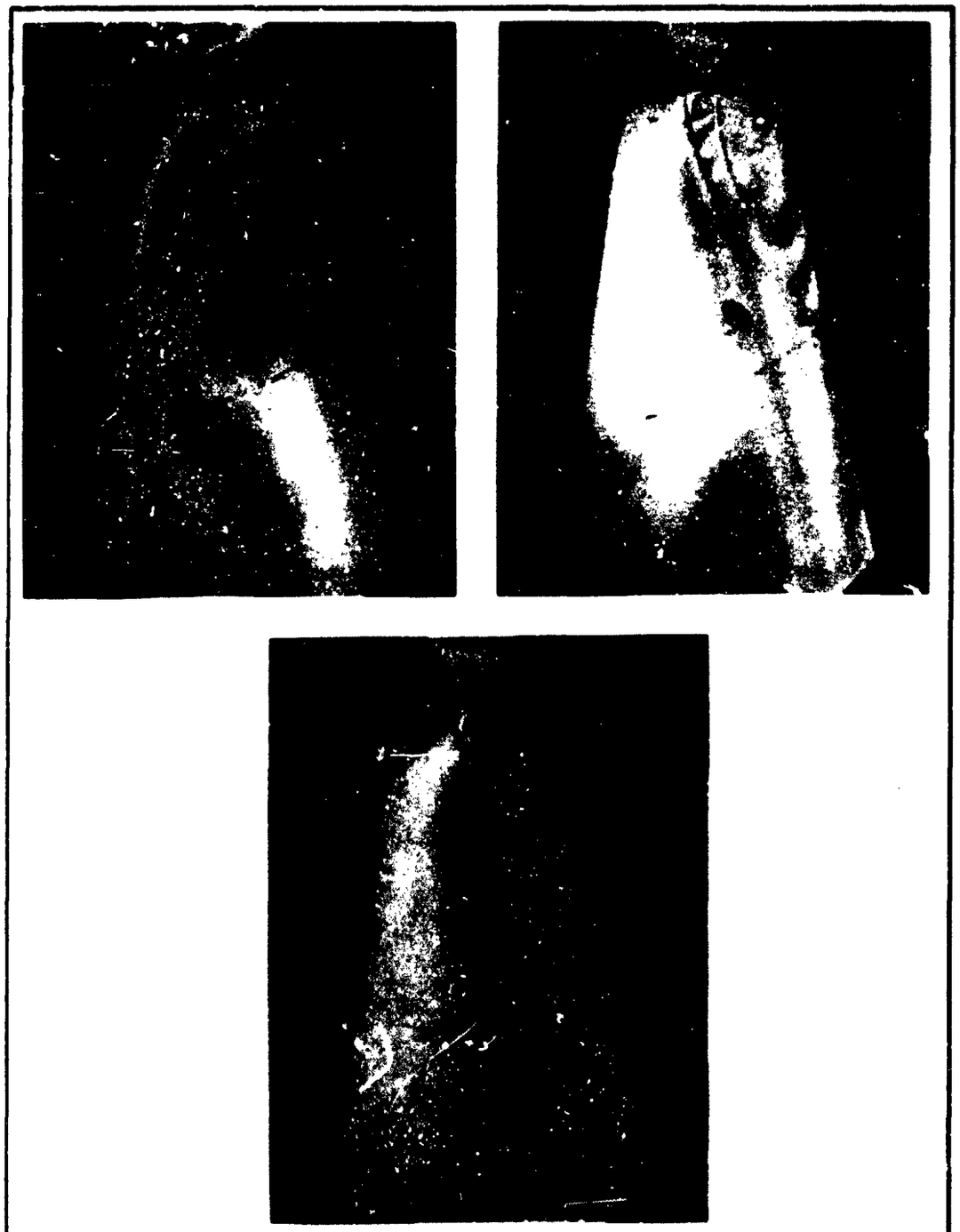

Parallel Injection Sequence - Left to Right

Fig. 14

Thrust Vectoring Sequence: Interferometer, d/b = 4; P_o/P_a = 2.89

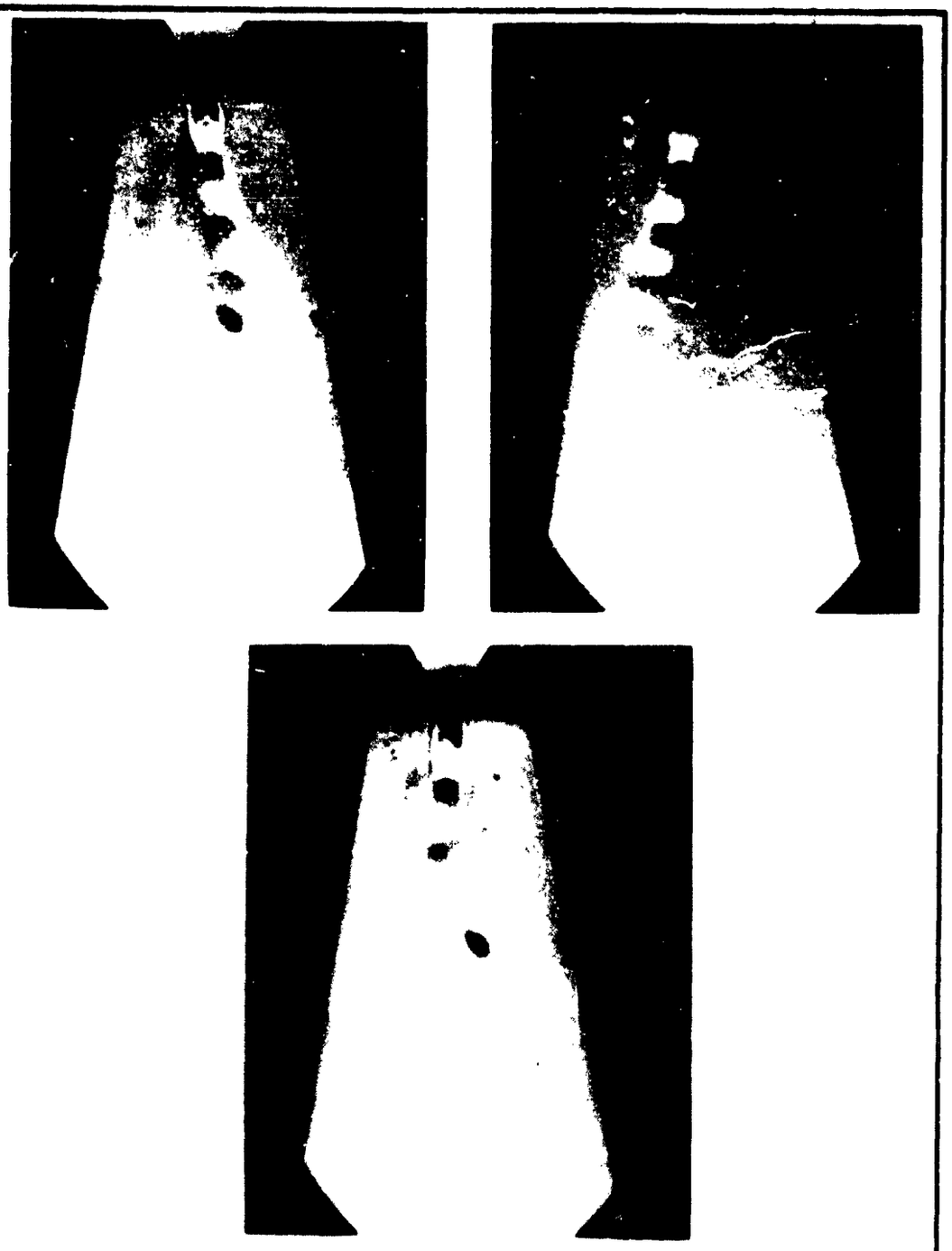

Parallel Injection Sequence - Right to Left

Fig. 15

Thrust Vectoring Sequence: Schlieren, d/b = 4; P_o/P_a = 3.39

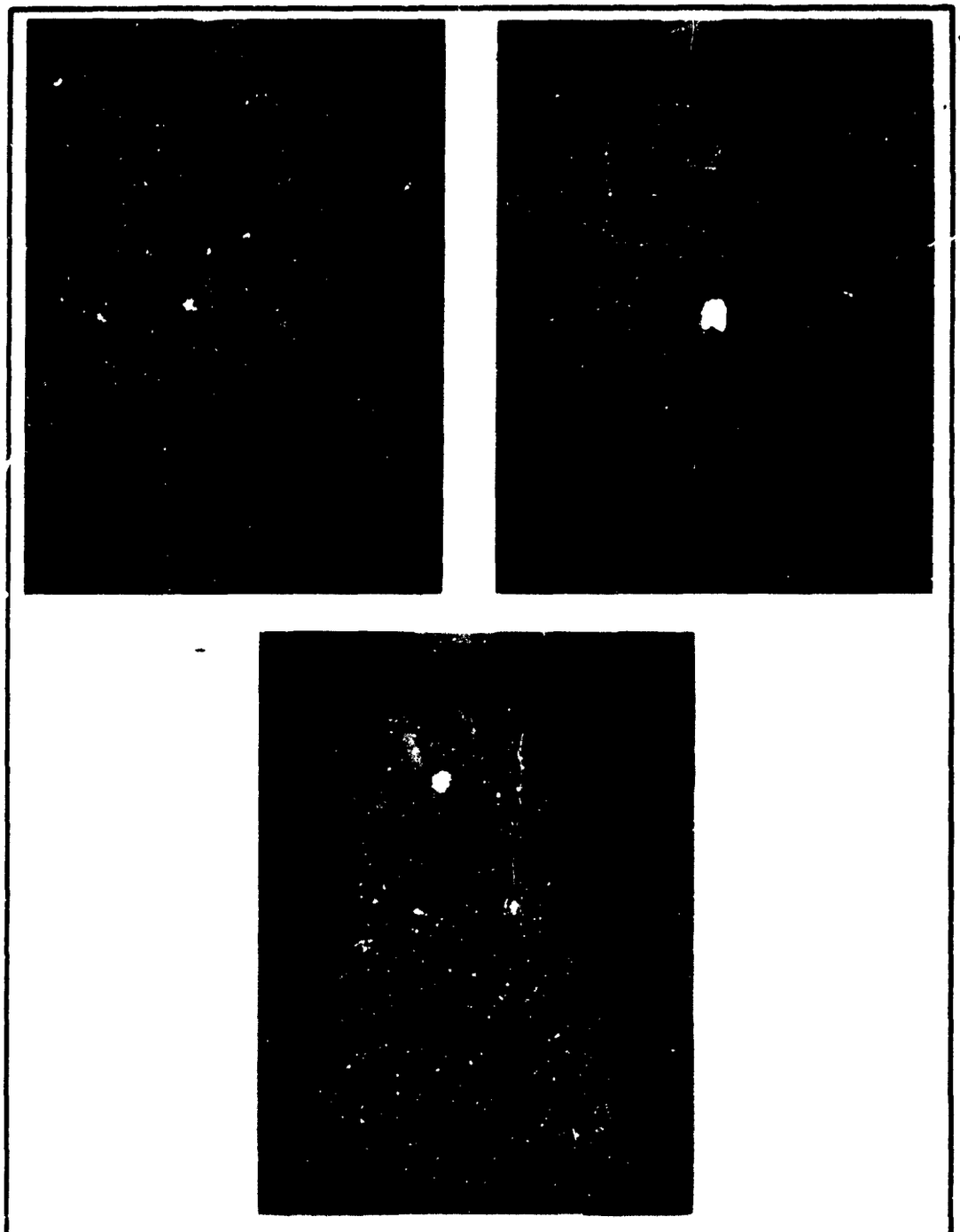

Parallel Injection Sequence - Right to Left

Fig. 16

Thrust Vectoring Sequence: Interferometer, d/b = 4; P_o/P_a = 3.39

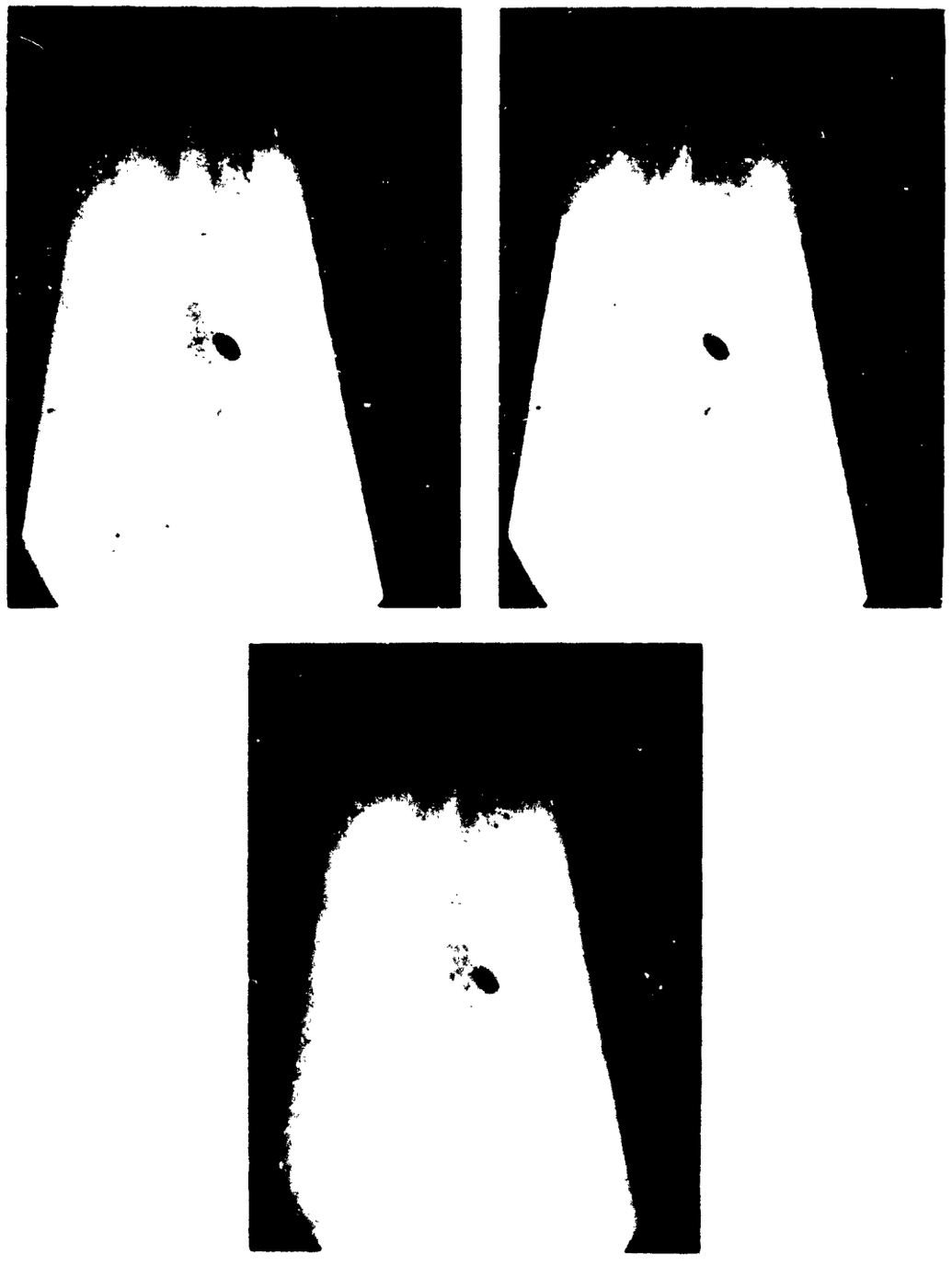

Parallel Injection Sequence - Right to Left

Fig. 17

Thrust Vectoring Sequence: Schlieren, d/b = 5; $P_o/P_a = 1.86$

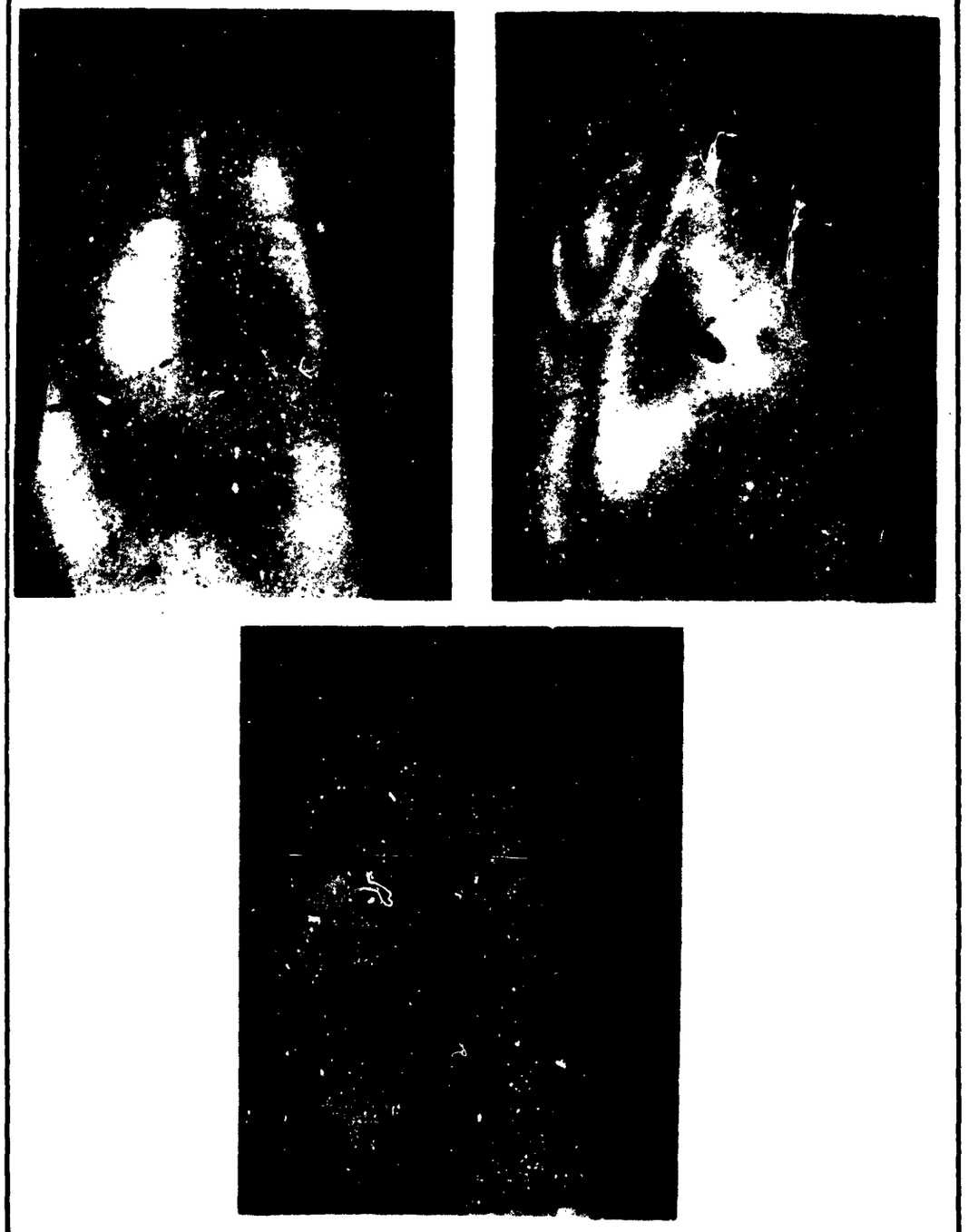

Parallel Injection Sequence - Right to Left

Fig. 18

Thrust Vectoring Sequence: Interferometer, d/b = 5; P_o/P_a = 1.86

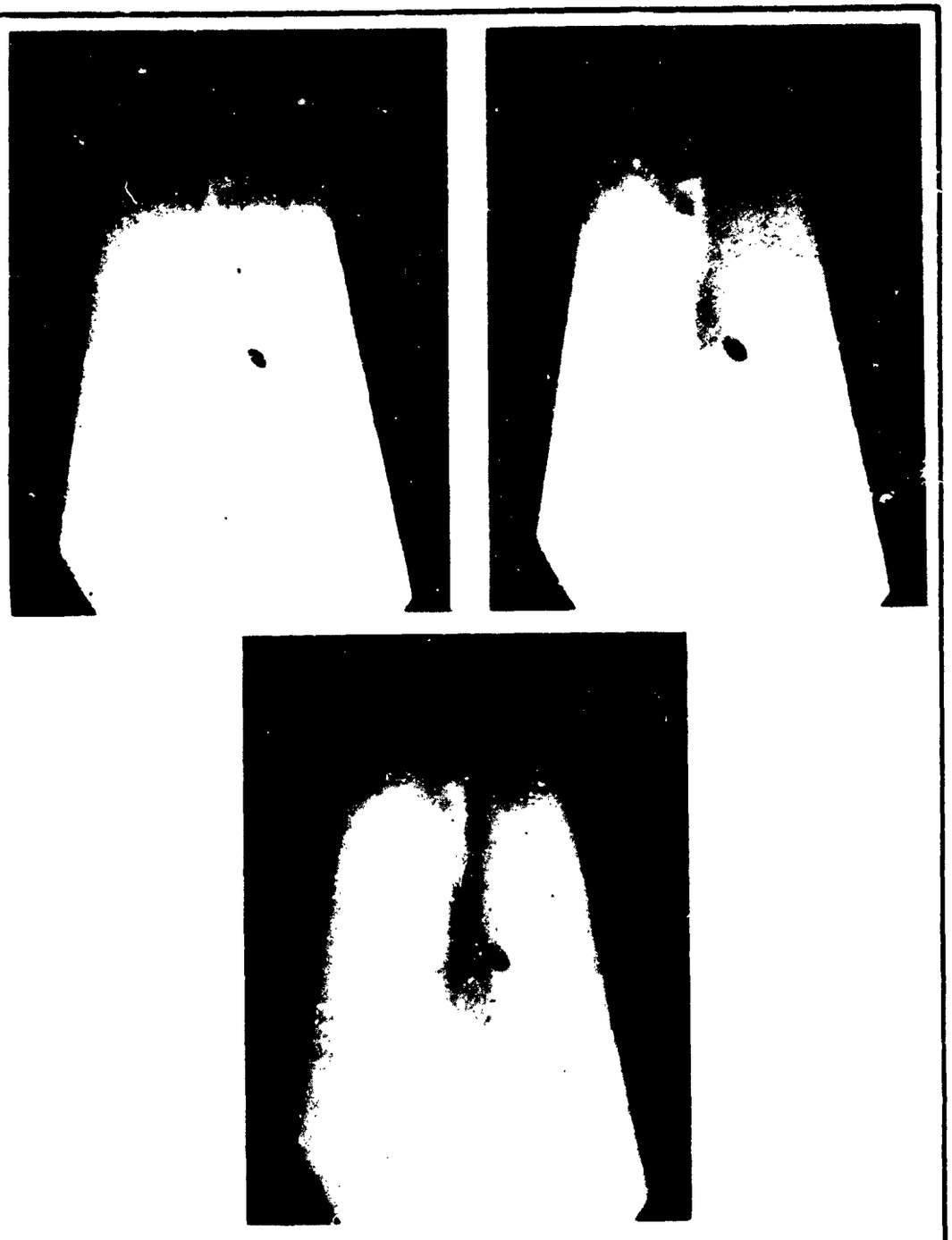

Parallel Injection Sequence - Right to Left

Fig. 19

Thrust Vectoring Sequence: Schlieren, d/b = 5; P_o/P_a = 2.20

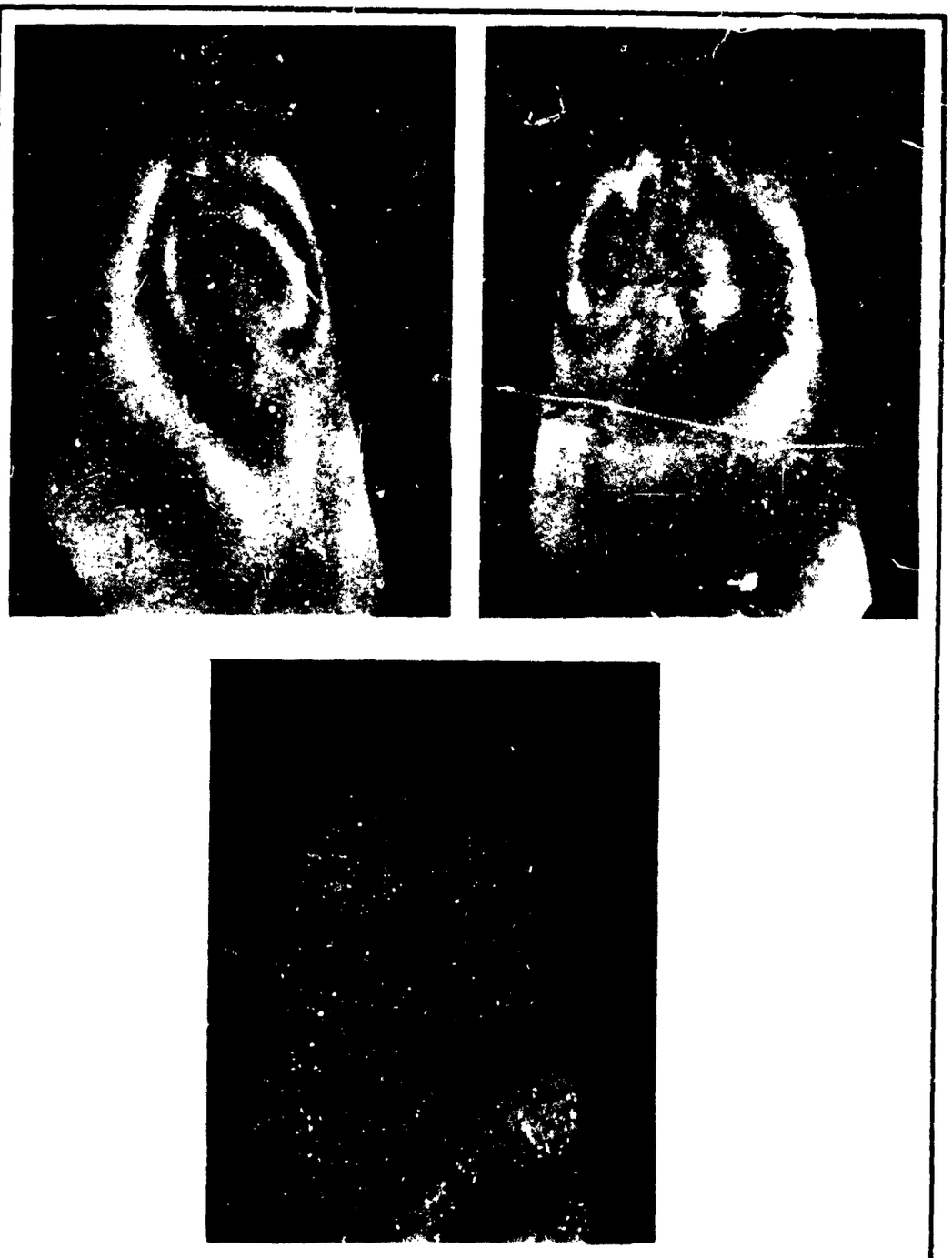

Parallel Injection Sequence - Right to Left

Fig. 20

Thrust Vectoring Sequence: Interferometer, d/b = 5; P_o/P_a = 2.20

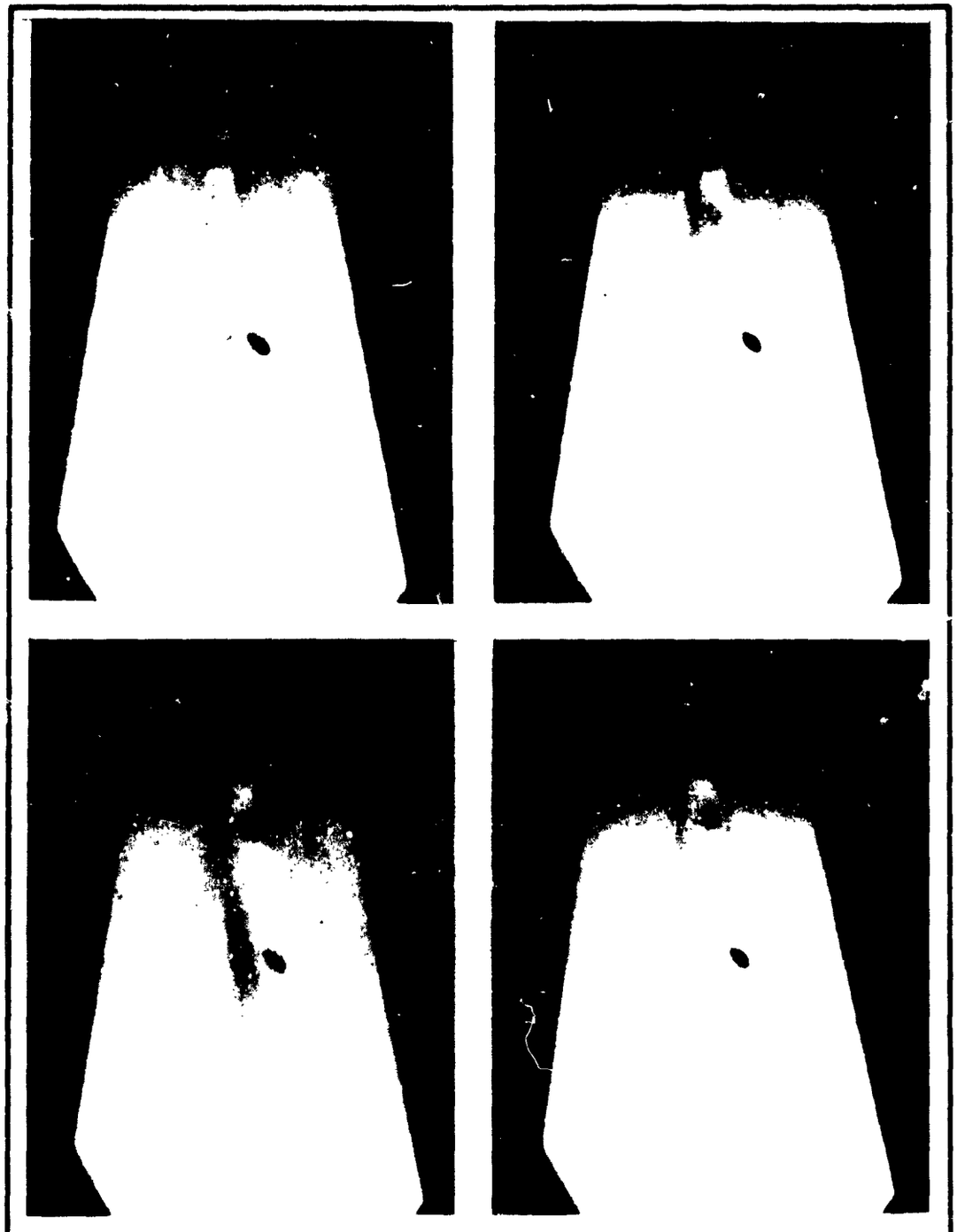

Parallel Injection Sequence - Left to Right

Fig. 21

Thrust Vectoring Sequence: Schlieren, d/b = 5; P_o/P_a = 2.89

Parallel Injection Sequence - Left to Right

Fig. 22

Thrust Vectoring Sequence: Interferometer, d/b = 5; P_o/P_a = 2.89

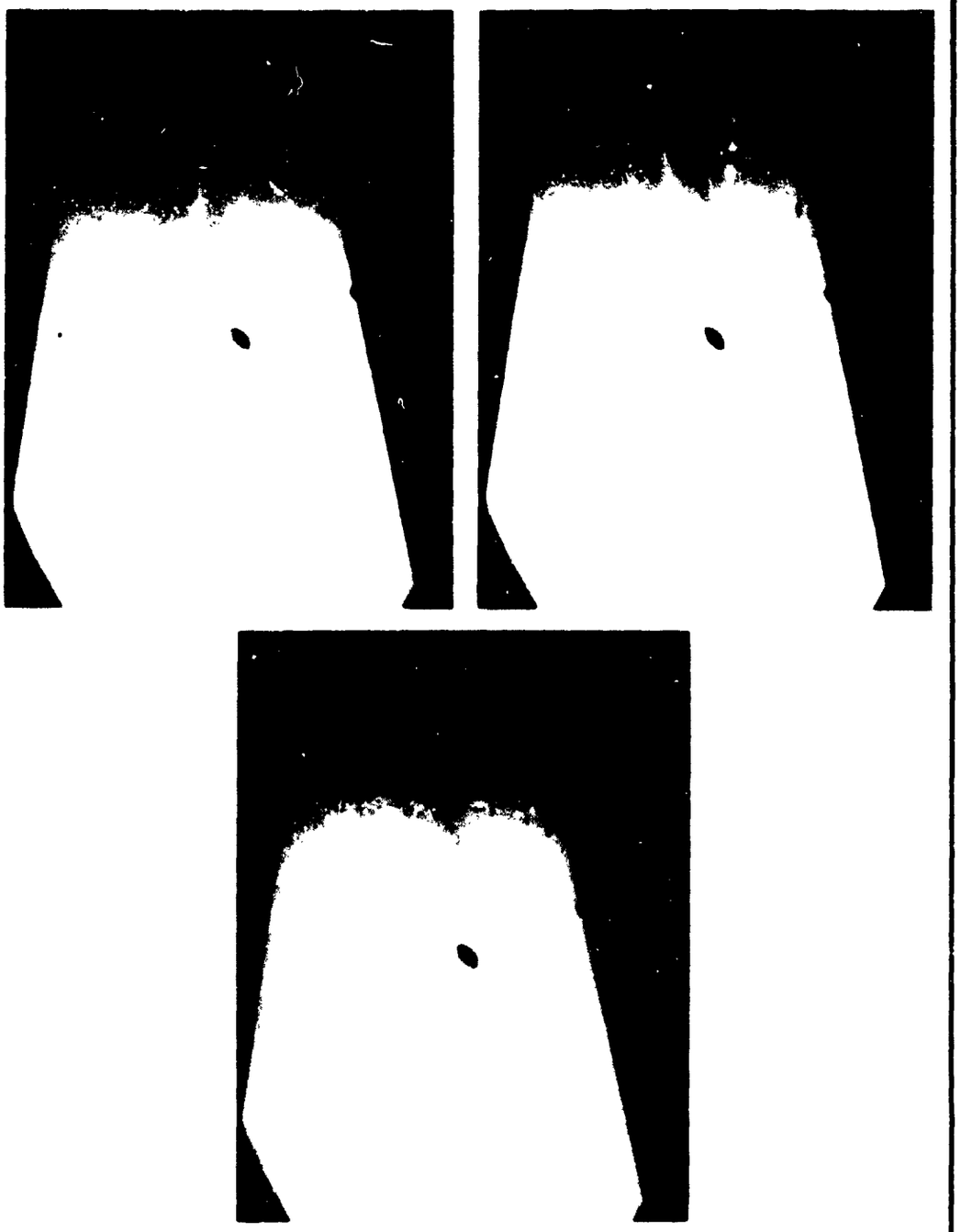

Parallel Injection Sequence - Left to Right

Fig. 23

Thrust Vectoring Sequence: Schlieren, d/b = 6; $P_o/P_a = 1.87$

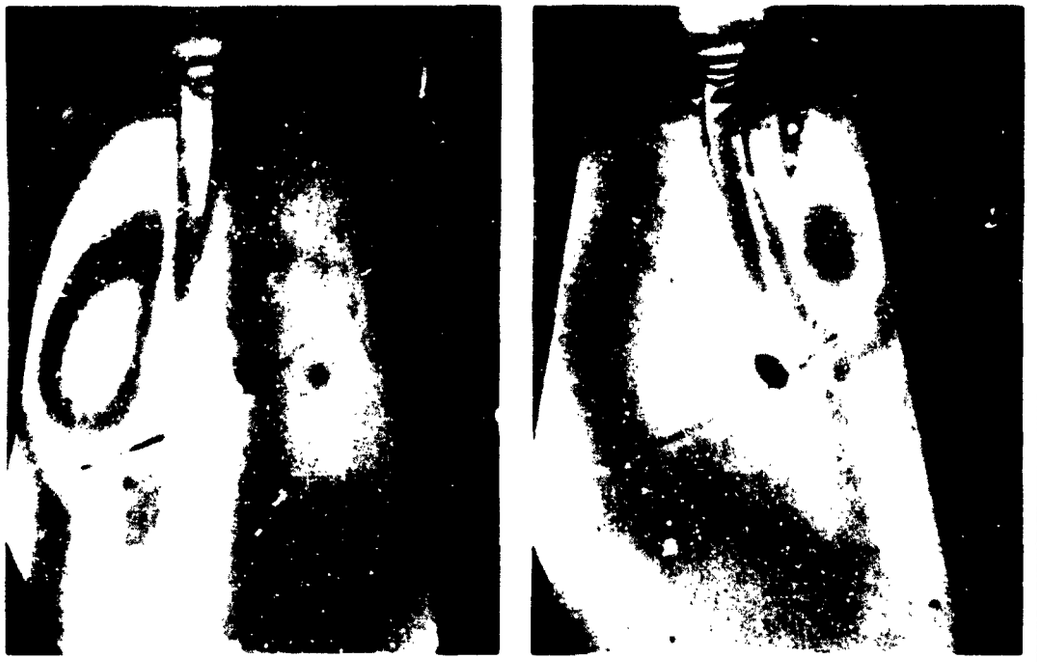

Parallel Injection Sequence - Left to Right

Fig. 24

Thrust Vectoring Sequence: Interferometer, d/b = 6; P_o/P_a = 1.87

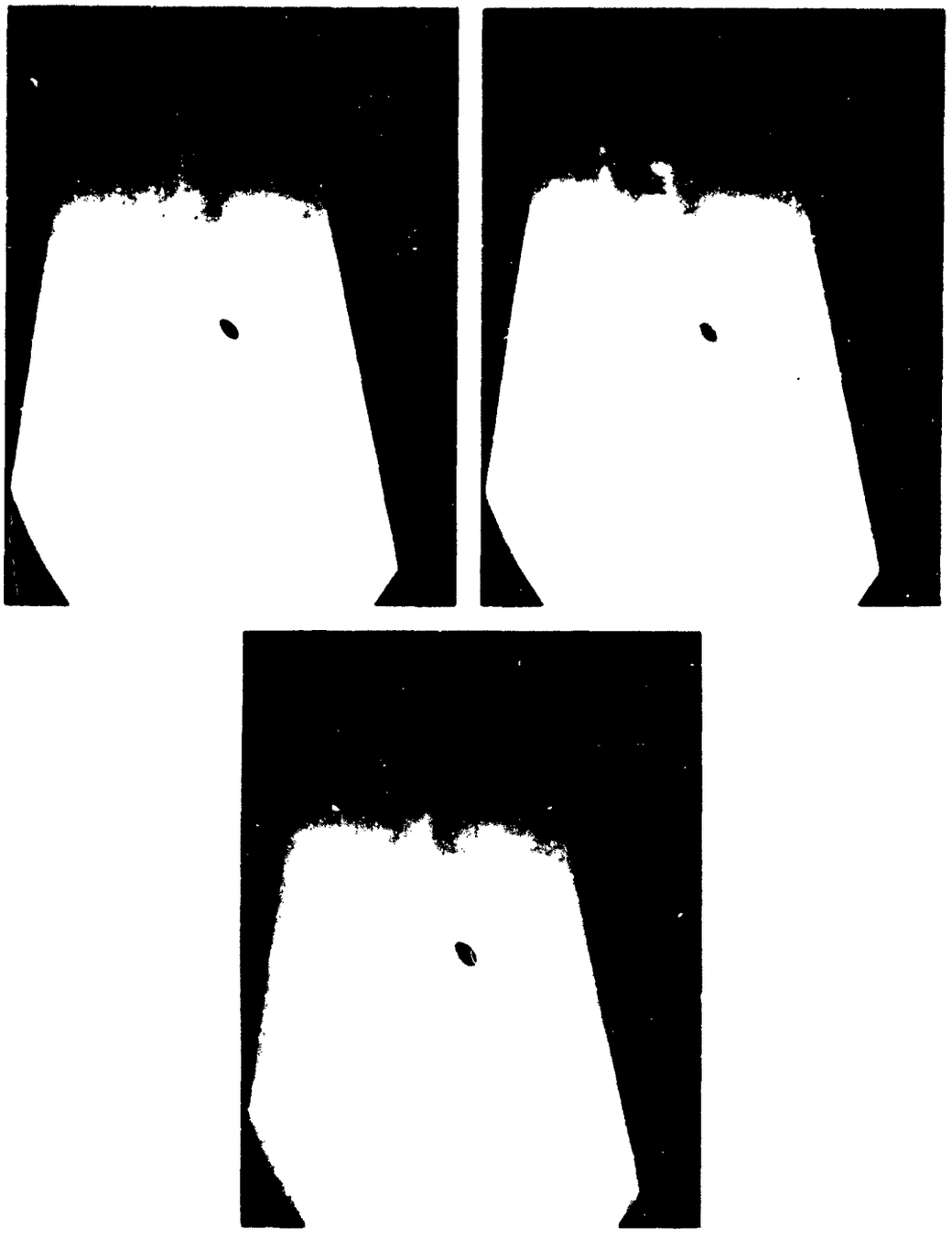

Parallel Injection Sequence - Right to Left

Fig. 25

Thrust Vectoring Sequence: Schlieren, d/b = 6; P_o/P_a = 2.22

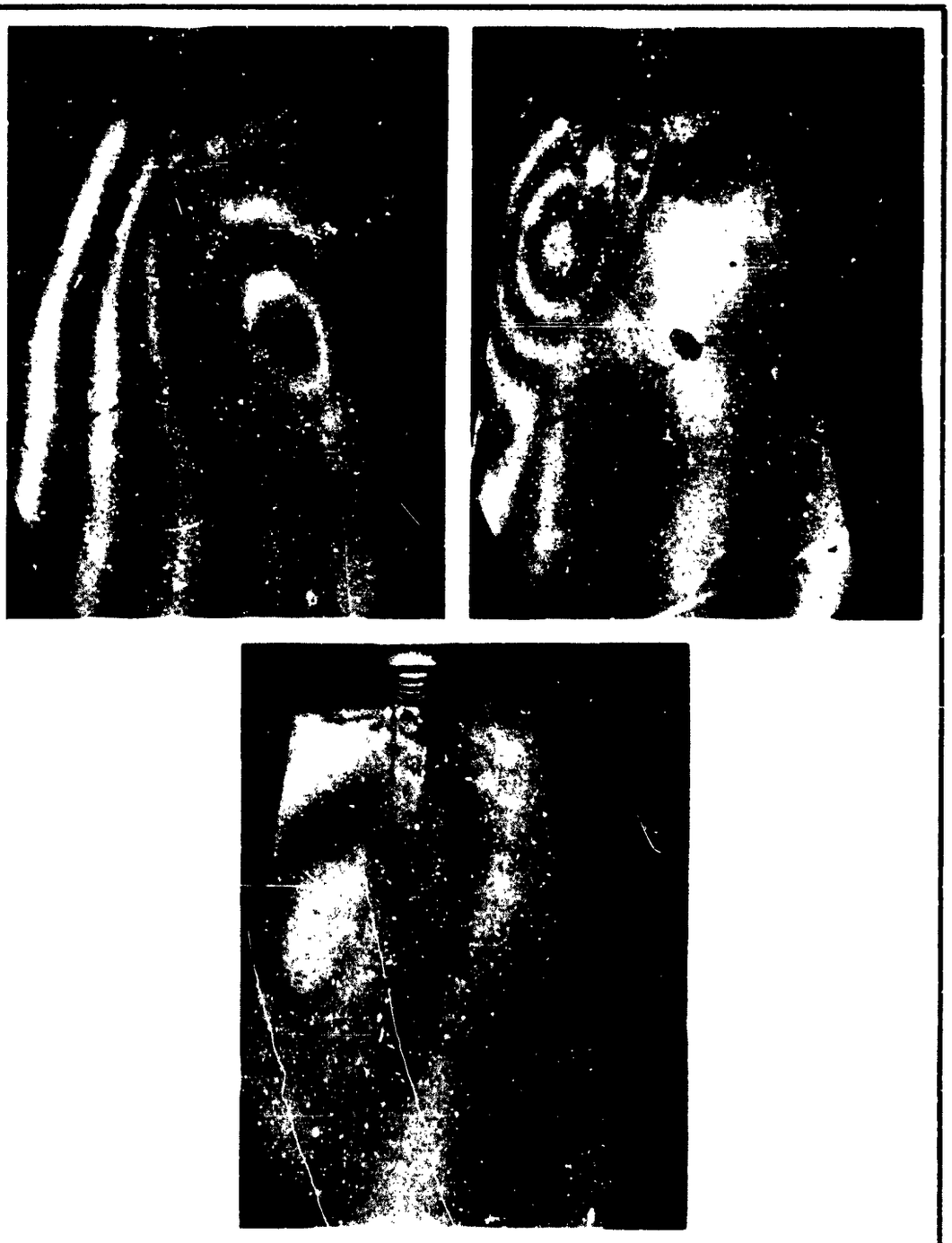

Parallel Injection Sequence - Right to Left

Fig. 26

Thrust Vectoring Sequence: Interferometer, d/b = 6; P_o/P_a = 2.22

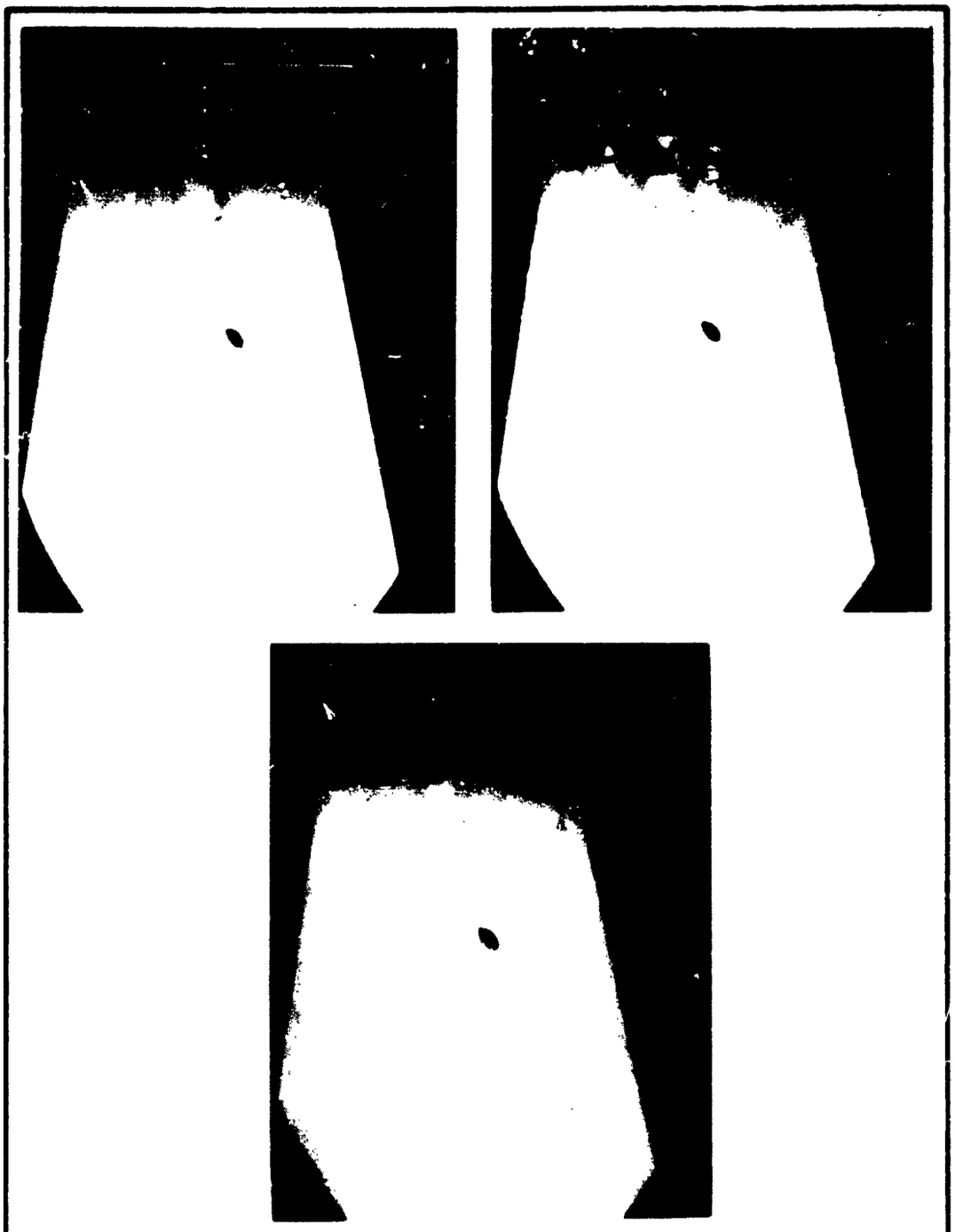

Parallel Injection Sequence - Right to Left

Fig. 27

Thrust Vectoring Sequence: Schlieren, d/b = 6; P_o/P_a = 2.35

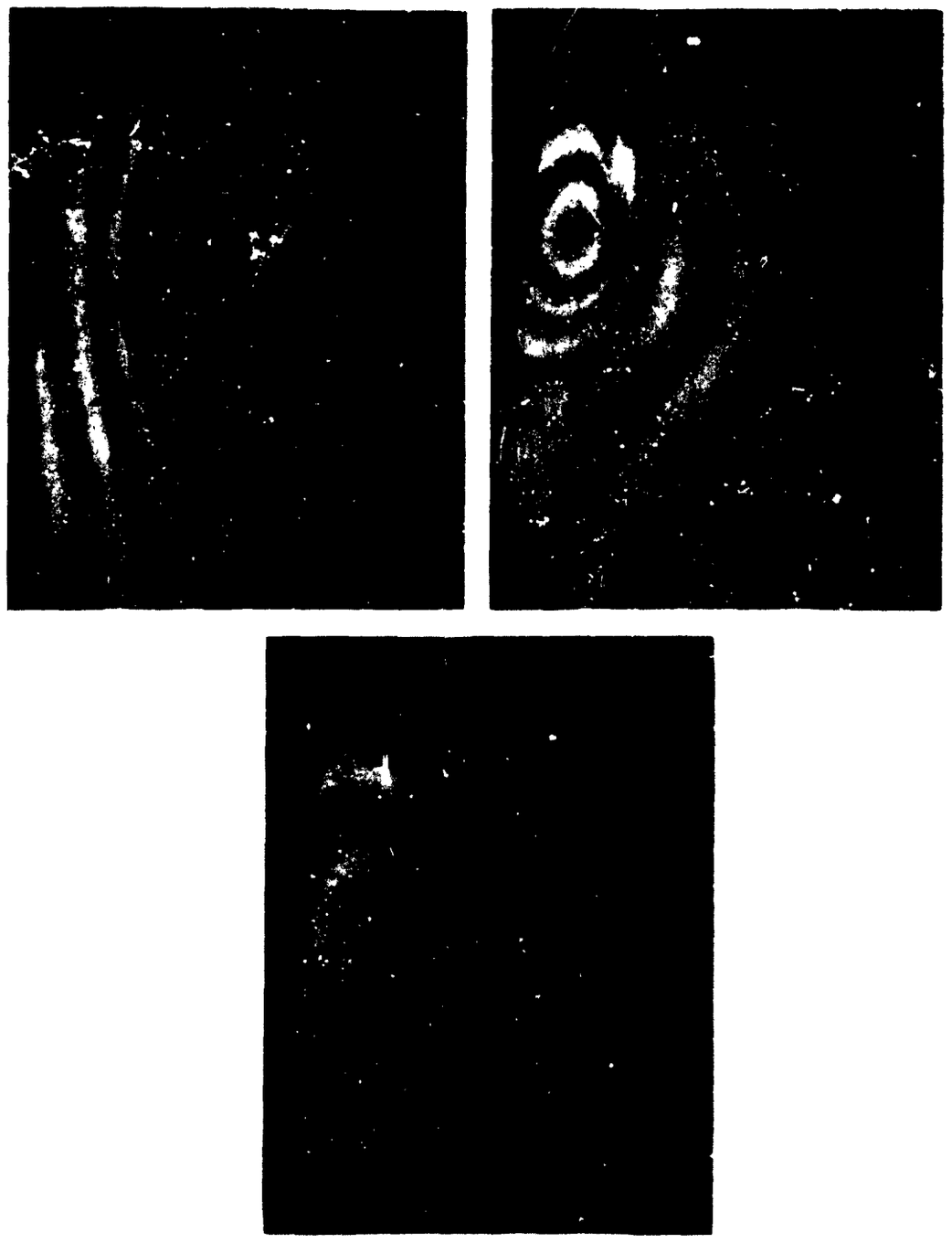

Parallel Injection Sequence - Right to Left

Fig. 28

Thrust Vectoring Sequence: Interferometer, d/b = 6; P_o/P_a = 2.35

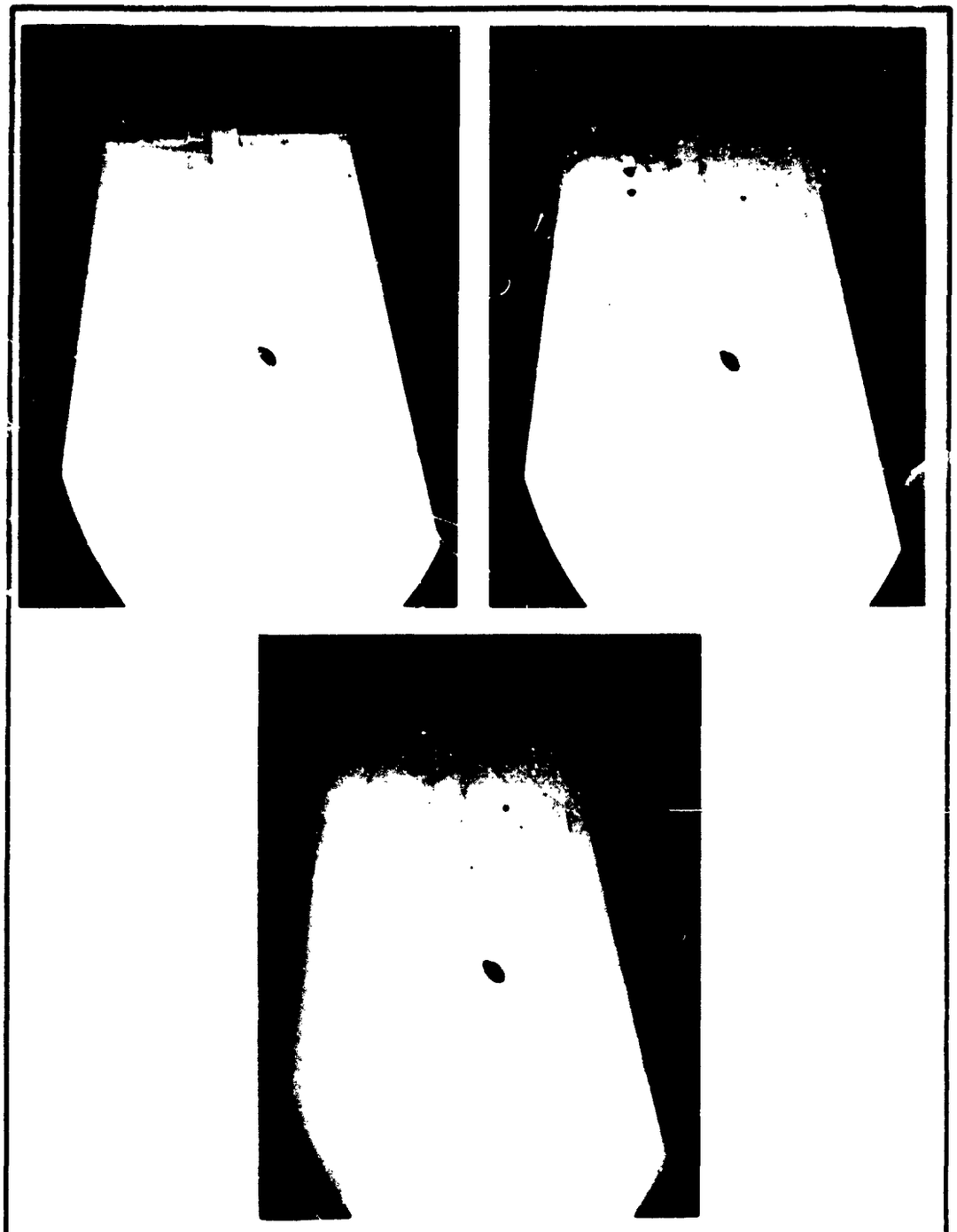

Parallel Injection Sequence - Right to Left

Fig. 29

Thrust Vectoring Sequence: Schlieren, d/b = 7; P_o/P_a = 1.70

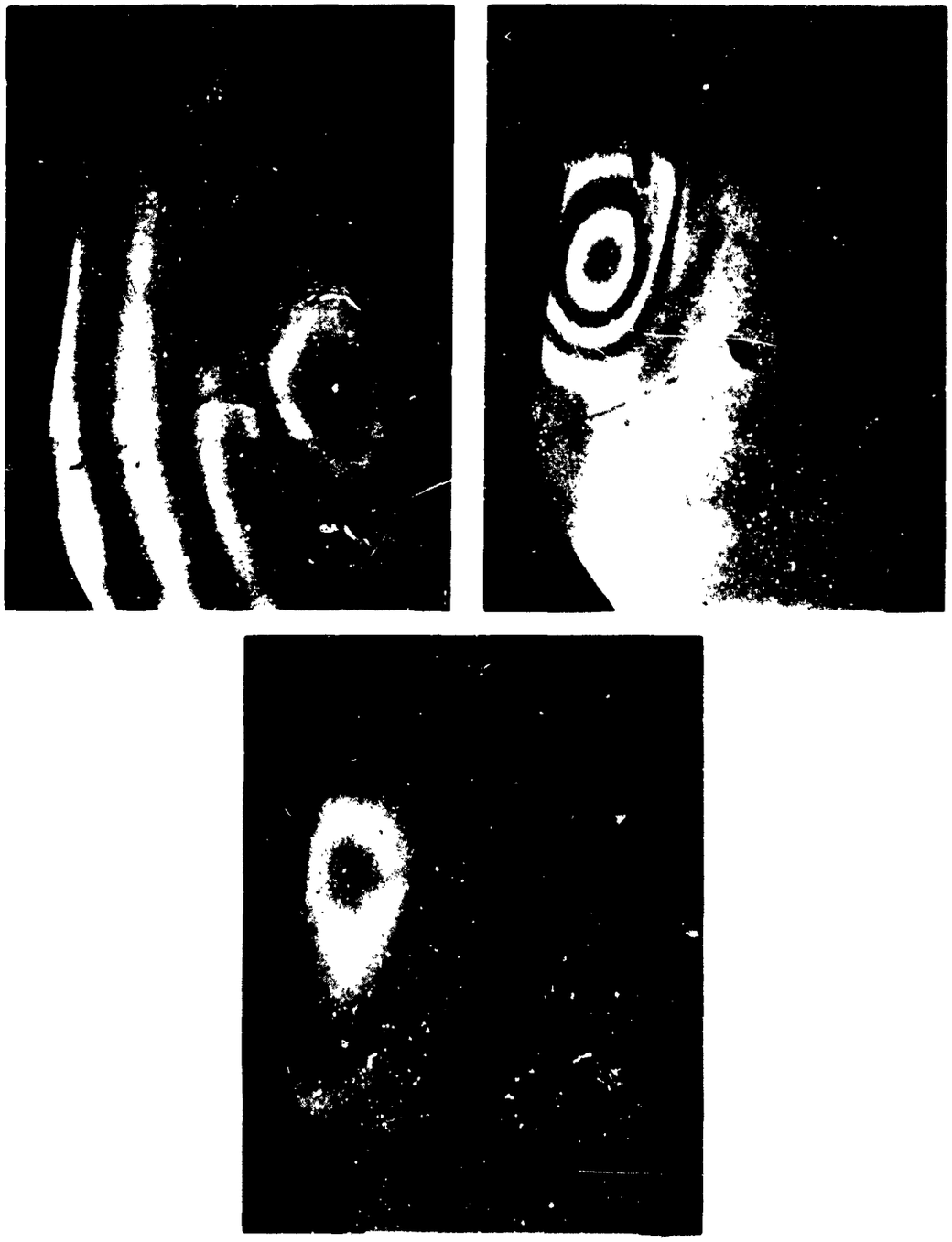

Parallel Injection Sequence - Right to Left

Fig. 30

Thrust Vectoring Sequence: Interferometer, d/b = 7; P_o/P_a = 1.70

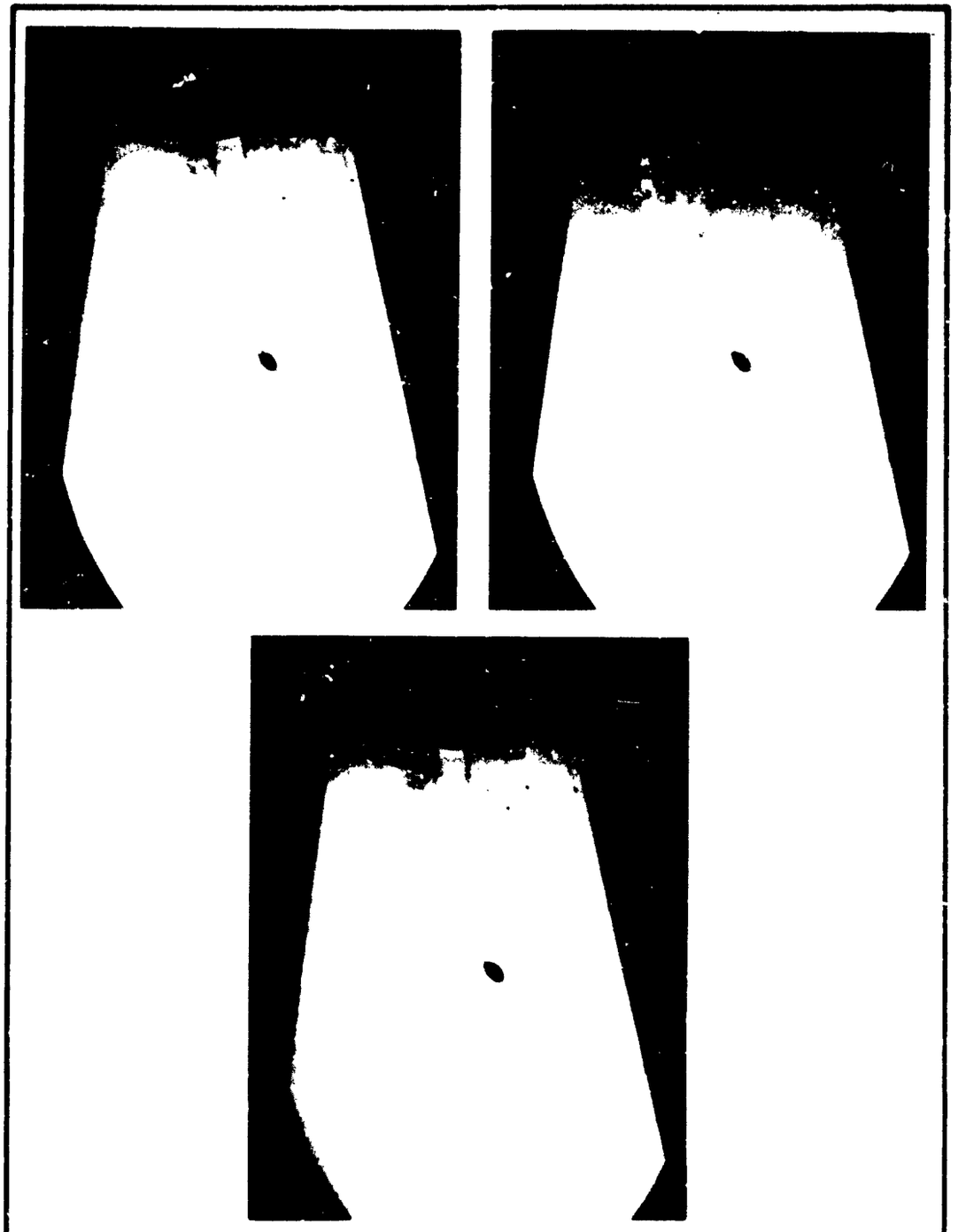

Parallel Injection Sequence - Right to Left

Fig. 31

Thrust Vectoring Sequence: Schlieren, d/b = 7; P_o/P_a = 1.87

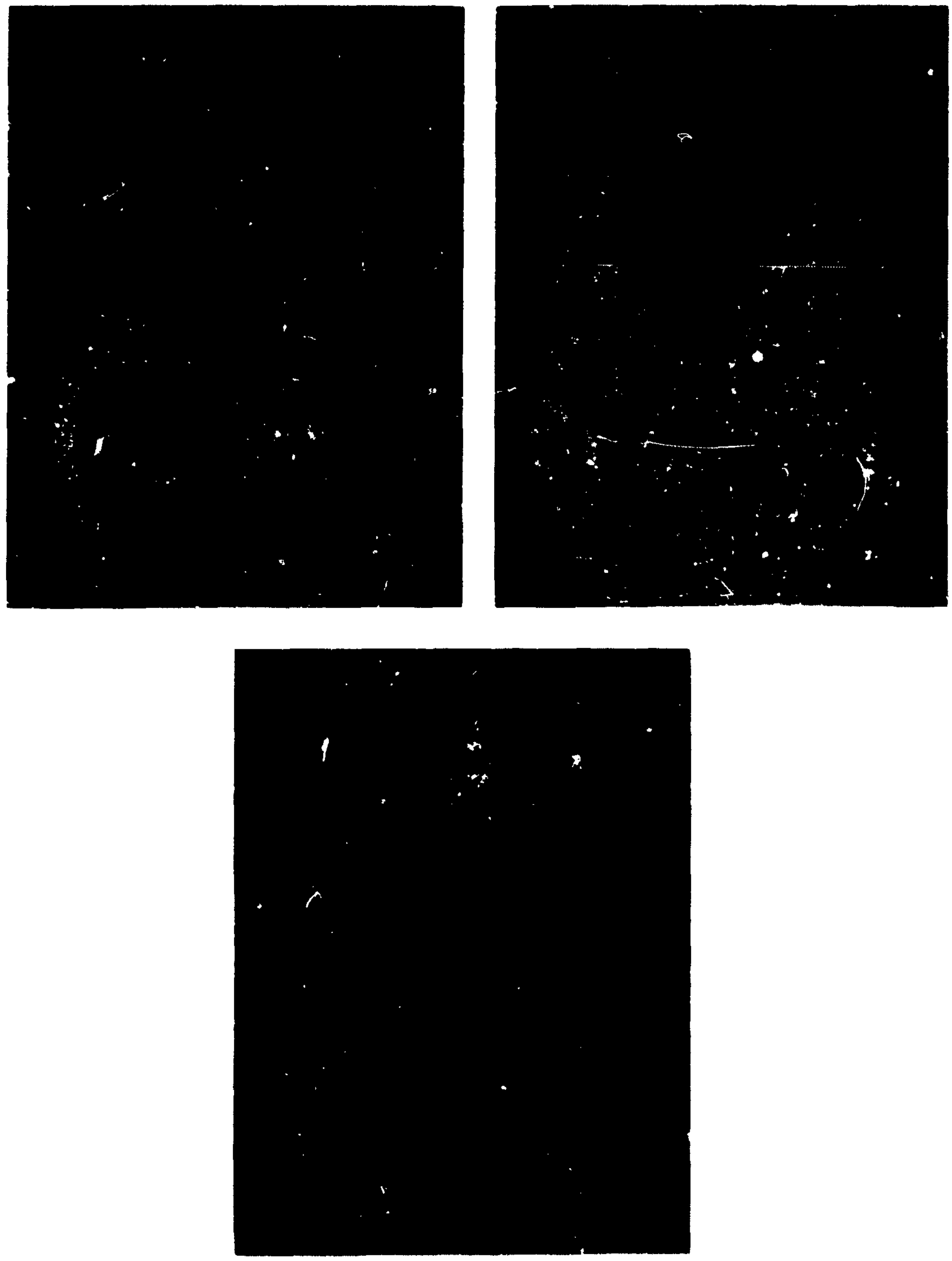

Parallel Injection Sequence - Right to Left

Fig. 32

Thrust Vectoring Sequence: Interferometer, d/b = 7; P_c/P_a =1.87

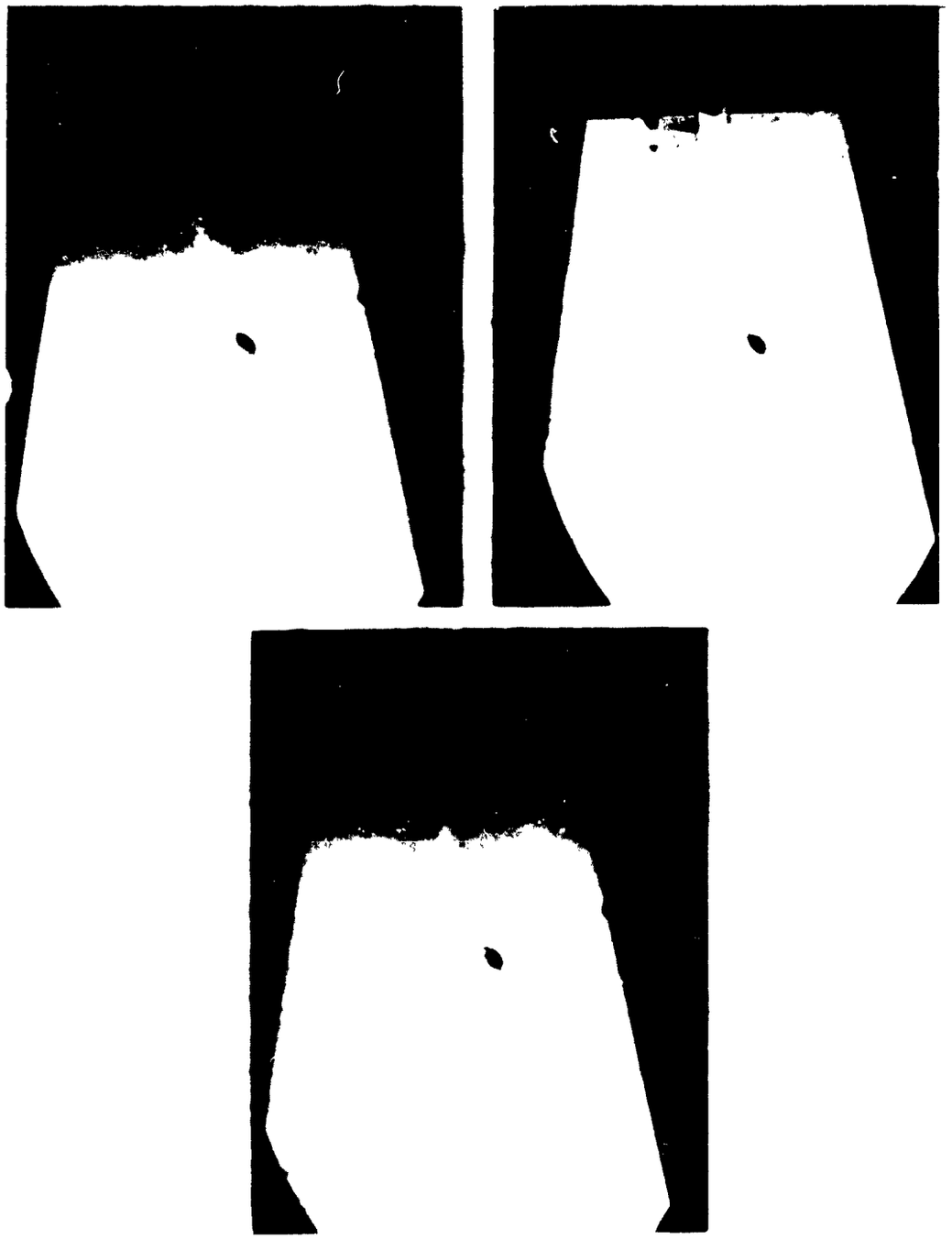

Parallel Inje tion Sequence - Right to Left

Fig. 33

Thrust Vectoring Sequence: Schlieren, d/b = 7; P_o/P_a =1.90

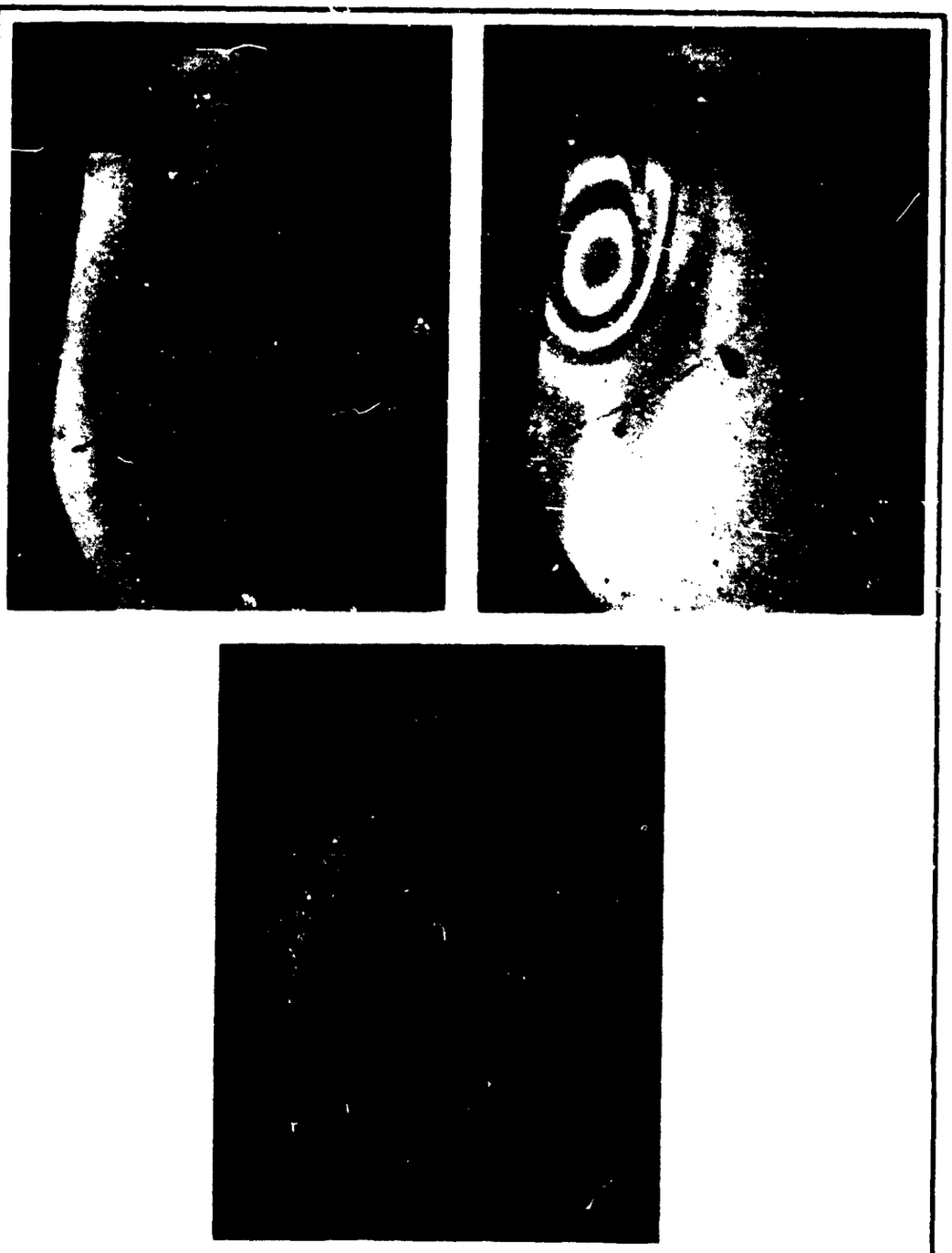

Parallel Injection Sequence - Right to Left

Fig. 34

Thrust Vectoring Sequence: Interferometer, d/b = 7; P_o/P_a = 1.90

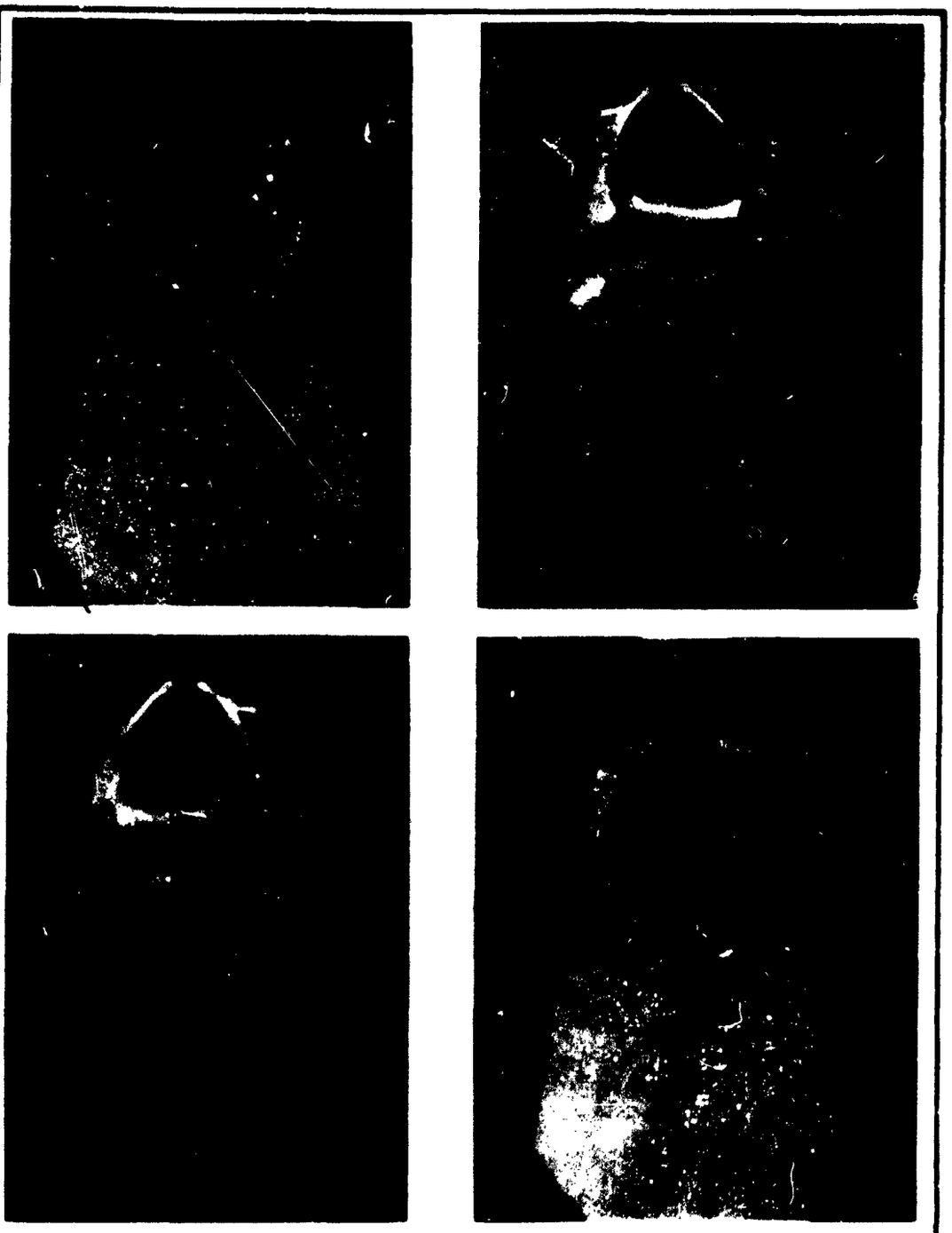

Fig. 35

Expanded Flow Sequence: Schlieren, d/b = 4; P_o/P_a = 6.05

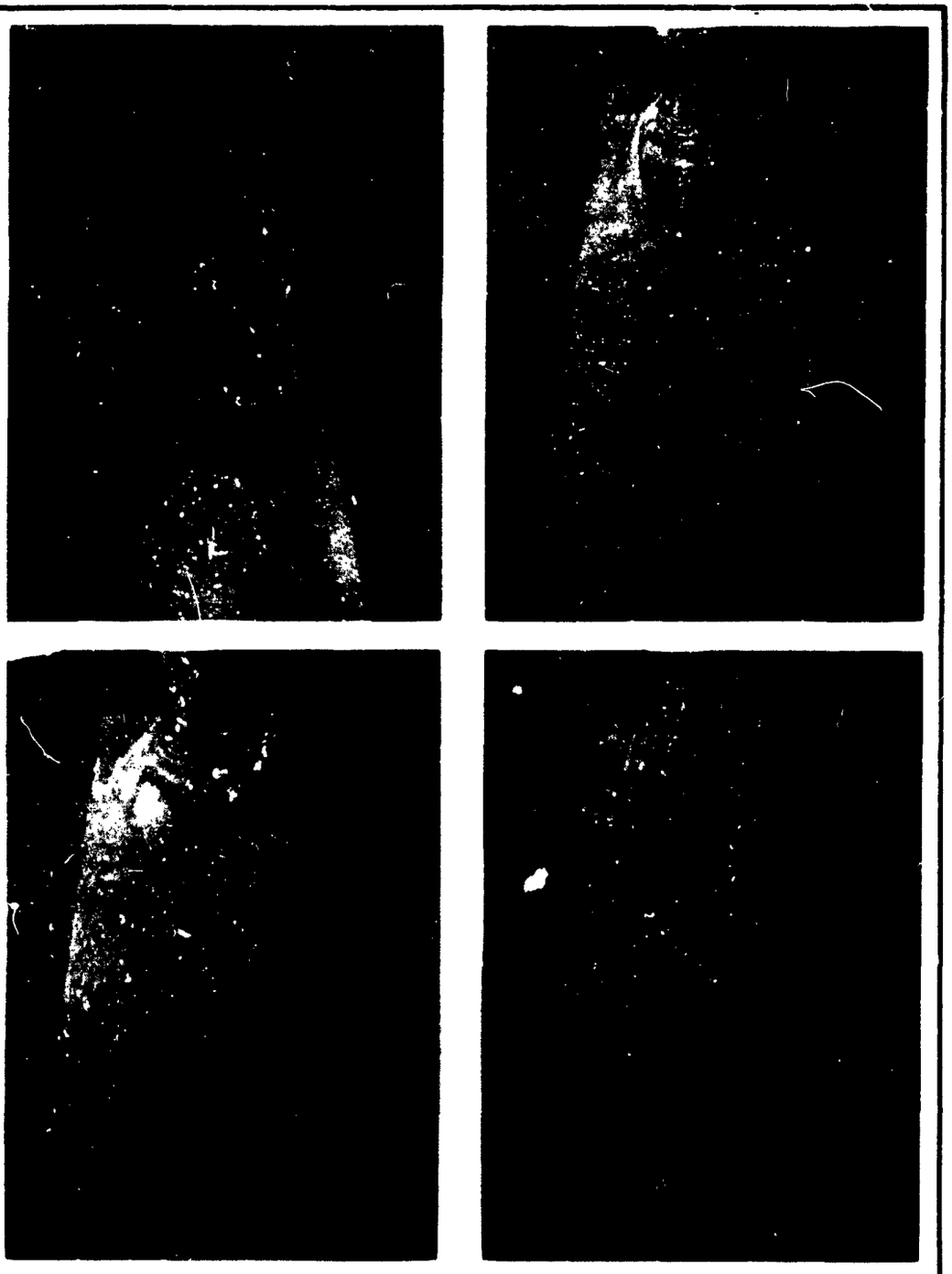

Fig. 36

Expanded Flow Sequence: Interferometer, $d/b = 4$, $P_o/P_a = 6.05$

Appendix B

Plotted Data

All of the plotted data referenced in the body of this report have been collected in this appendix.

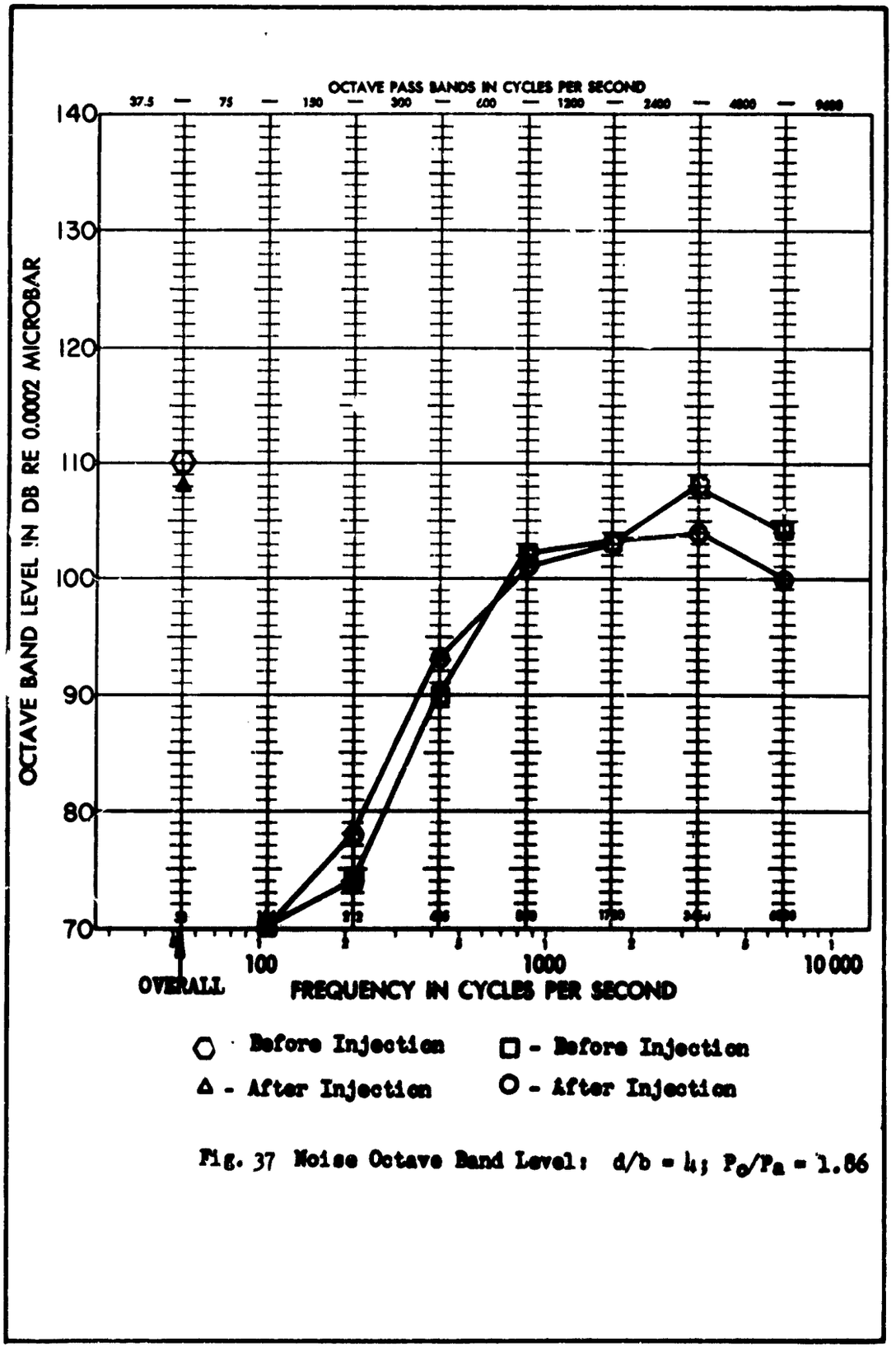

Fig. 37 Noise Octave Band Level: $d/b = 4$; $P_o/P_a = 1.86$

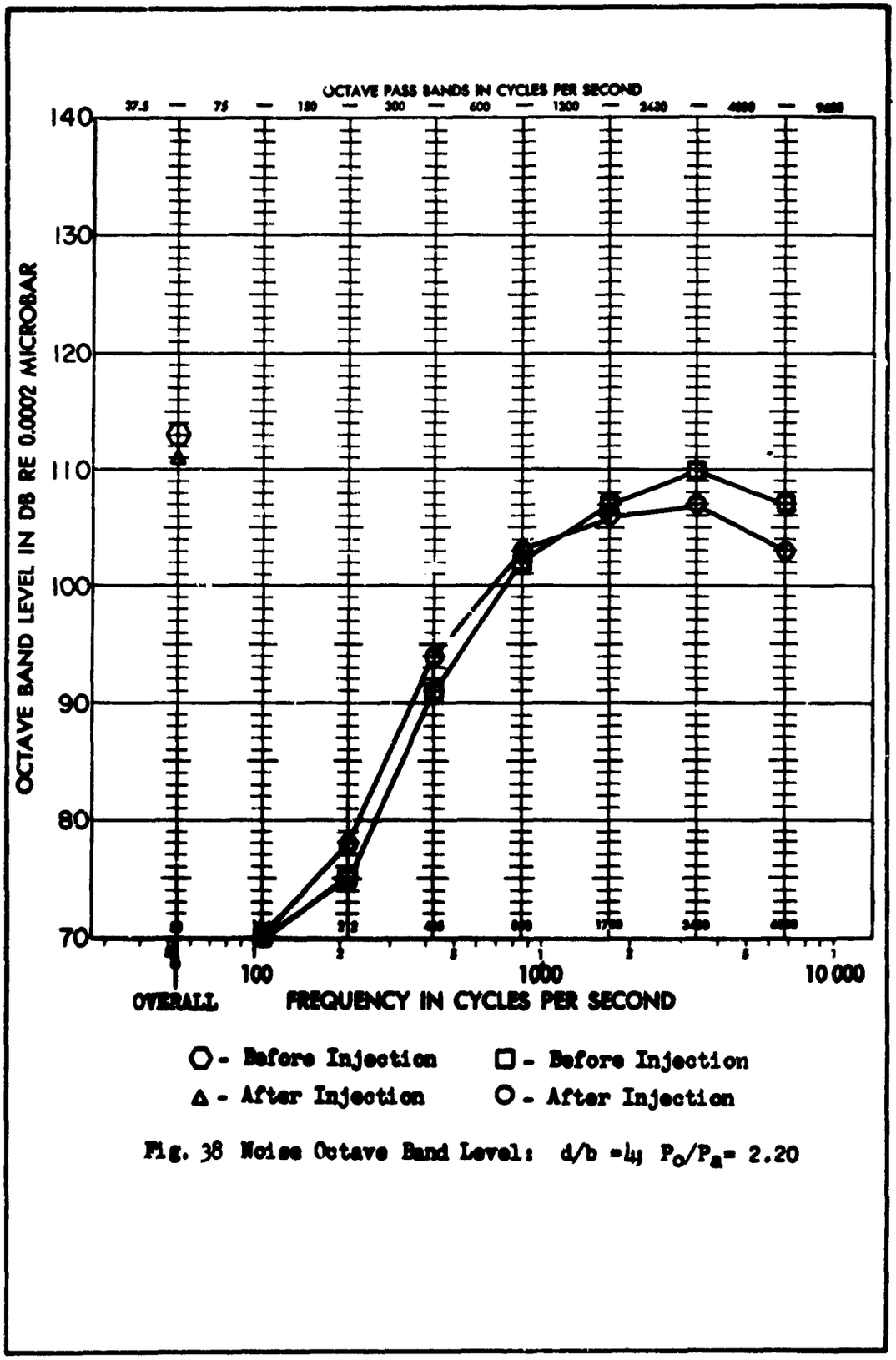

Fig. 38 Noise Octave Band Level: d/b =4; P_o/P_a= 2.20

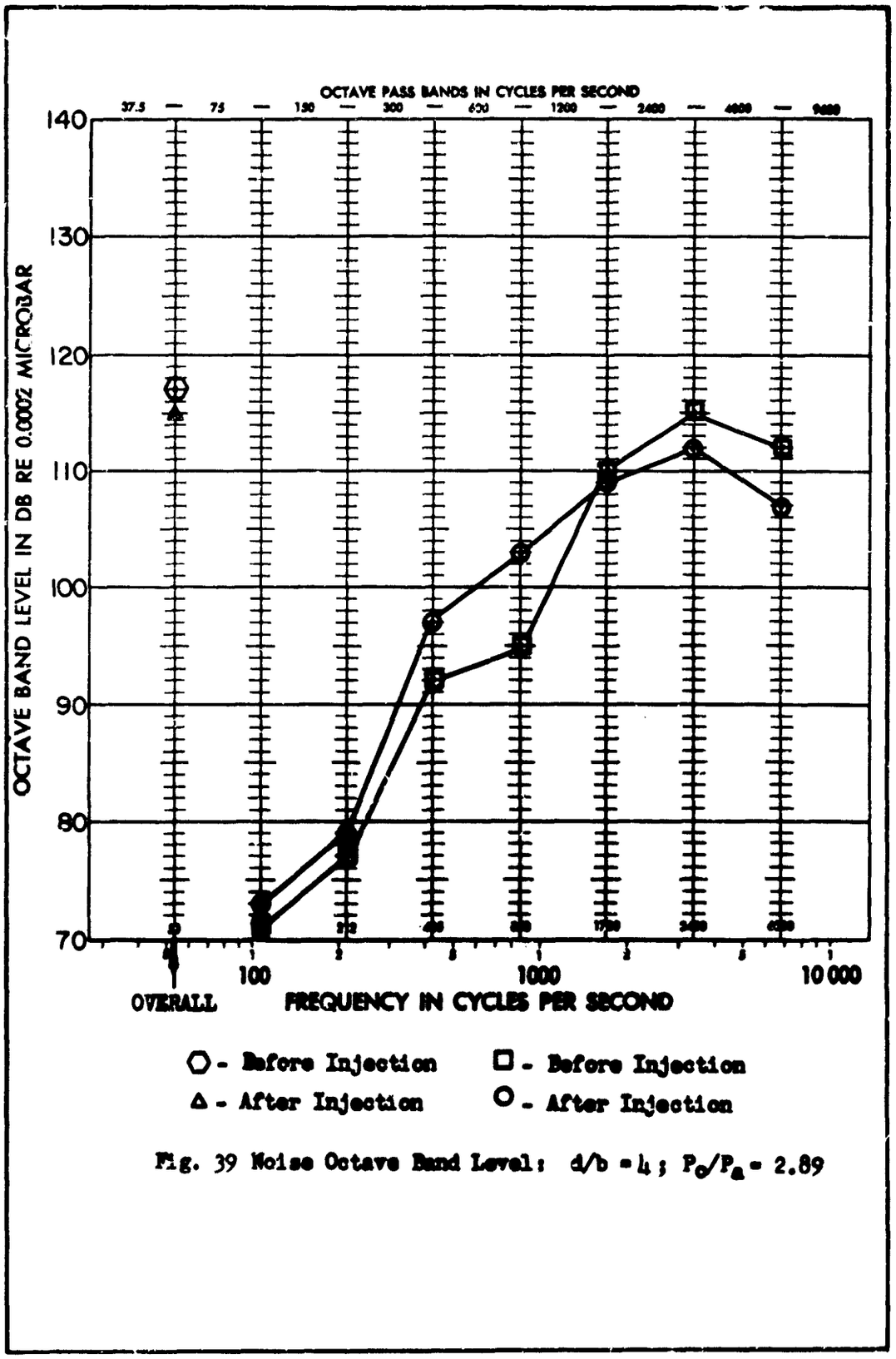

Fig. 39 Noise Octave Band Level: $d/b = 4$; $P_o/P_a = 2.89$

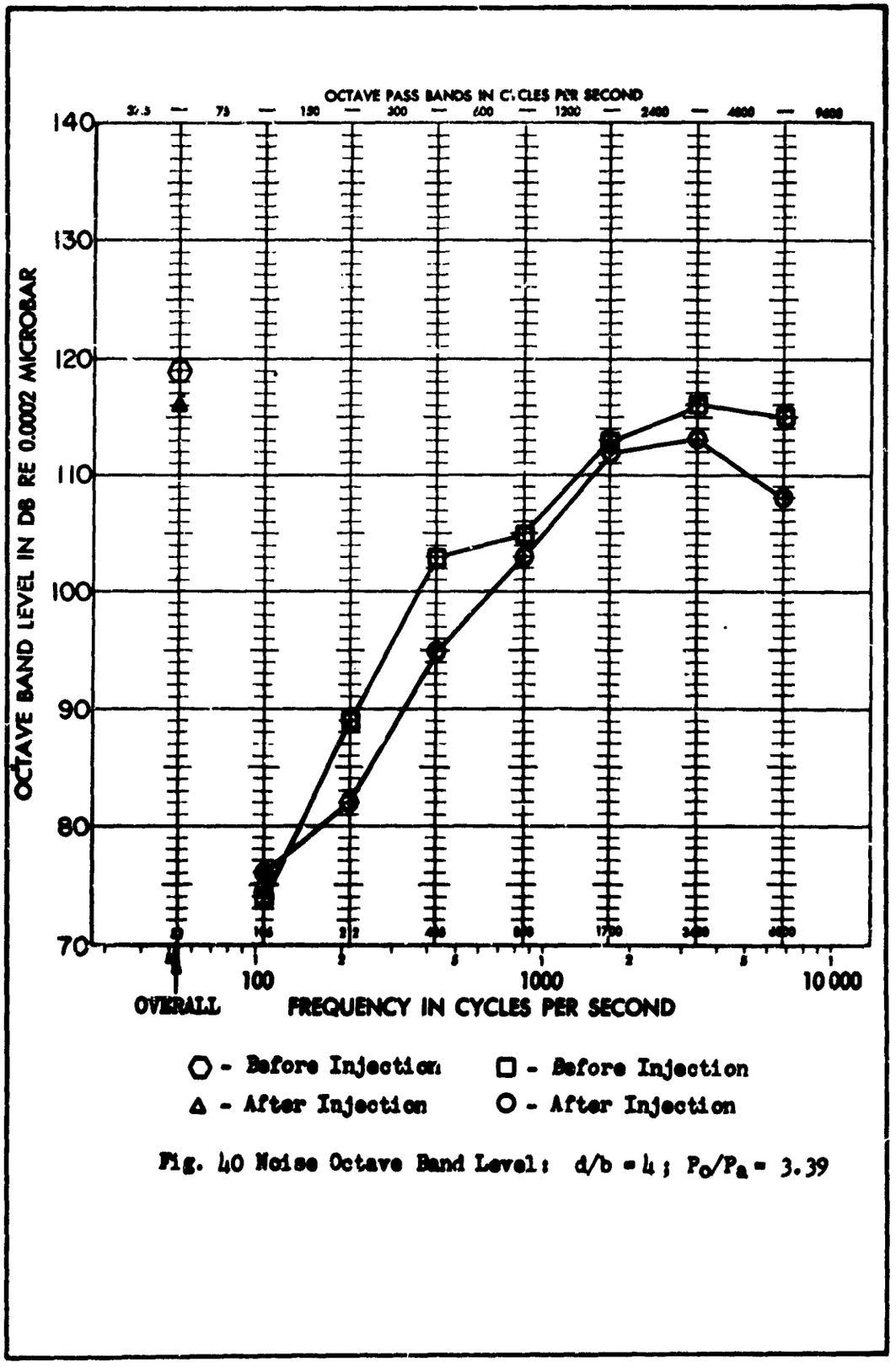

Fig. 40 Noise Octave Band Level: d/b = 4 ; P_o/P_a = 3.39

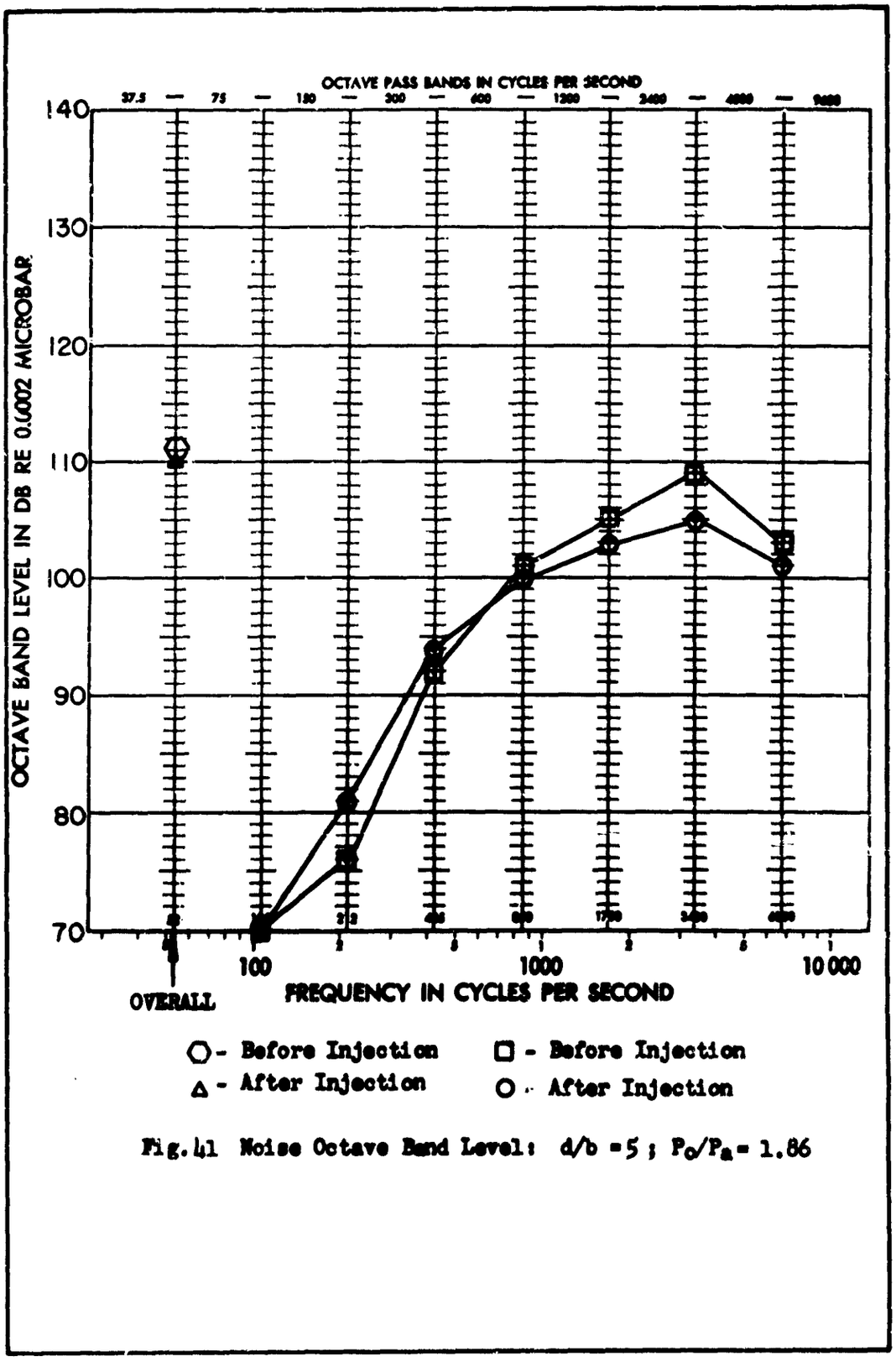

Fig.41 Noise Octave Band Level: d/b = 5 ; P_o/P_a = 1.86

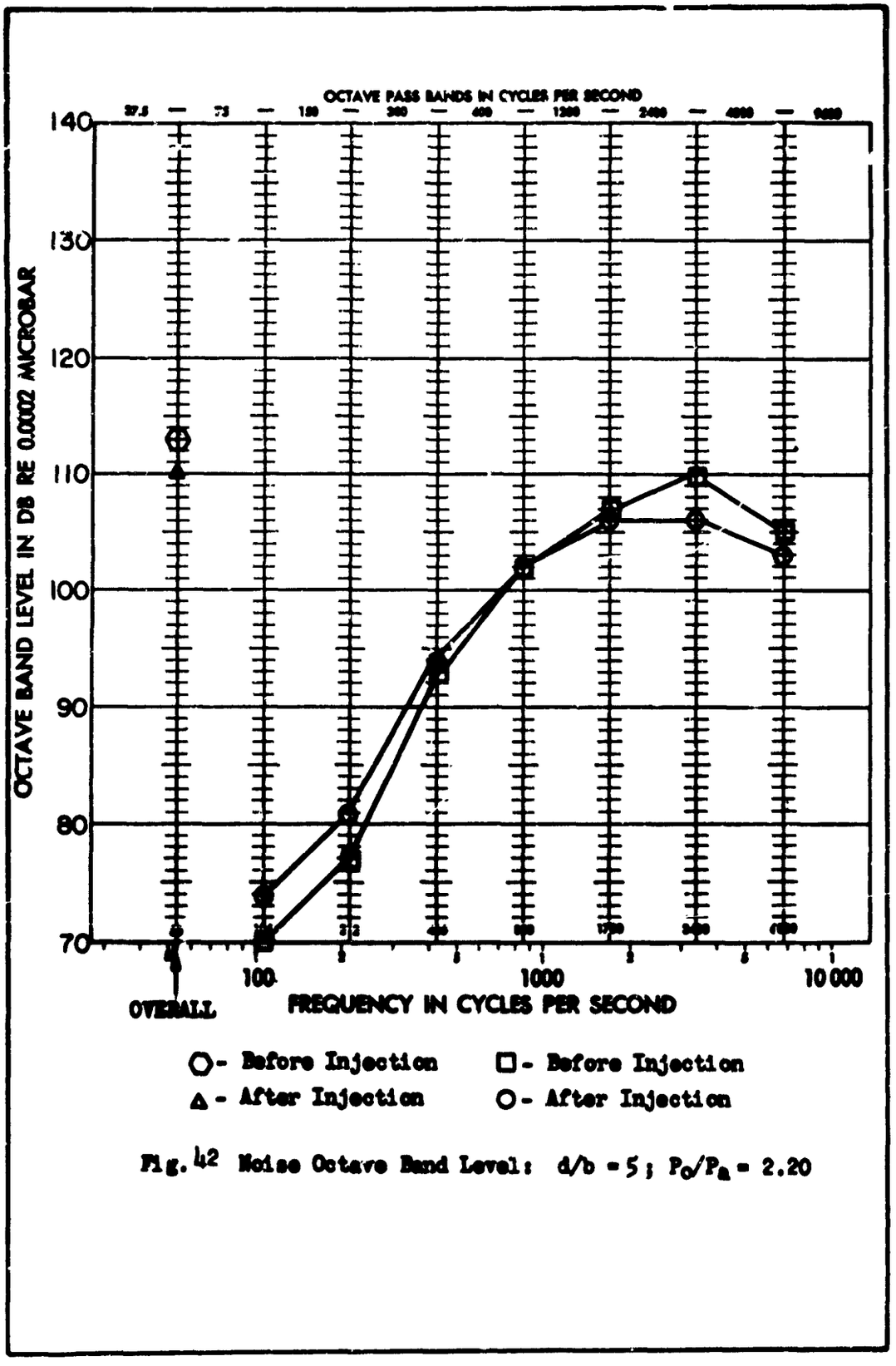

Fig. 42 Noise Octave Band Level: d/b = 5; P_o/P_a = 2.20

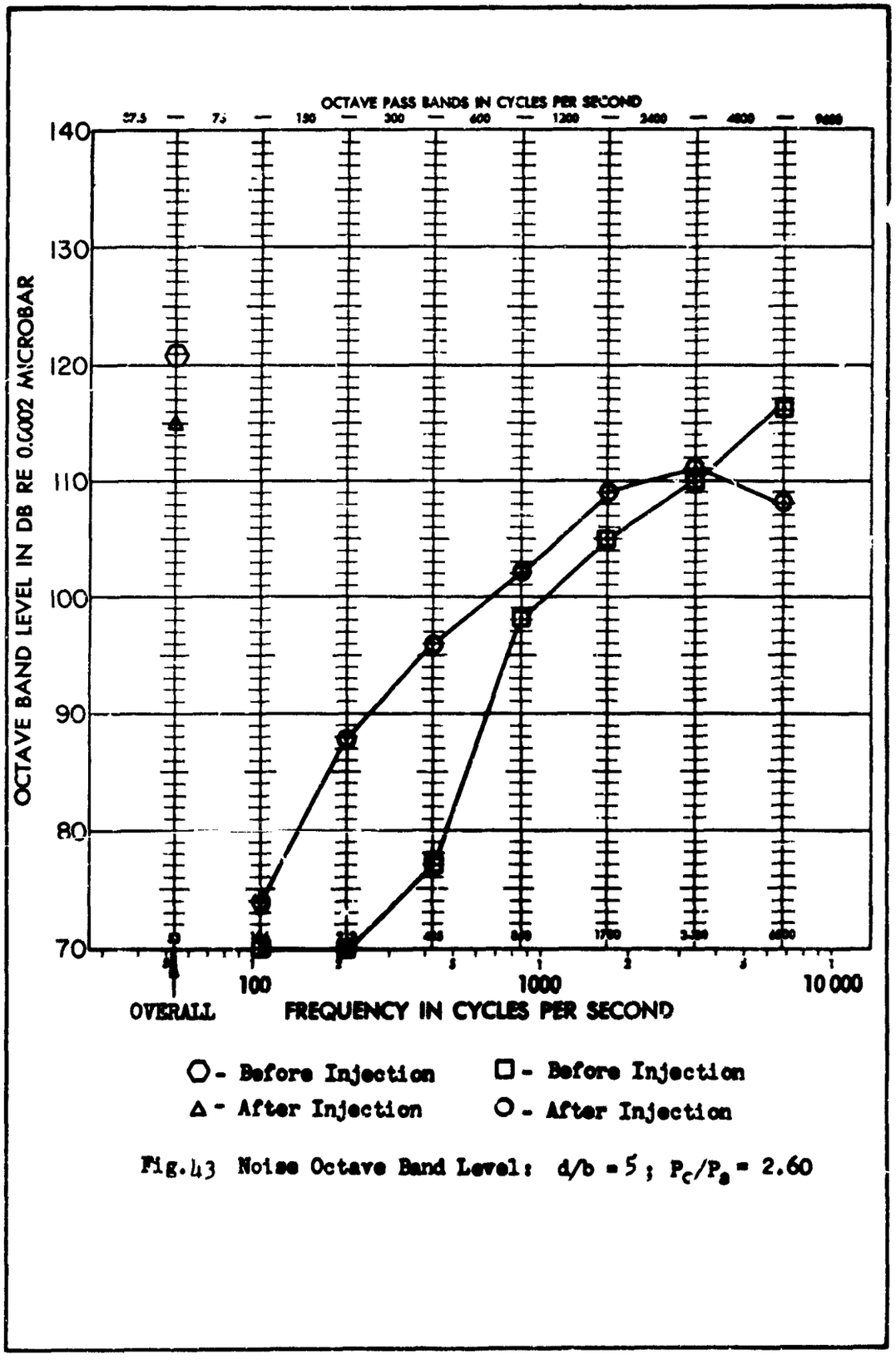

Fig.43 Noise Octave Band Level: $d/b = 5$; $P_c/P_s = 2.60$

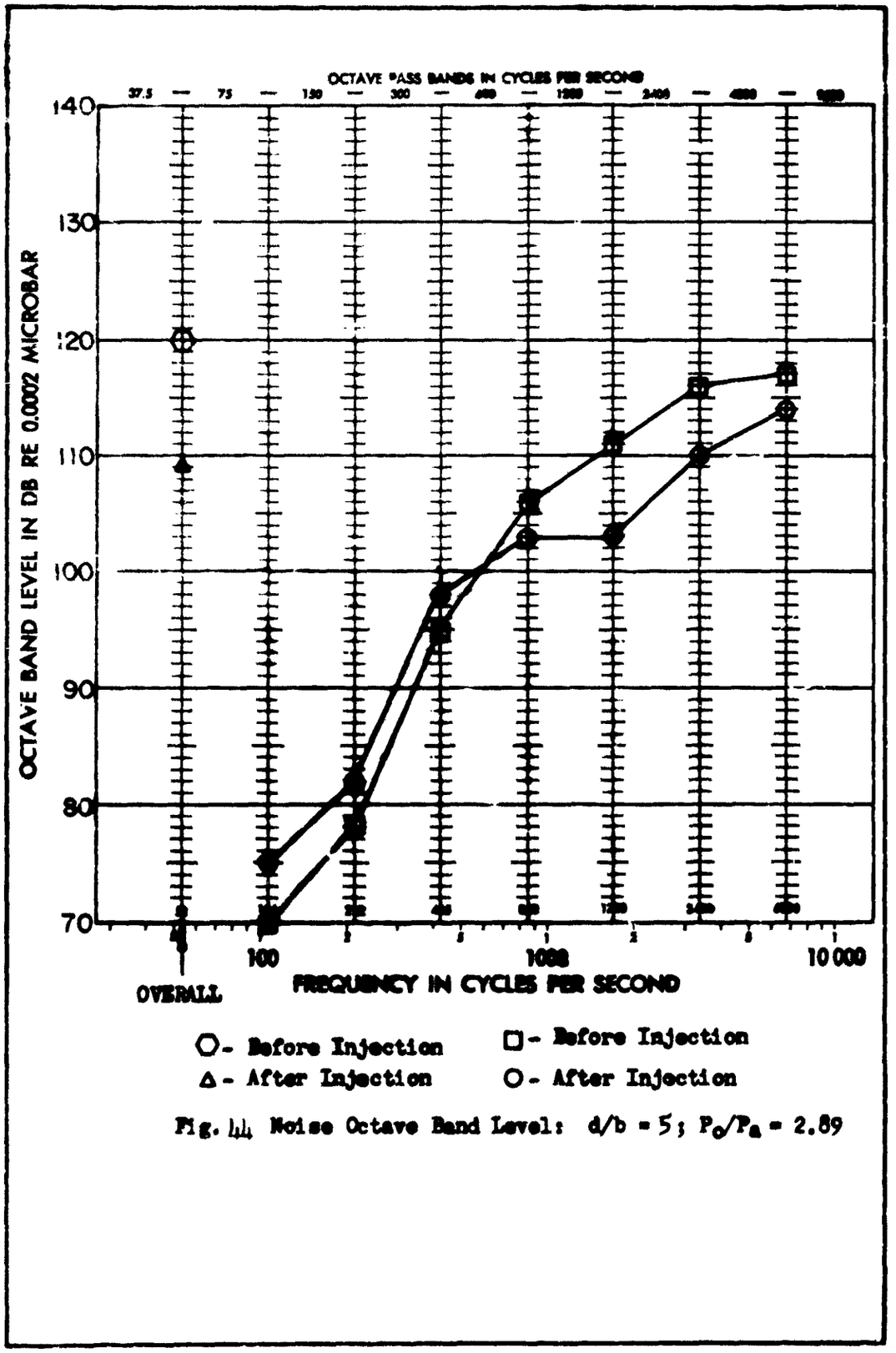

Fig. 44 Noise Octave Band Level: d/b = 5; P_o/P_a = 2.89

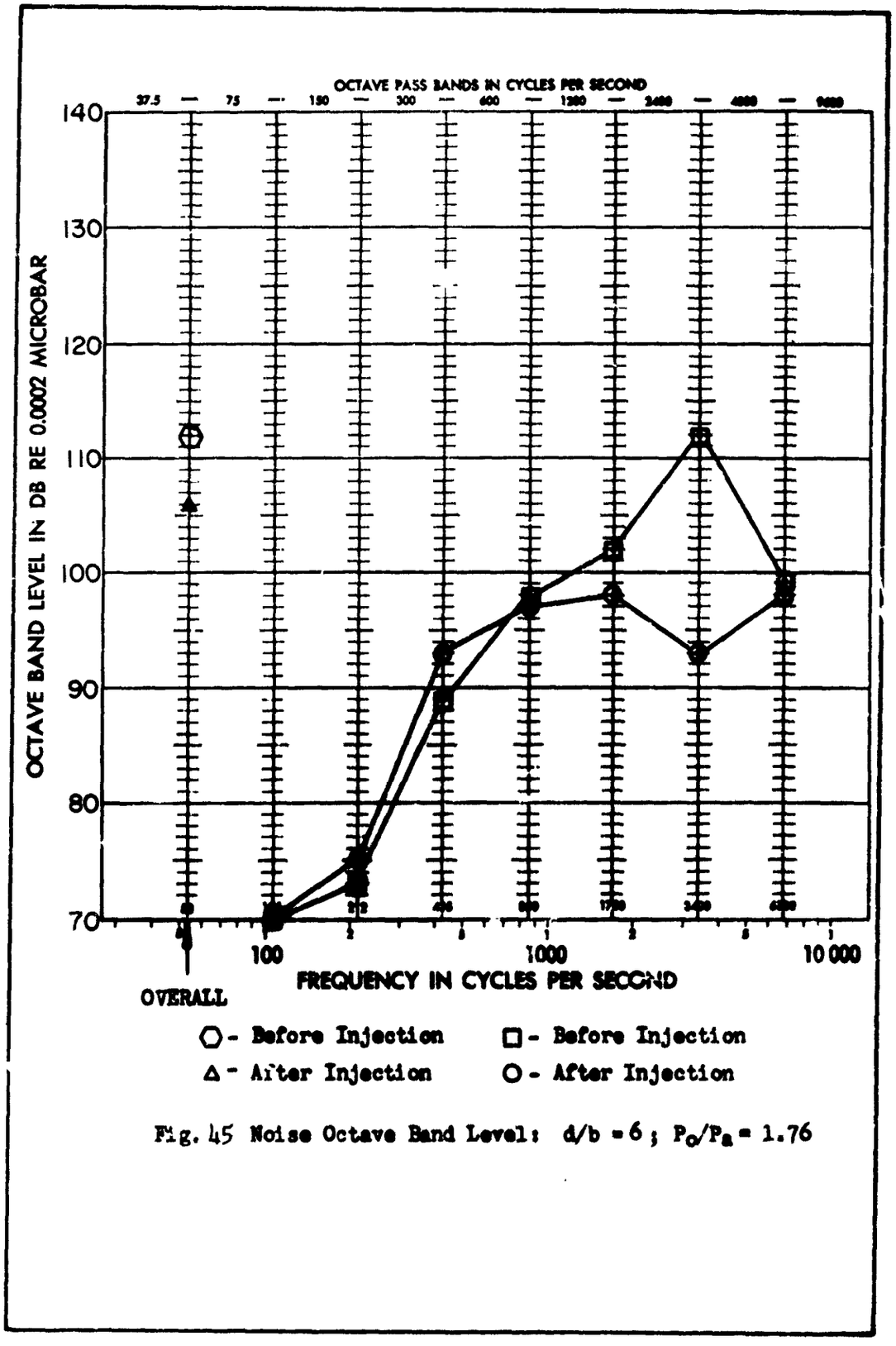

Fig. 45 Noise Octave Band Level: d/b = 6 ; P_o/P_a = 1.76

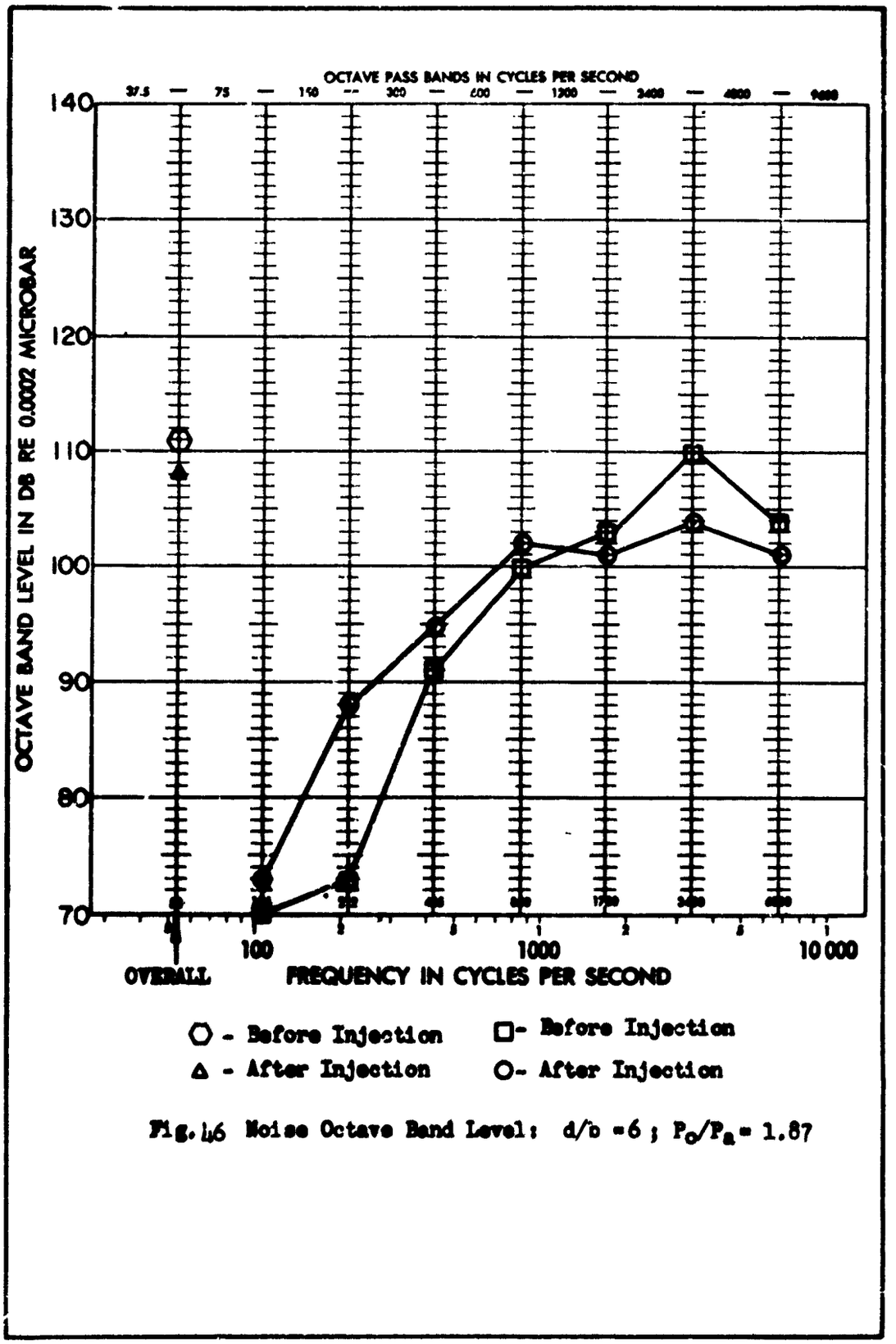

Fig. 46 Noise Octave Band Level: d/b = 6 ; P_o/P_a = 1.87

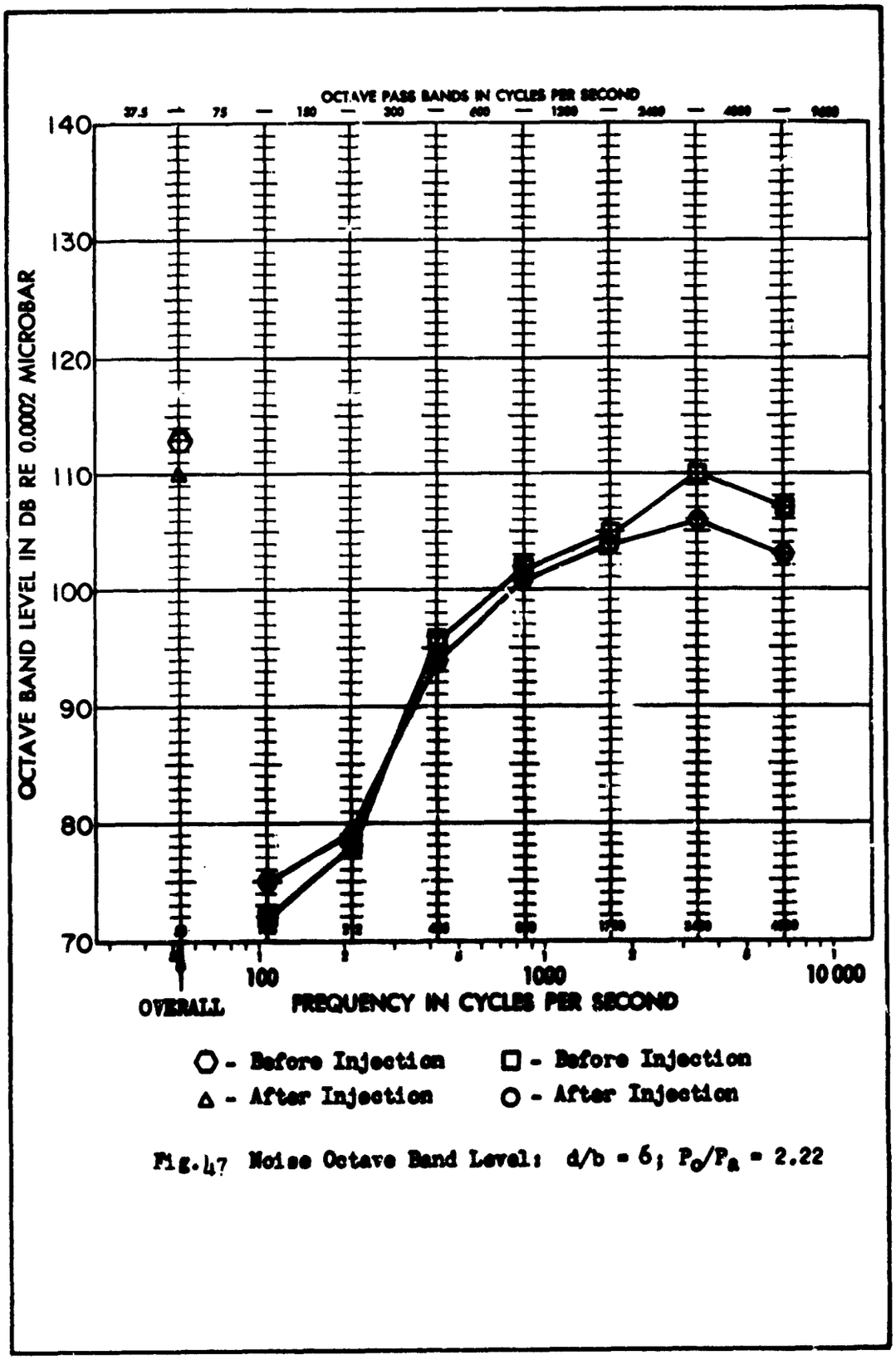

Fig.47 Noise Octave Band Level: d/b = 6; P_o/P_a = 2.22

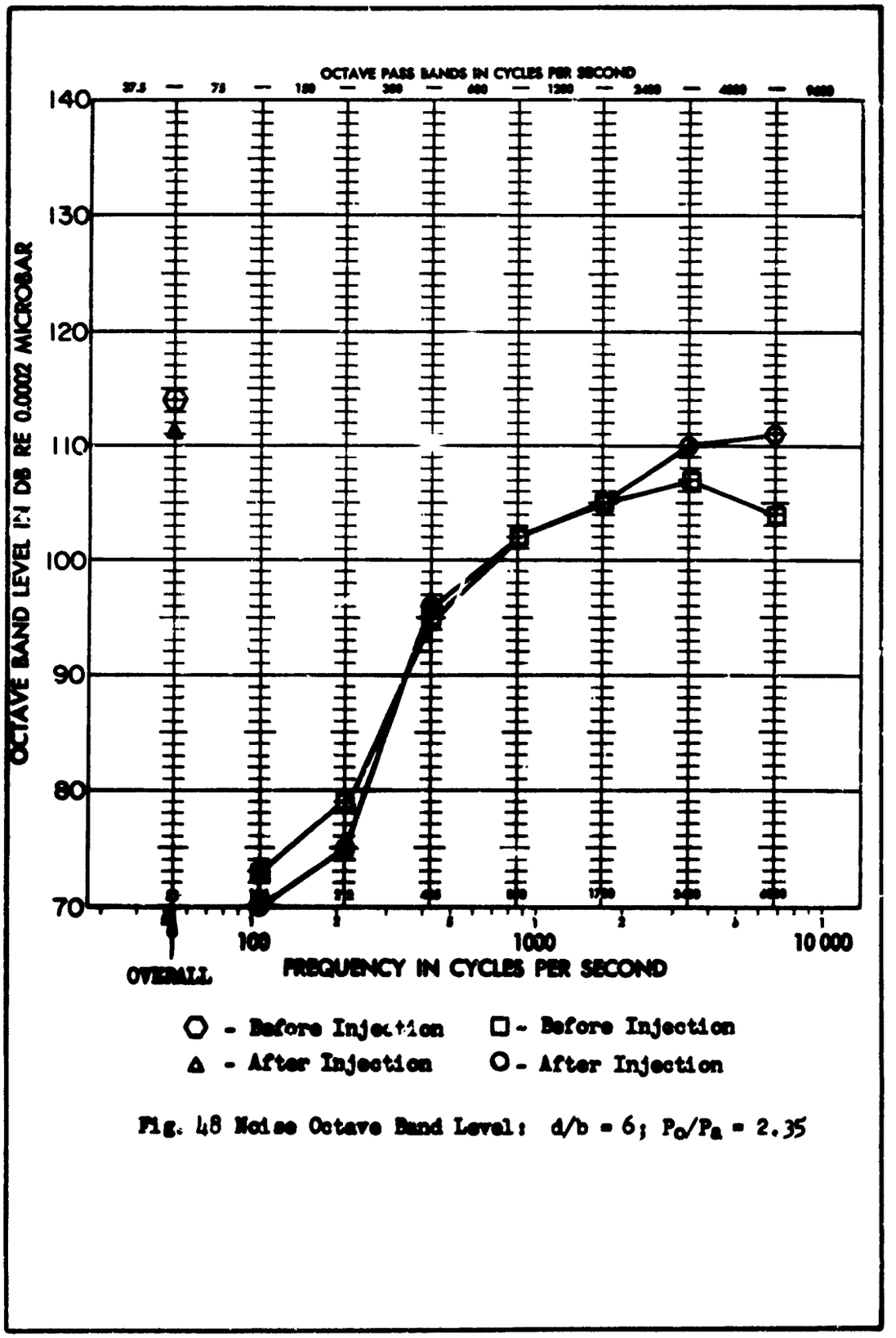

Fig. 48 Noise Octave Band Level: d/b = 6; P_o/P_a = 2.35

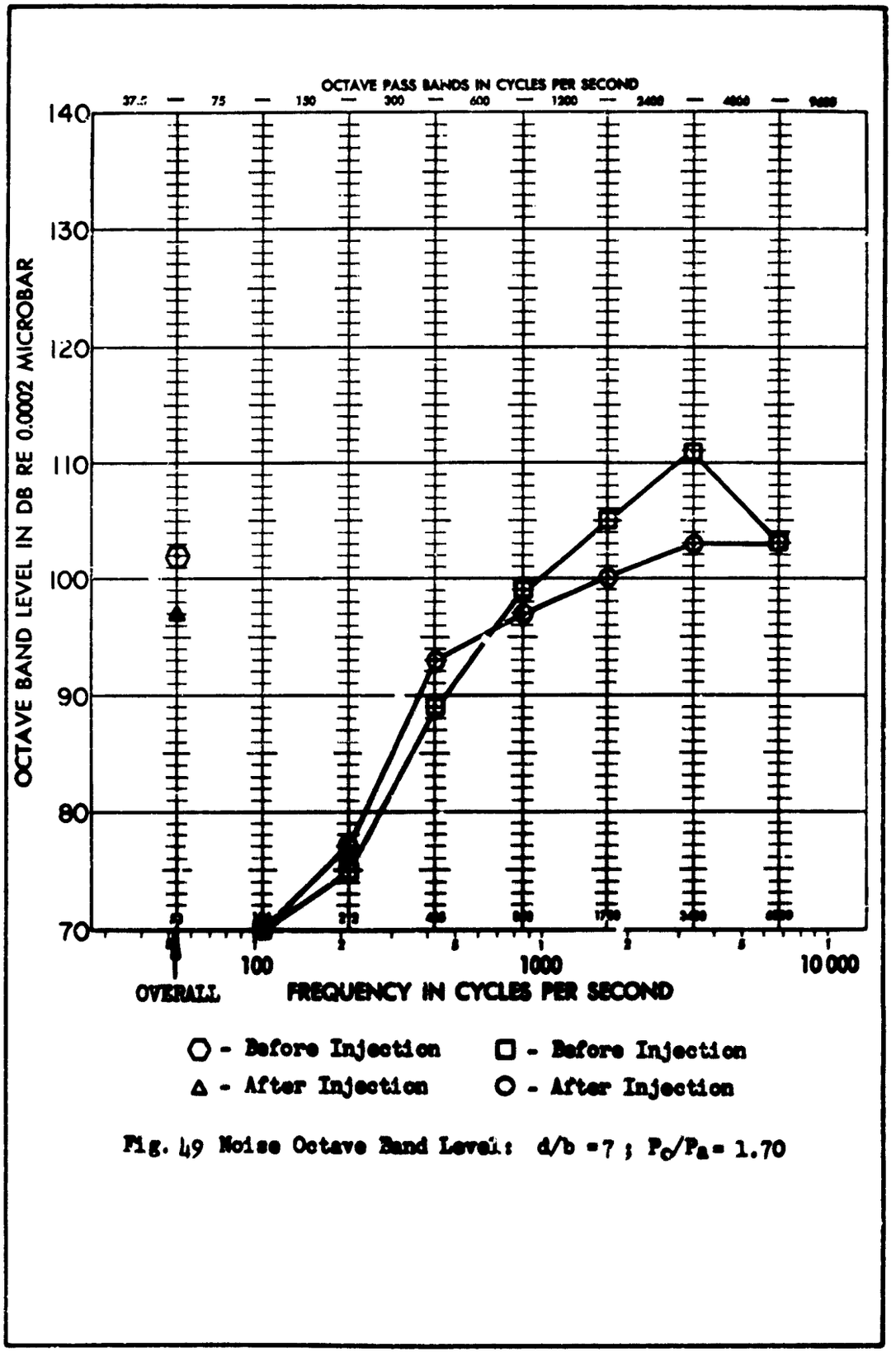

Fig. 49 Noise Octave Band Level: d/b = 7 ; P_c/P_a = 1.70

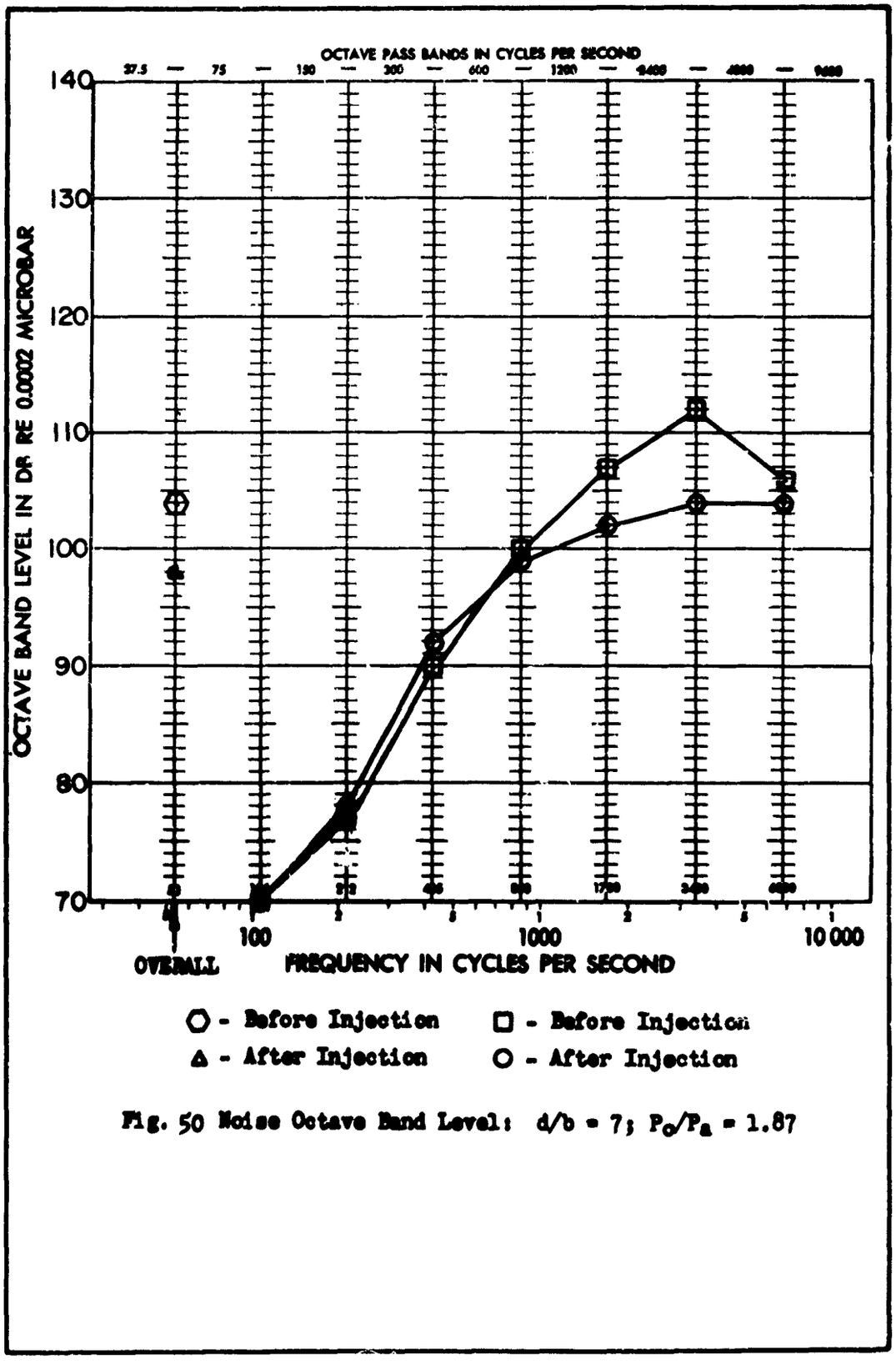

Fig. 50 Noise Octave Band Level: d/b = 7; P_o/P_a = 1.87

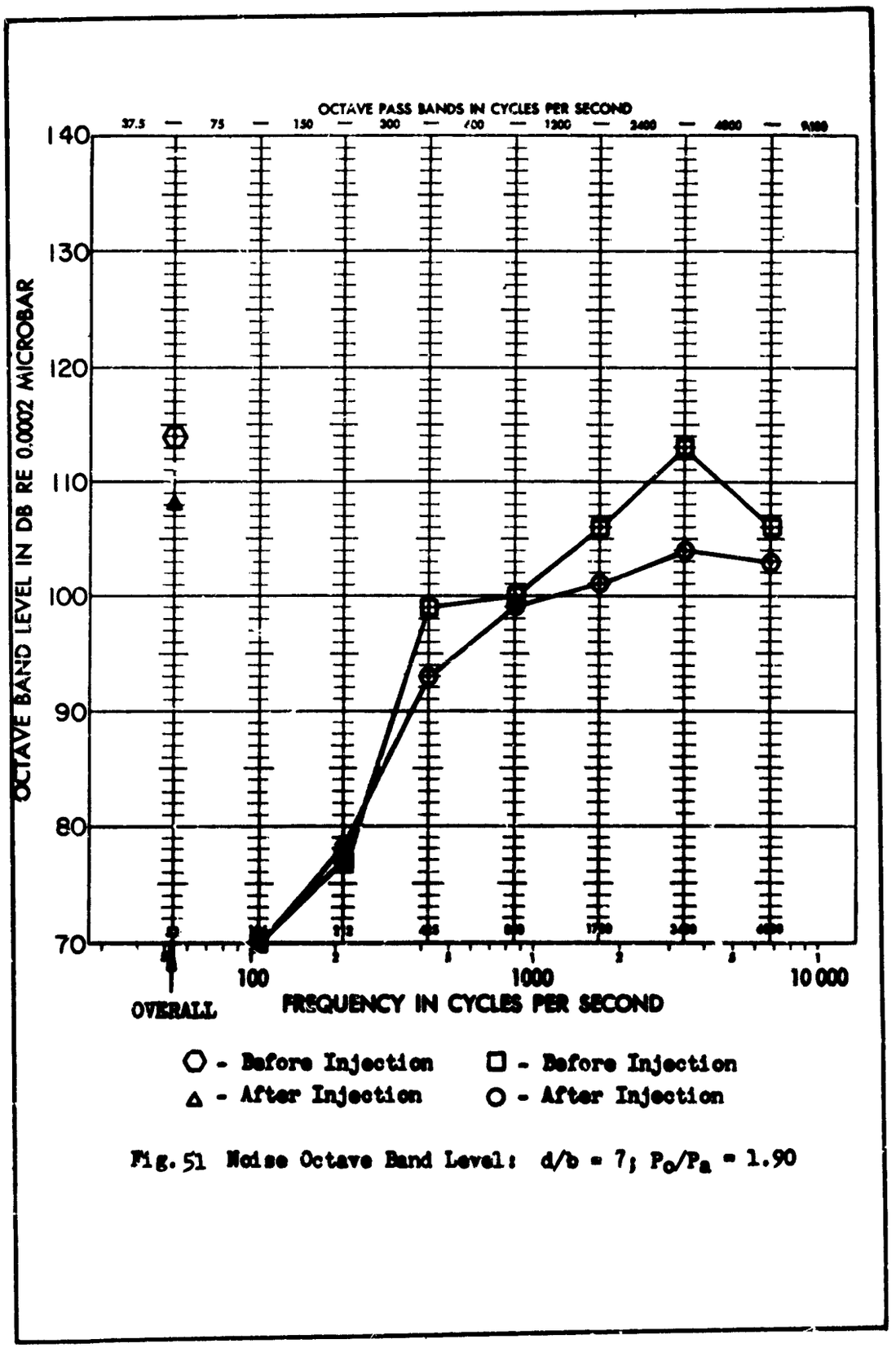

Fig. 51 Noise Octave Band Level: d/b = 7; P_o/P_a = 1.90

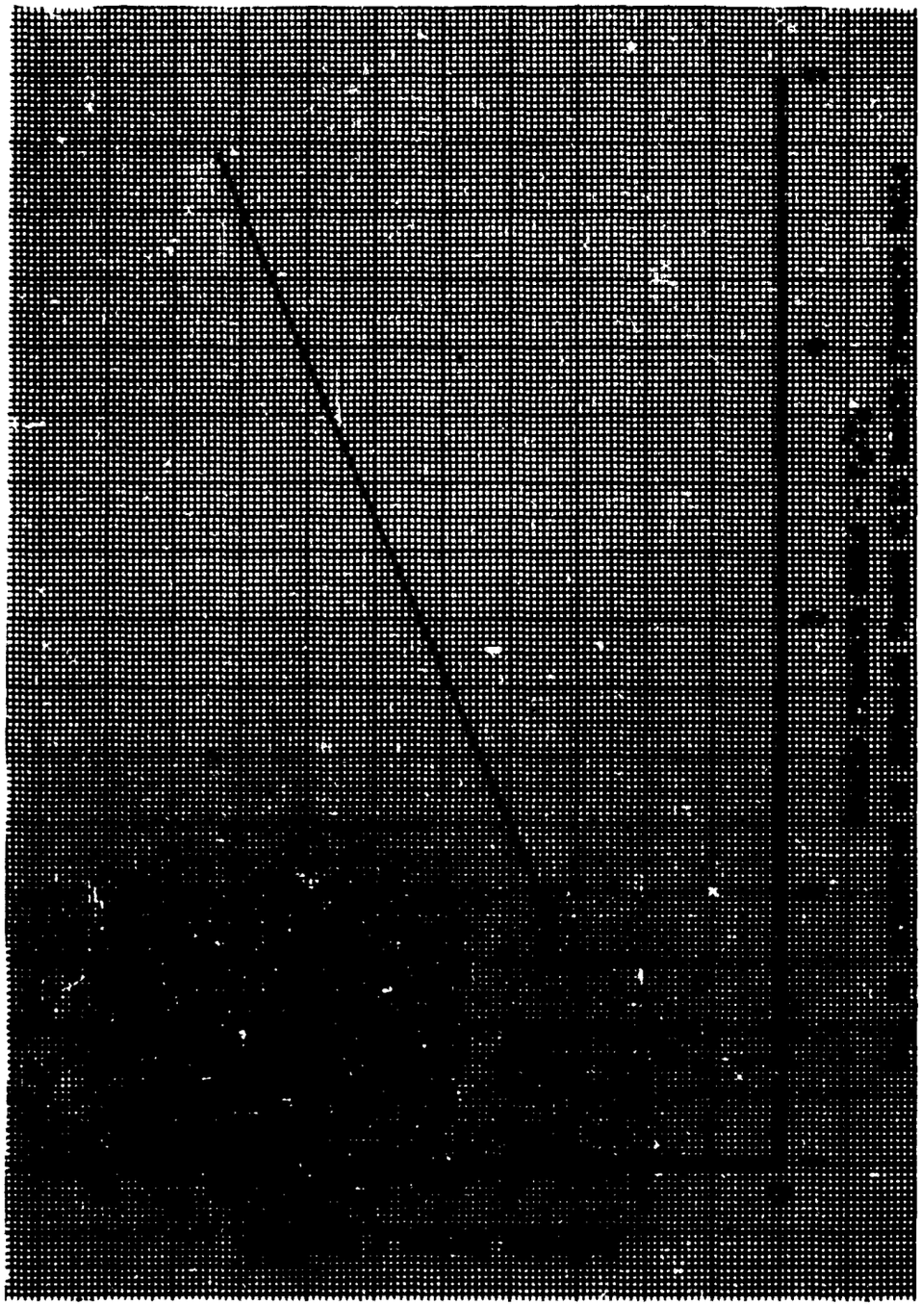

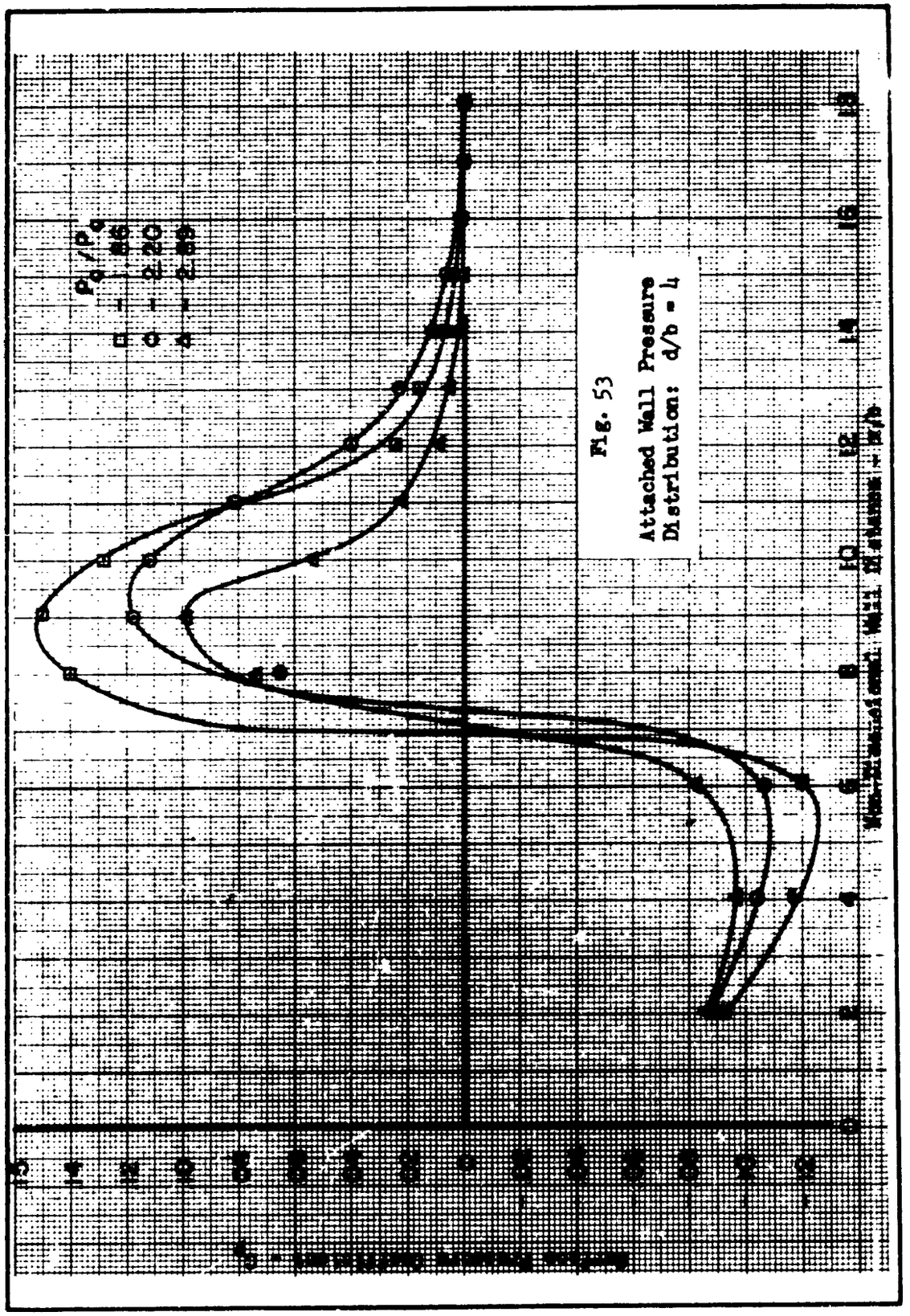

Fig. 53
Attached Wall Pressure
Distribution: d/b = 4

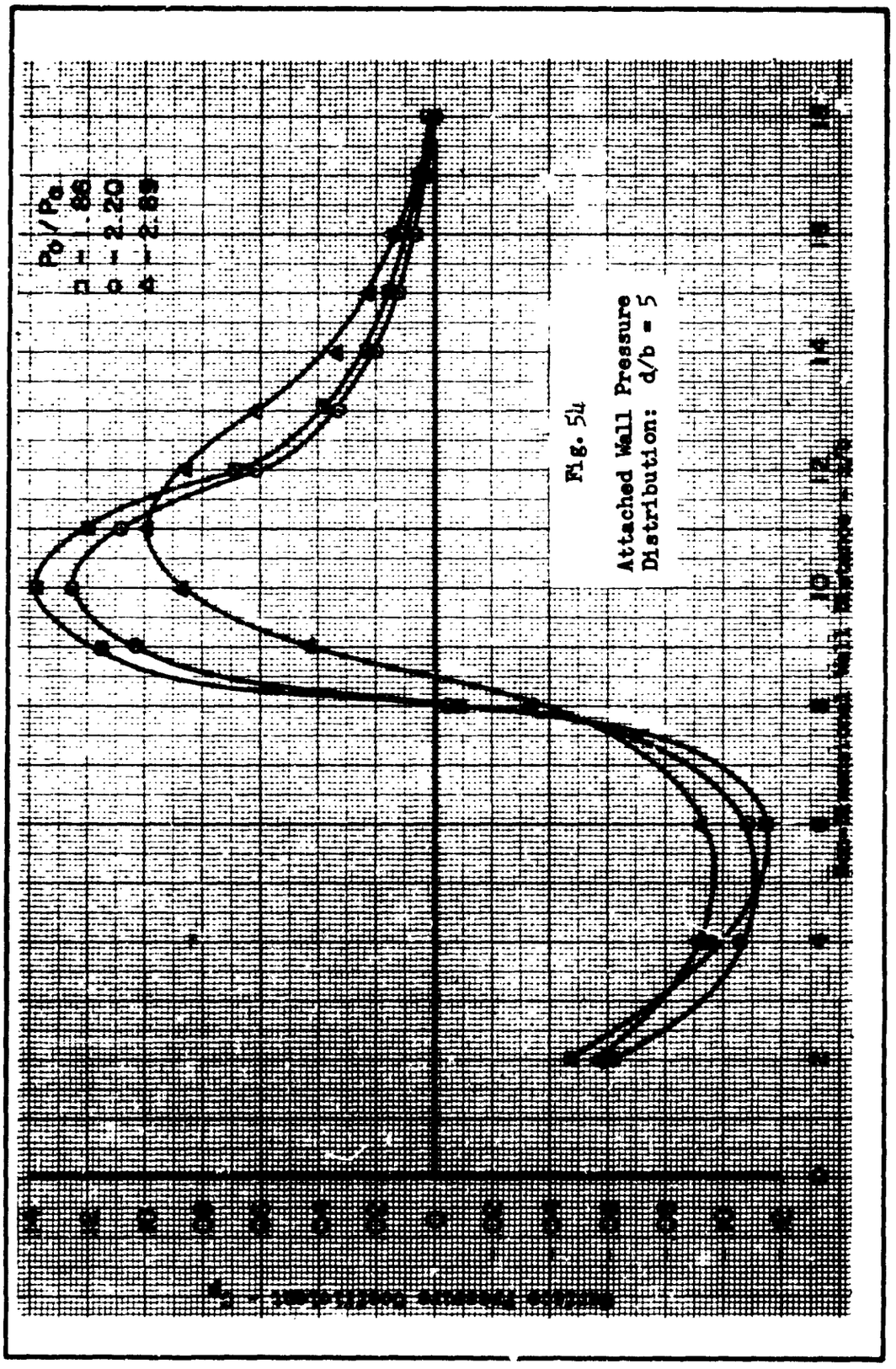

Fig. 54

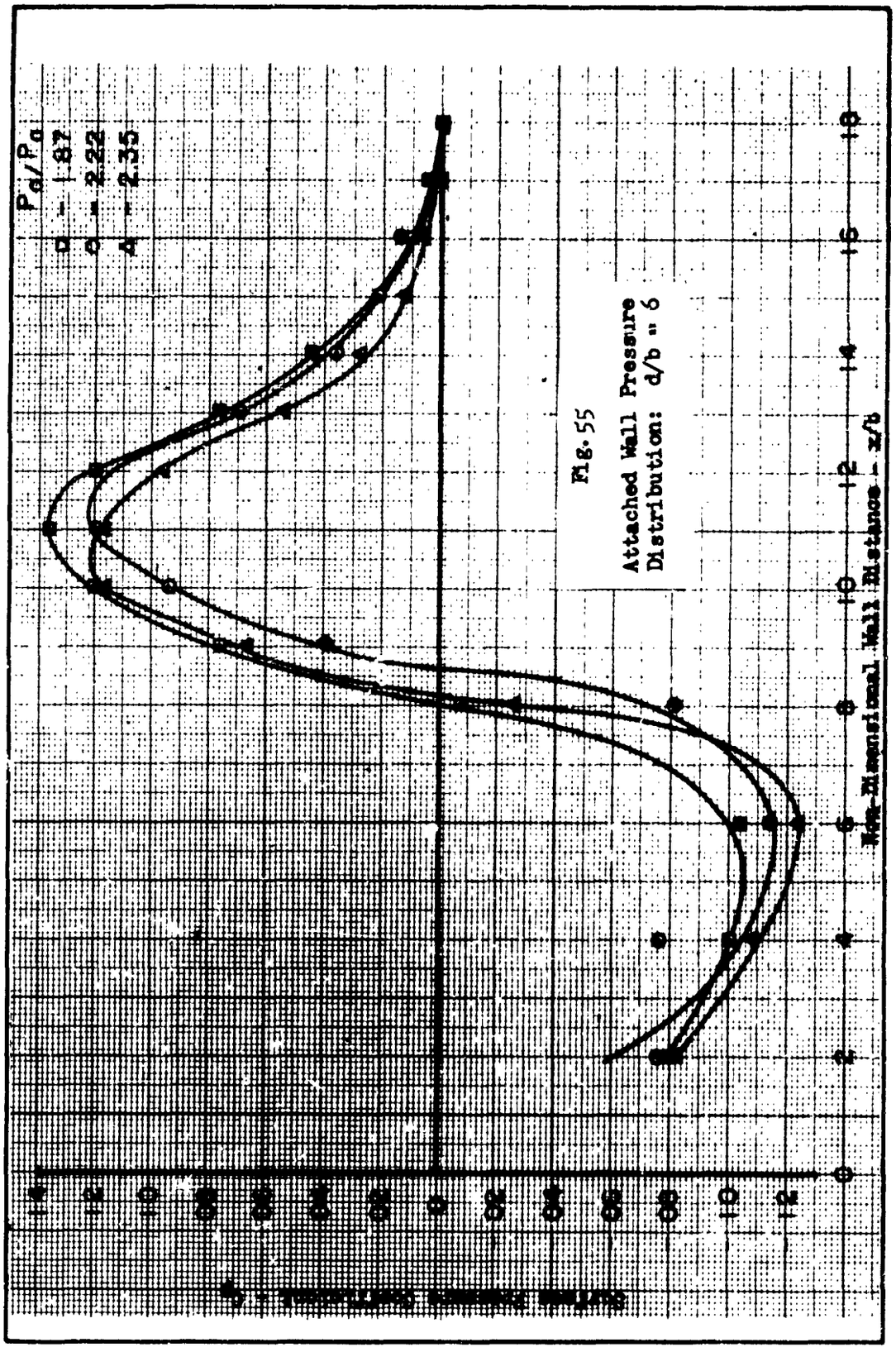
P_d/P_a
D = 1.87
C = 2.22
A = 2.35
Fig. 55
Attached Wall Pressure Distribution: d/b = 6
Non-Dimensional Wall Distance - x/b

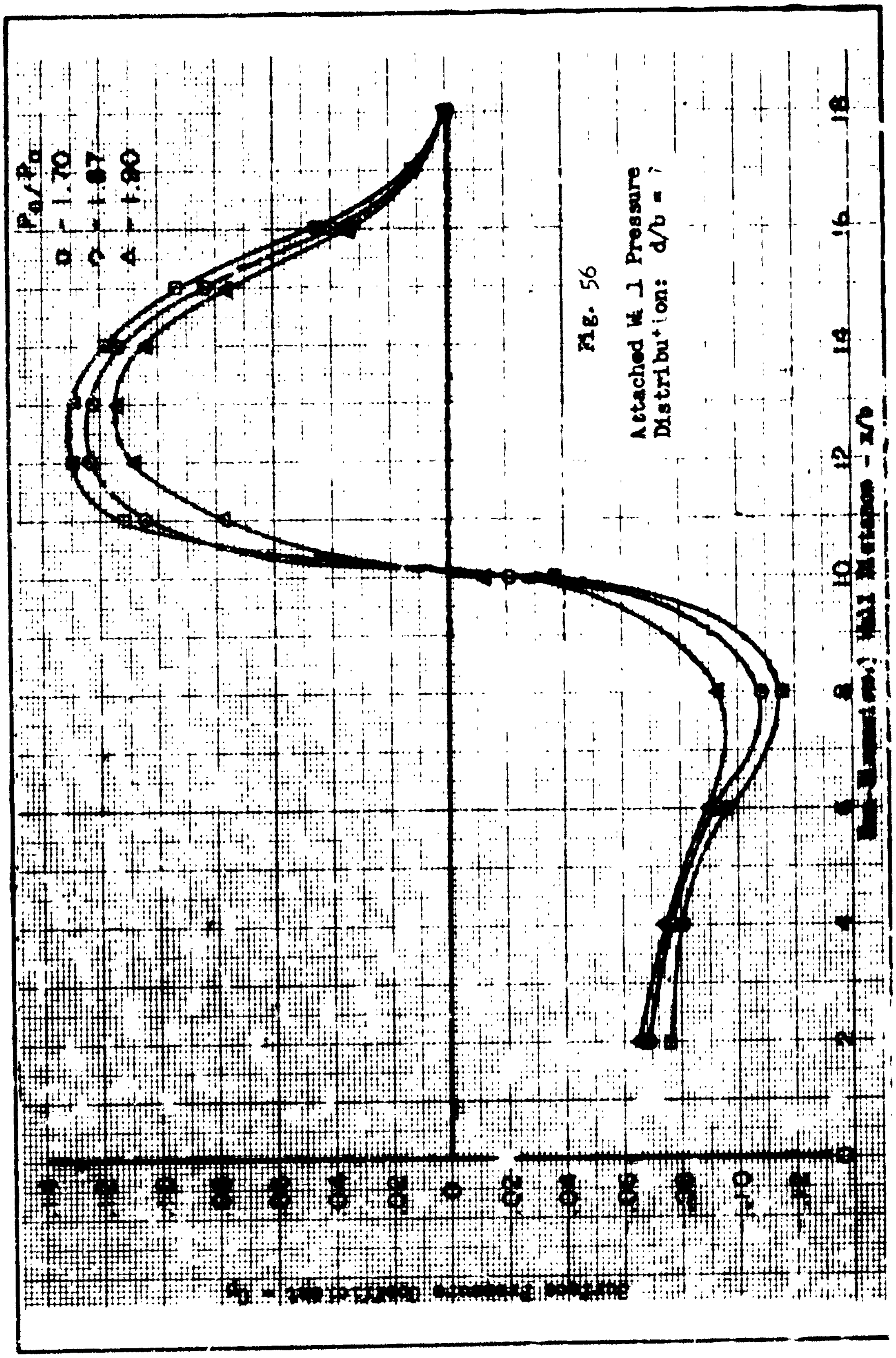

Fig. 56

Attached Wall Pressure Distribution: d/b = 7

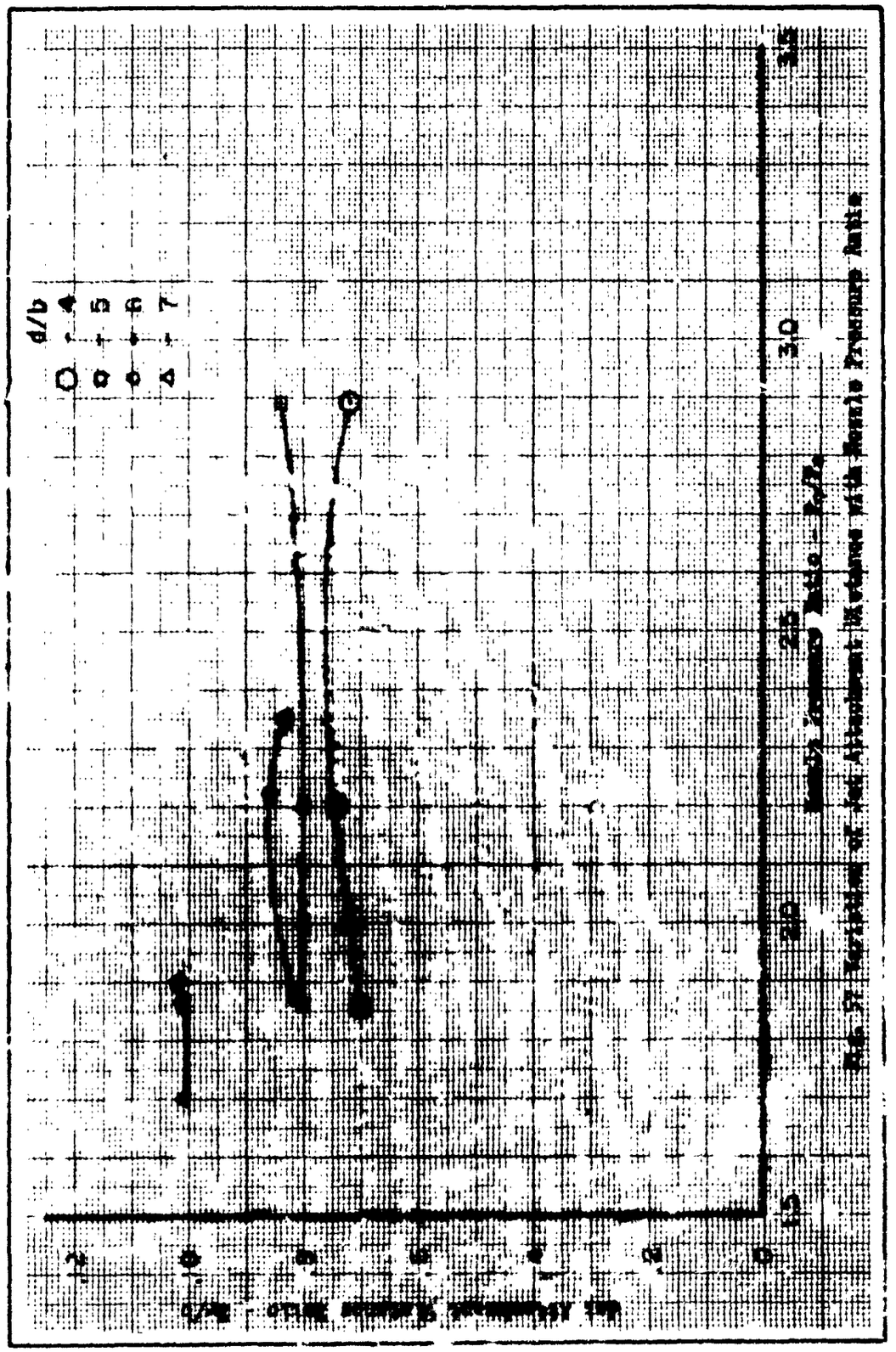
d/b
4
5
6
7
3.0
2.5
2.0
1.5
1.0

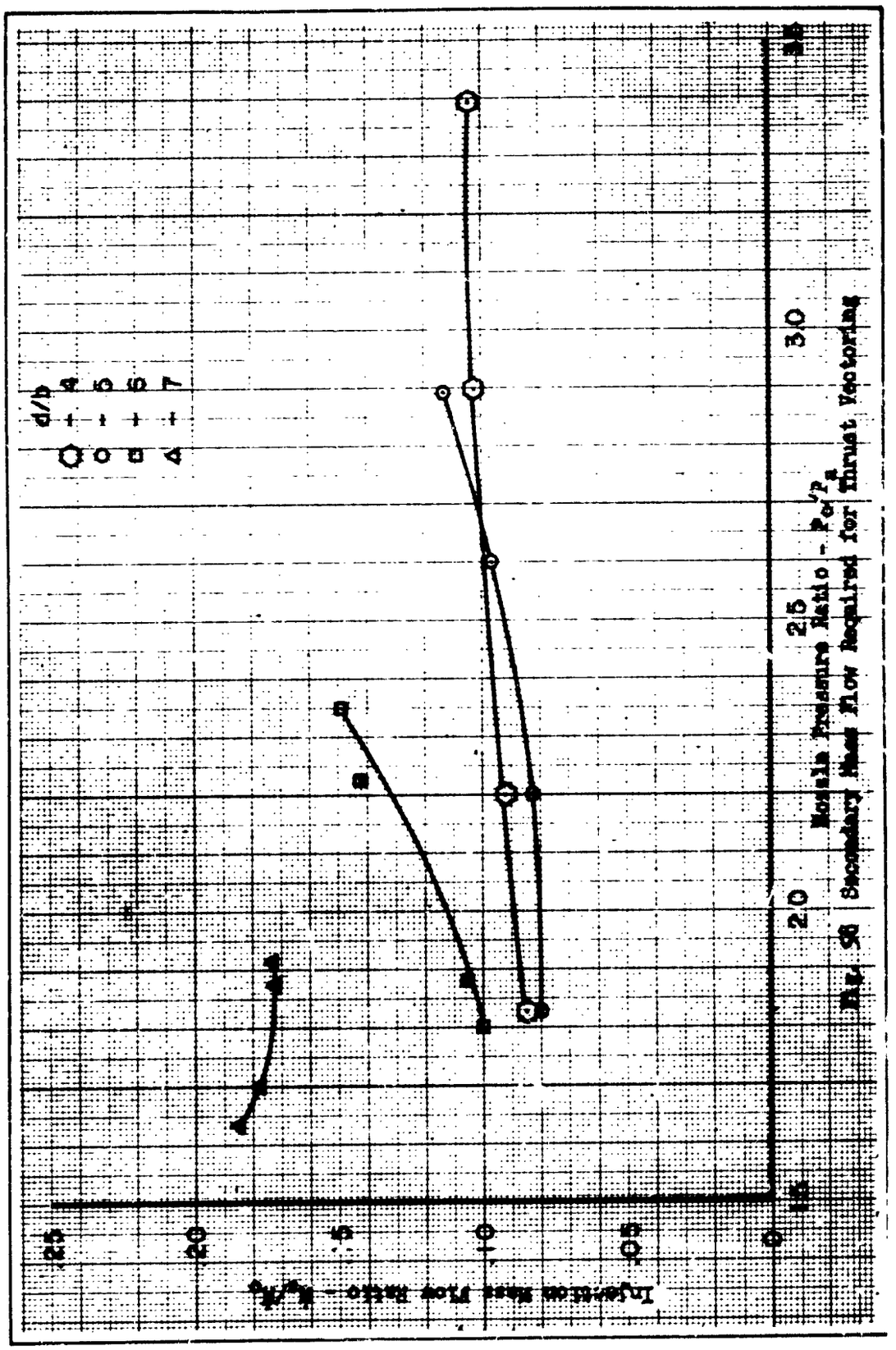
Ratio Pressure Ratio - $P_{o'}/P_a$
Fig. 58 Secondary Mass Flow Required for Thrust Vectoring
Injection Mass Flow Ratio - W_j/W_p
d/b
4
5
6
7
3.0
2.5
2.0
1.5
1.0
.5
0
.5
1.0
2.0
2.5

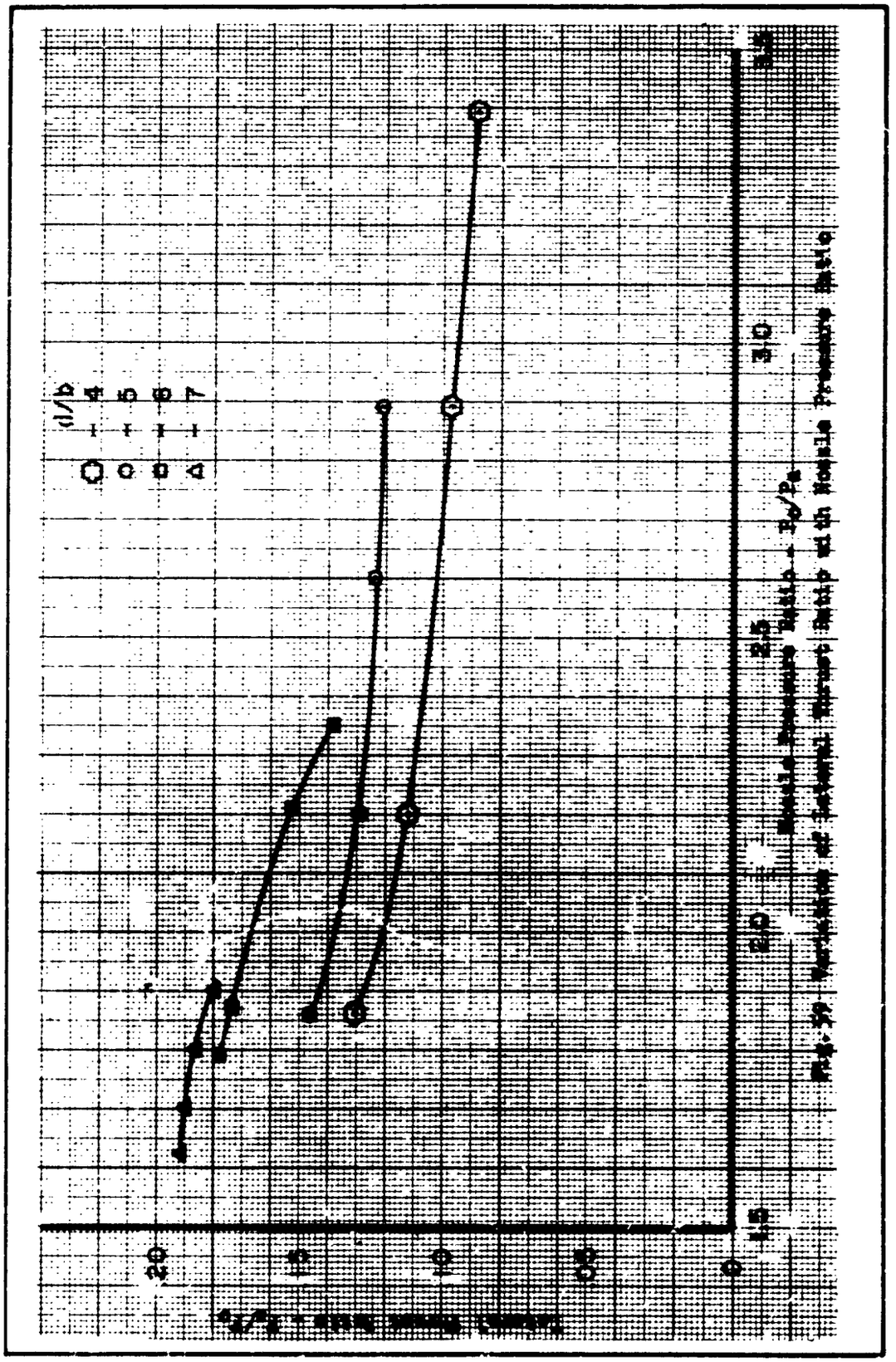

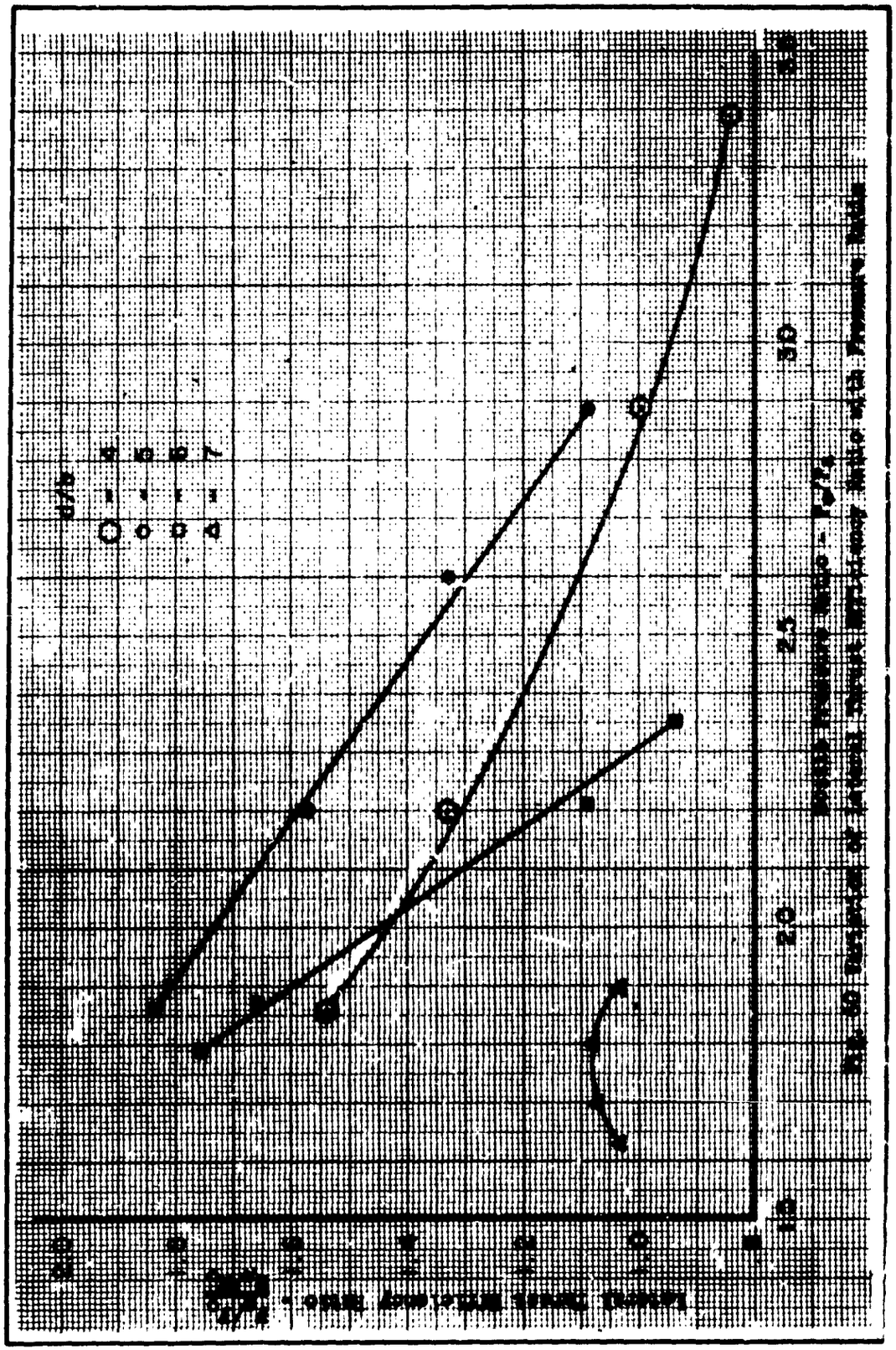

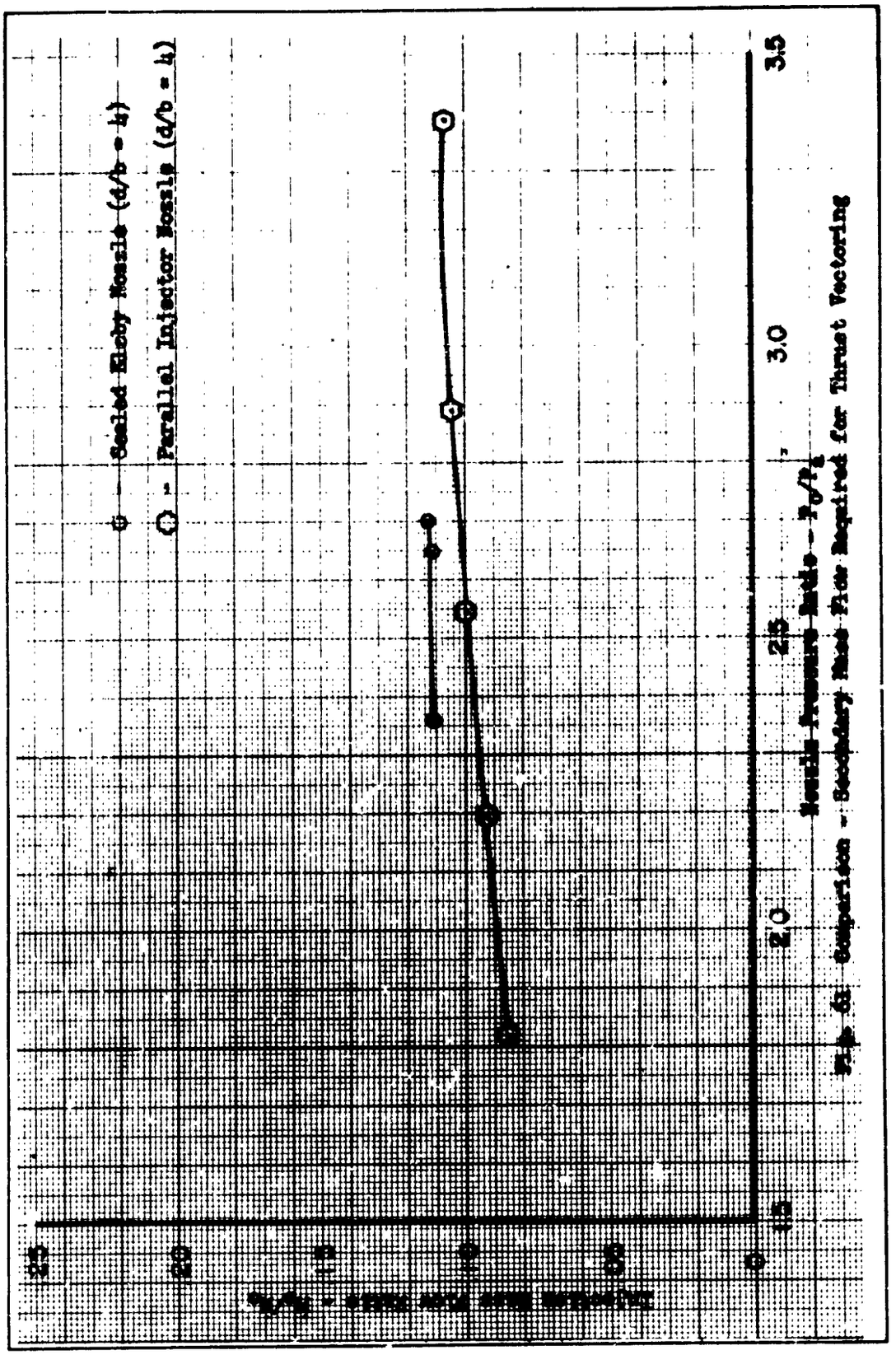

Fig. 61 Comparison - Secondary Mass Flow Required for Thrust Vectoring

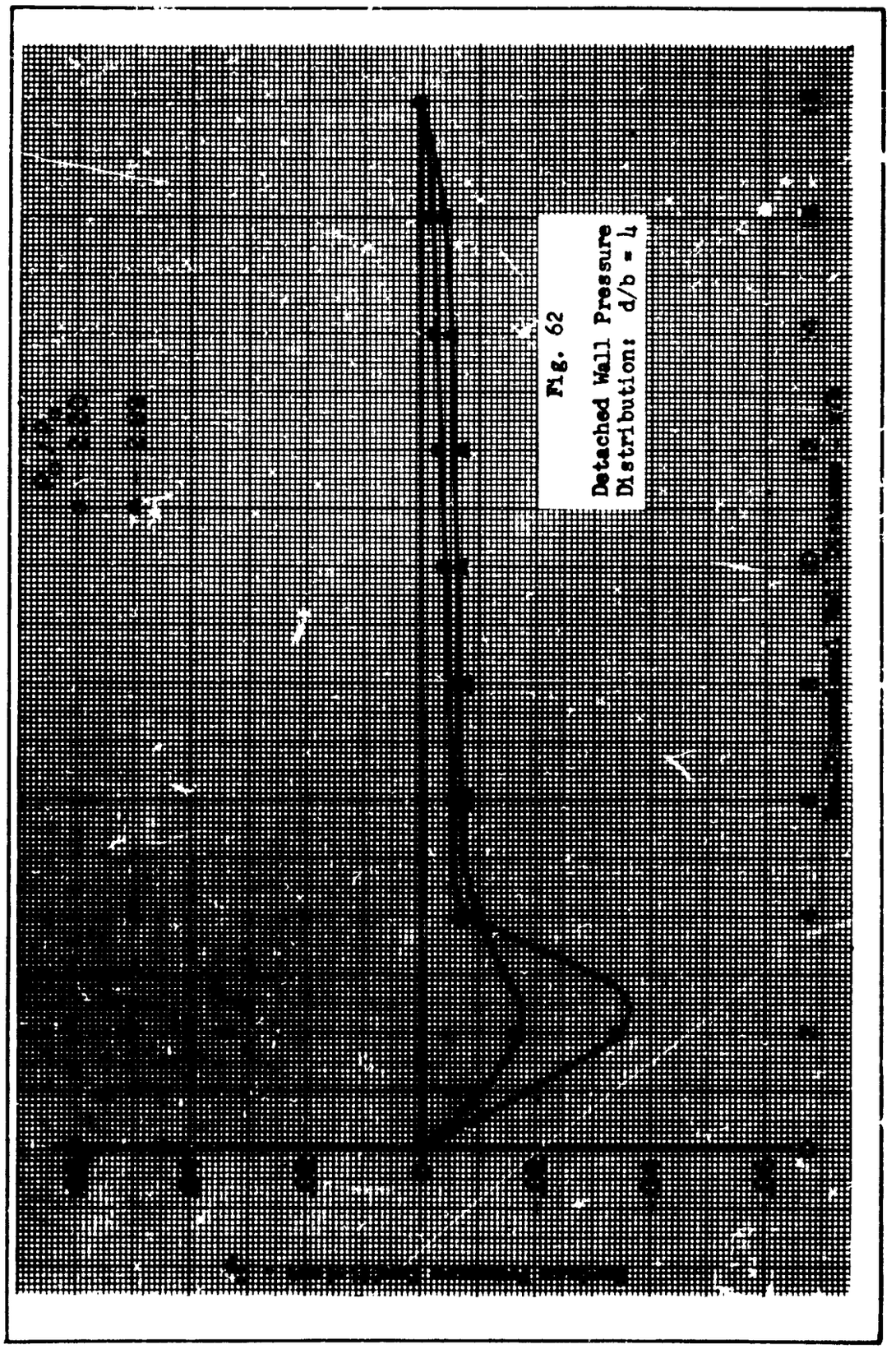

Fig. 62
Detached Wall Pressure Distribution: d/b = 4

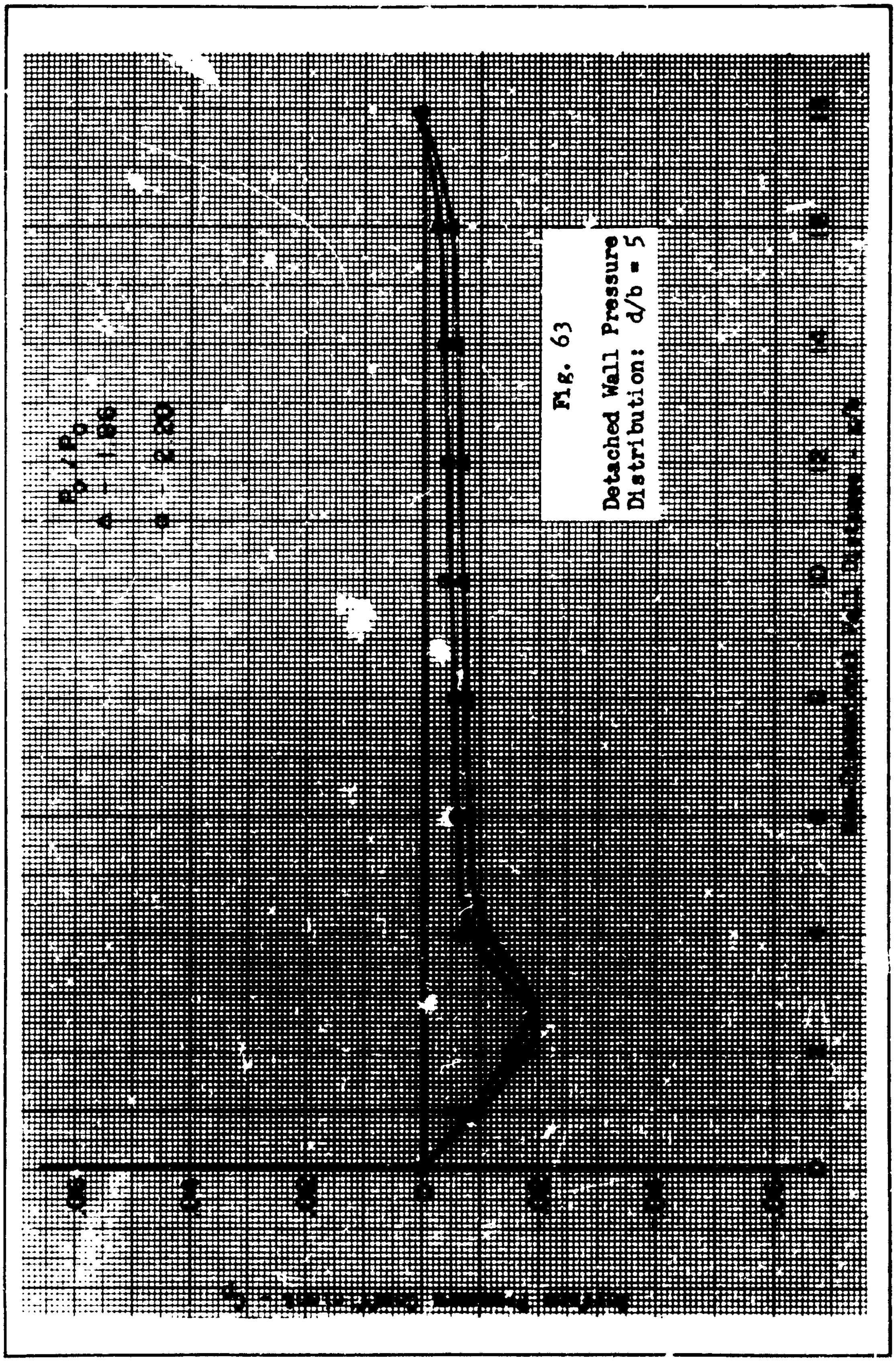

Fig. 63

Detached Wall Pressure Distribution: d/b = 5

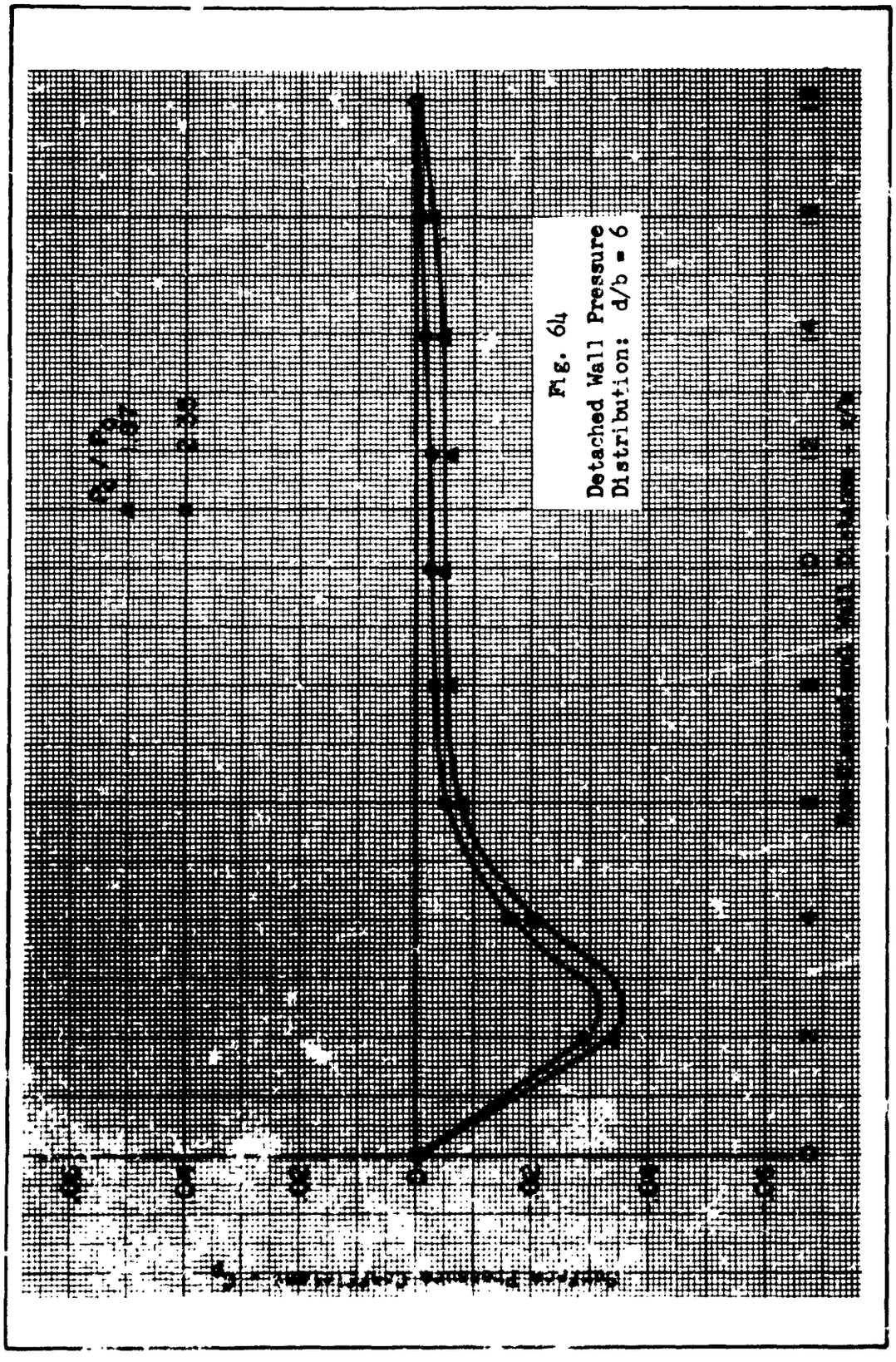

Fig. 64
Detached Wall Pressure
Distribution: d/b = 6

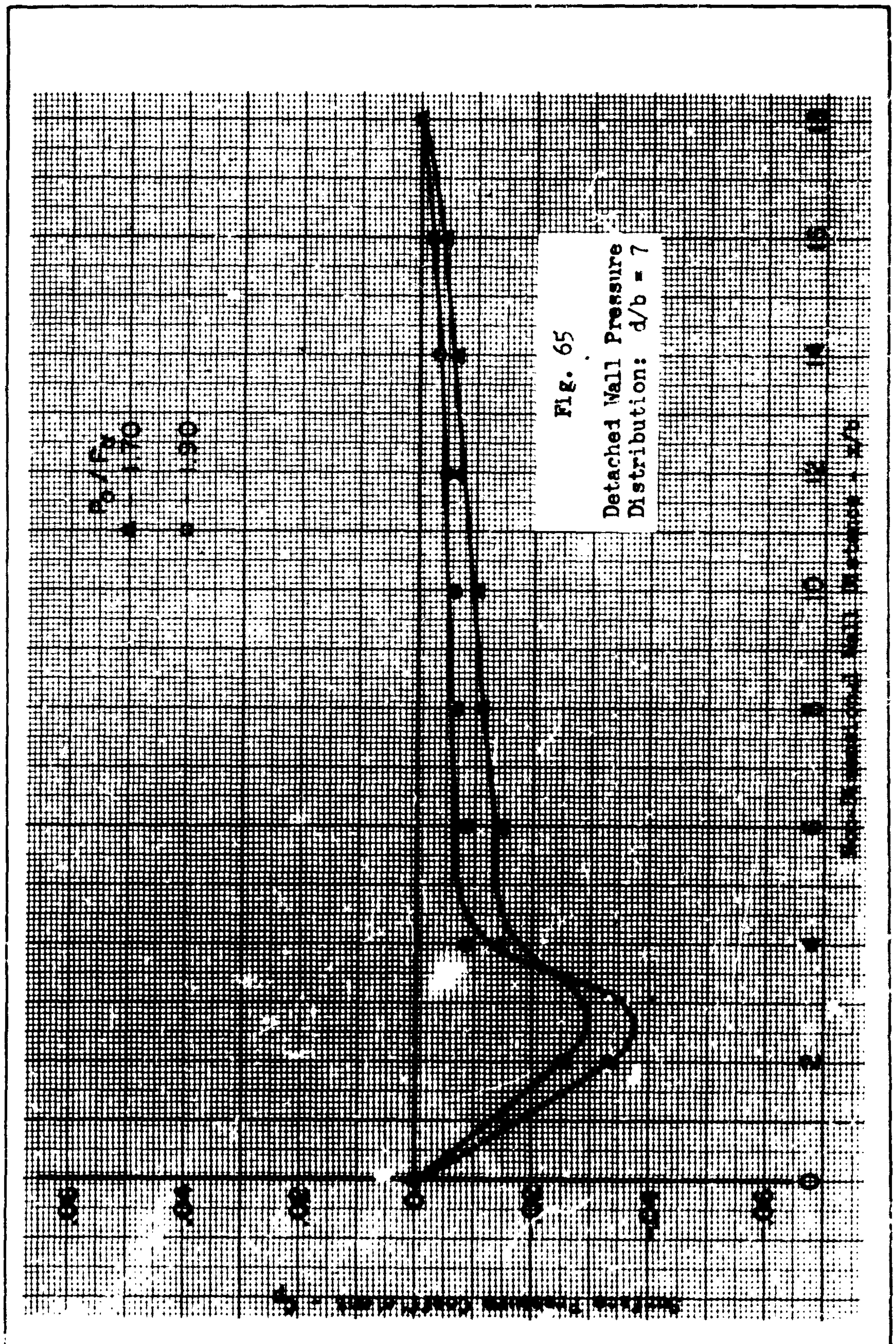

Fig. 65

Detached Wall Pressure Distribution: d/b = 7

Appendix C

Test Nozzle Dimensions

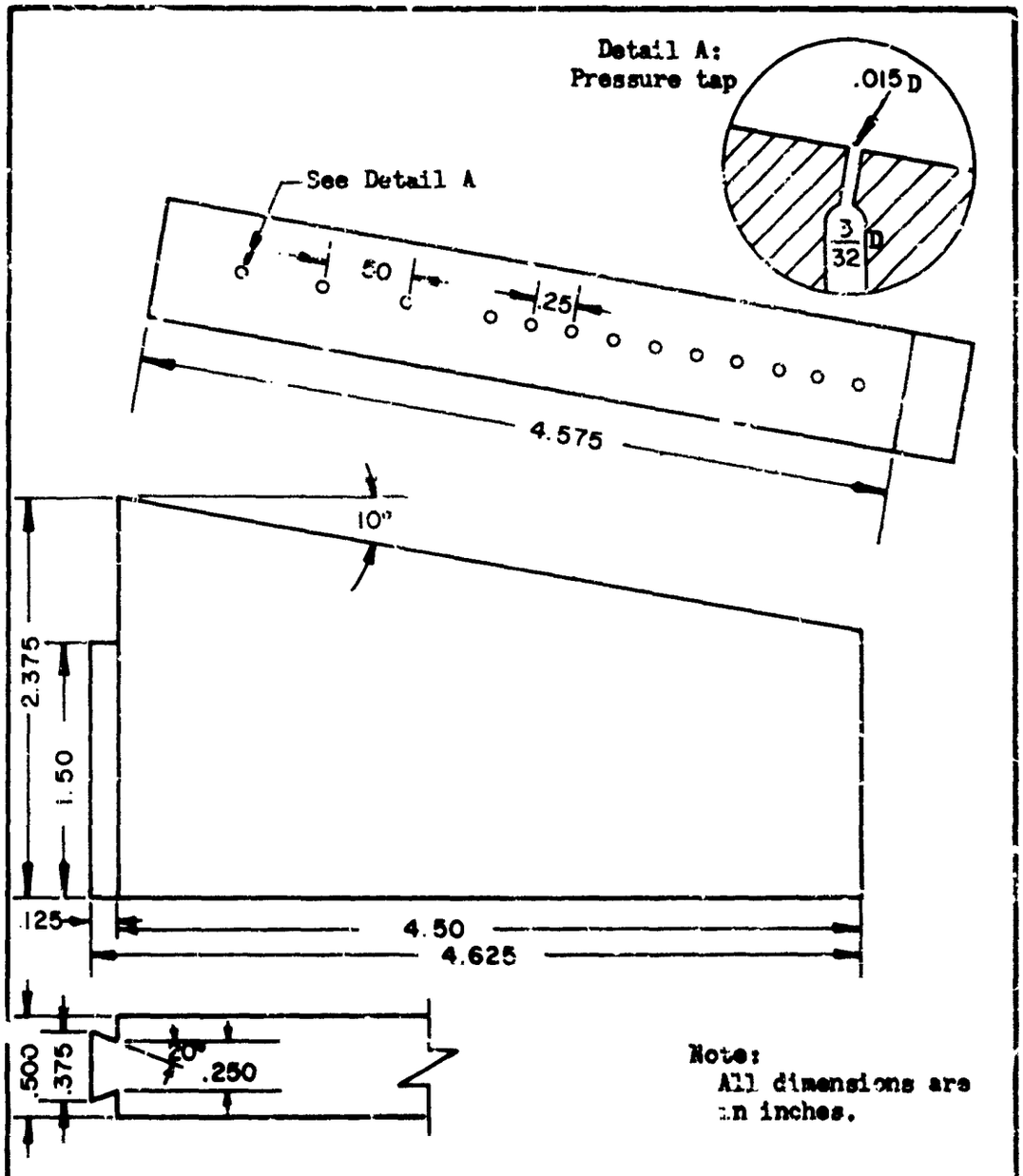

Fig. 66

Diverging Block Dimensions

Note: All dimensions are in inches.

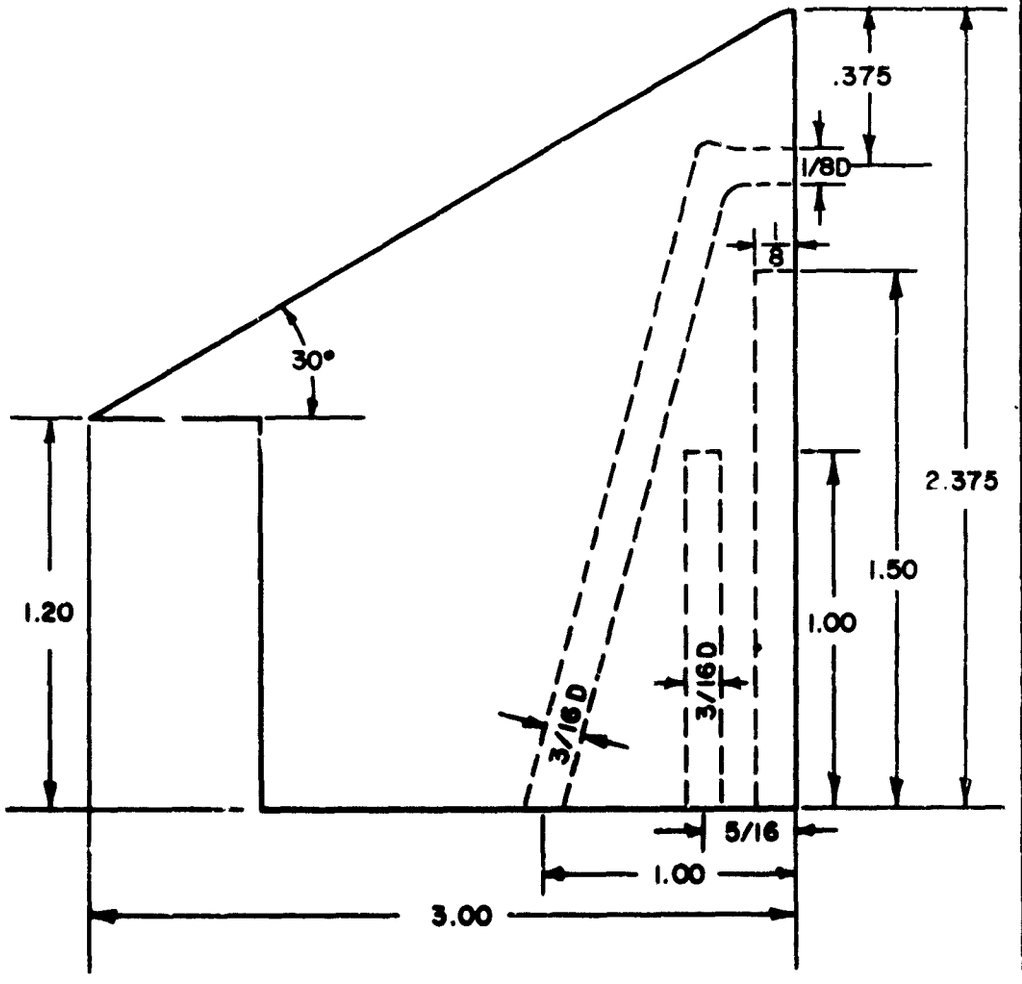

Fig. 67

Converging Block Dimensions

Appendix D

Additional References

Appendix D

Additional References

The following is a listing of additional reference material found by the author during a literature survey on pure fluid control devices. The list is presented for the convenience of future researchers in this field. A listing of 348 references can be found in additional Ref 10.

1. Angrist, S. W. "Fluid Control Devices". Scientific American 6: 80-88 (December 1964).

2. Bowles, R. E. State of the Art of Pure Fluid Systems. New York: ASME, Symposium on Fluid Jet Control Devices, 1962.

3. Brown, F. T. A Combined Analytical and Experimental Approach to the Development of Fluid-Jet Amplifiers. New York: ASME, Symposium on Fluid Jet Control Devices, 1962.

4. Dosanjh, D. S. and W. T. Sheeran. "Experiments with Two-Dimensional Transversely Impinging Jets". American Institute of Aeronautics and Astronautics Journal, 1: 329-333 (February 1963).

5. Greber, I. Bubble Pressures under Reattaching Laminar Jets and Boundary Layers. New York: ASME, Symposium on Fluid Jet Control Devices, 1962.

6. von Glahn, V. H. Use of the Coanda-Effect for Jet Deflection and Vertical Lift with Multiple Flat Plate and Curved Plate Deflection Surfaces. NASA TN 4377, September 1958.

7. Gooderum, R. B., et al. Investigation with an Interferometer of the Turbulent Mixing of a Free Supersonic Jet. NASA TR-963, 1950.

8. Kompass, E. J. "The State of the Art in Fluid Amplifier". Control Engineering, 10: 88-93 (January 1963).

9. Korst, H. H., et al. A Theory for Base Pressures in Transonic and Supersonic Flow. ME-TN-55-89. University of Illinois Experimental Station, 1955.

10. Long, T. A. and E. E. Thompson. A DDC Report Bibliography, January 1953 - October 1963. Alexandria, Virginia: Defense Documentation Center, AD-344 243 (Confidential), September 1963.

11. Sridar, K. An Experimental Investigation of the Flow in and Behind Two-Dimensional Jet Sheets Bounding a Cavity. Report No. 94, Toronto, Canada: Institute of Aerospace Studies, University of Toronto, August 1963.

12. Torda, T. P. Symmetric Laminar Mixing of Two Parallel Streams. AD-5202, University of Illinois, Urbana, Illinois, October 1951.

13. Wuerer, Josef. Experiments on the Control of Plane Jets by Auxilliary Flows. AD-420 578, University of California, Los Angeles, July, 1963.

14. Yakovlevskii, O. V. Laws of Turbulent Mixing of Co-Axial Flows in a Channel of Constant Cross-Section. Translated from Russian by Ministry of Aviation, London, England, July 1964.